

FINAL REPORT FOR CONTRACT YEAR 1
Origins Of Energetic Ions in the Earth's Magnetosheath
Contract NAS5-31213
(for the period ending 5 June 1992)

This final report describes activities under NASA contract NAS5-31213 to Lockheed Missiles and Space Company. The report covers the period from 8 May 1991 to 5 June 1992, the first year of the three year contract. This is a contract under the NASA Guest Investigator Program for the analysis and interpretation of the combined scientific data from the Hot Plasma Composition Experiment (HPCE) and the Charge Energy Mass (CHEM) spectrometer on the AMPTE/Charge Composition Explorer (CCE) spacecraft. These combined data sets have and will be used to survey the energetic ion environment in the Earth's magnetosheath to determine the origins and relative strengths of the energetic ion populations found there.

DATA ANALYSIS ACTIVITIES

A significant amount has been accomplished during the first contract year for this analysis of energetic ion populations. Much of the work early in the first year centered around the development of computer code to analyze and interpret the combined CHEM and HPCE data sets. This code development was used as a means to become familiar with the CHEM data and the capabilities of the CHEM instrument.

In the process of developing an understanding of the CHEM instrument, Dr. Fuselier was able to contribute to a study of radial pulsations observed on the AMPTE and GOES spacecraft. This study led directly to a paper submitted to the Journal of Geophysical Research. The paper entitled "The spatial extent of radial magnetic pulsation events observed in the dayside near synchronous orbit" has been accepted by the journal and is currently in press. A preprint of the paper can be found in Appendix B of this report.

Once familiar with the CHEM data, analysis of energetic ion events in the Earth's magnetosheath proceeded throughout the first year of the contract. The focus of the first year was on the determination of the contribution of leaked magnetospheric protons to the total energetic proton population. Emphasis was placed on intervals when the AMPTE spacecraft was in the plasma depletion layer because it was argued that in this region, only the leaked population

contributes to the energetic ion population. The results of this study are described in a paper entitled "Energetic magnetospheric protons in the plasma depletion layer" which was submitted to the Journal of Geophysical Research. This paper has been accepted and is currently in press. A preprint of the paper can be found in Appendix B of this report.

Manipulation of the CHEM data and comparison of the CHEM and HPCE data over their common energy range near the magnetopause also contributed directly to a second study of that region. Results from this work were used in a study to look at the conservation of mass across the magnetopause. Under conditions of steady state reconnection, the magnetopause is a rotational discontinuity and the mass density, ρ , appropriately modified by the anisotropic pressure term $(1-\alpha)$, where $\alpha = (P_{\parallel}-P_{\perp})\mu_0/B^2$ is constant across the discontinuity. To test this relation, accurate estimates of the mass density and pressure terms are needed. These can only come from composition measurements and AMPTE was uniquely instrumented to test this relation. The HPCE instrument had an upper energy cutoff of 17.1 keV/q. This upper energy is approximately equal to the thermal energy of the hot magnetospheric component found in the outer magnetosphere and in the low latitude boundary layer. Thus, by using the HPCE instrument alone, the mass density and pressure contributions from the magnetosphere are typically underestimated. However, by combining the HPCE and CHEM instruments, these contributions can be correctly accounted for. This procedure was used to determine the conservation of $\rho(1-\alpha)$ across the magnetopause for 28 magnetopause crossings observed in the AMPTE/CCE data. Results from this study are described in a paper entitled "Mass density and pressure changes across the dayside magnetopause" which was submitted to the Journal of Geophysical Research. This paper is currently under review and a preprint of it can be found in Appendix B of this report.

SUMMARY OF PUBLICATIONS

Engebretson, M. J., D. L. Murr, K. N. Erickson, R. J. Strangeway, D. M. Klumpar, S. A. Fuselier, L. J. Zanetti, and T. A. Potemra, The spatial extent of radial magnetic pulsation events observed in the dayside near synchronous orbit, *J. Geophys. Res.*, in press, 1992.

Fuselier, S. A., Energetic magnetospheric protons in the plasma depletion layer, *J. Geophys. Res.*, in press, 1992.

Fuselier, S. A., E. G. Shelley, and D. M. Klumpar, Mass density and pressure changes across the dayside magnetopause, *J. Geophys. Res.*, submitted, 1992.

SUMMARY OF PRESENTATIONS

Lockheed Space Sciences Seminar

Fuselier, S. A., Energetic ions in the Earth's magnetosheath and upstream region, 16 January, 1992, Palo Alto, CA.

University of Maryland Space Sciences Seminar

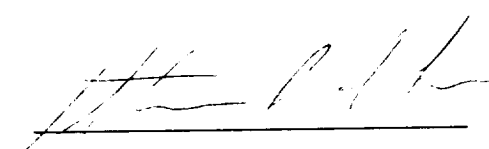
Fuselier, S. A., Energetic ions in the Earth's magnetosheath, 1 March, 1992, College Park, MD.

American Geophysical Union Spring Meeting, Montréal Canada, 12-16 May, 1992.

Fuselier, S. A., Energetic magnetospheric protons in the plasma depletion layer (Abstract), *EOS Trans. Amer. Geophys. Union*, 73(14), Spring Meeting Suppl., 250, 1992.

Shelley, E. G., S. A. Fuselier, and D. M. Klumpar, Mass density conservation across the magnetopause (Abstract), *EOS Trans. Amer. Geophys. Union*, 73(14), Spring Meeting Suppl., 256, 1992.

Copies of the above abstracts and papers are found in Appendices A and B, respectively.



Stephen A. Fuselier

APPENDIX A: PRESENTATIONS

LOCKHEED PALO ALTO RESEARCH LABORATORIES

SPACE SCIENCE SEMINAR

Thursday, 9:00 a.m. to 10:00 a.m.

3170 PORTER DRIVE, BUILDING 255

Back Conference Room

Note to outside visitors: This schedule is subject to change. Please call Loreen at (415) 424-3258 for confirmation before making a special trip.

January 16, 1991 Dr. Stephen A. Fuselier
Lockheed Palo Alto Research Laboratories
Palo Alto, CA 94304

Energetic ions in the Earth's magnetosheath and upstream region

Since the discovery of energetic ions (>10 keV/q) upstream from the Earth's quasi-parallel bow shock and in the Earth's magnetosheath, a controversy has raged over the origin (or origins) of these ions. Early on, it was realized that there are two competing sources of energetic ions, one related to the Earth's bow shock and the other related to the magnetosphere. It is widely accepted that solar wind ions undergo first order Fermi acceleration in the turbulent regions upstream and downstream from the Earth's bow shock, providing the energetic ion population related to the Earth's bow shock. It is also widely accepted that energetic ions leak from the Earth's magnetosphere onto magnetic field lines near the magnetopause, providing the energetic ion population related to the Earth's magnetosphere. Controversy continues over the level of importance of the two competing sources. Part of this controversy is the result of an incomplete understanding of several aspects of the energetic ion observations. This talk will focus on two of these aspects. In the first part of the talk, possible seed populations for ion acceleration at the bow shock will be discussed. In the second part of the talk, a technique for observing leaked energetic ions from the magnetosphere without interference from the bow shock related source will be presented.

Energetic Magnetospheric Protons in the Plasma Depletion Layer

S A Fuselier, (Lockheed Palo Alto Research Laboratory,
Palo Alto, California 94304; (415) 424-3334;
SPAN LOCKHD::FUSELIER)

When the angle between the Interplanetary Magnetic Field (IMF) and the X_{GSE} direction is larger than $\sim 60^\circ$, the quasi-parallel bow shock region is located on the flanks and magnetic field draping against the magnetopause results in the formation of a plasma depletion layer in the subsolar region near the magnetopause. Under these conditions, the leakage of energetic magnetospheric ions can be studied in the plasma depletion layer without interference from the bow shock accelerated energetic ion population. The proton components of the energetic ion population in the energy range from a few keV/q to ~ 100 keV/q were studied using 13 plasma depletion layer intervals identified in the AMPTE/CCE data. In general, the leaked energetic proton distributions in the plasma depletion layer were similar to those found in the magnetosphere except they had lower densities, much higher velocities, and similar but somewhat lower temperatures. The leaked energetic proton distributions also had much higher velocities along B than the magnetosheath proton distributions in the plasma depletion layer. The high velocities indicate that the leaked energetic protons will exit the plasma depletion layer and enter the magnetosheath and region upstream from the Earth's quasi-parallel bow shock. However, the contribution these protons make to the total energetic proton population is small when compared to the contribution from the bow shock acceleration source because the leaked magnetospheric proton densities were about 10 times smaller than typical upstream energetic proton densities.

1. 1992 Spring Meeting
2. 001025672
- 3 (a). S. A. Fuselier
Dept. 91-20, Bldg. 255
Lockheed Palo Alto Research
Laboratory
3251 Hanover St.
Palo Alto, CA 94304
(b). (415) 424-3334
4. (SM) Magnetospheric Physics
- 5 (a). none
(b). 2724 Magnetopause, Cusp
and boundary layers,
2728 Magnetosheath
6. Oral
7. None
8. Invoice \$60 to
Lockheed Palo Alto Research
Laboratory
P. O. #ZAP24678-0X
(attached)
Inquiries to:
Technical Information
Dept 90-11, Bldg 201
Lockheed
3251 Hanover Street
Palo Alto, CA 94304
Attn: Janet Thomas
9. C (Contributed)

Mass Density Conservation Across the Magnetopause

E G Shelley, S A Fuselier, and D M Klumpar (Lockheed Palo Alto Research Laboratory, Palo Alto, California 94304; (415) 424-3334; SPAN LOCKHD::FUSELIER)

For steady reconnection, the magnetopause is a time stationary rotational discontinuity. When this condition holds, the total mass density, ρ , modified by the anisotropic pressure term, $(1-\alpha)$, (where $\alpha=(P_{\parallel}-P_{\perp})\mu_o/B^2$) must be constant across the magnetopause. Using plasma composition measurements from the AMPTE/CCE spacecraft, this rotational discontinuity test can be attempted for the first time. We report on the results of a survey of 27 magnetopause crossings where composition measurements in the Low Latitude Boundary Layer (LLBL) and in the magnetosheath (or in magnetosheath (external) boundary layer if sampling permitted) were available. For these crossings, the mass density on both sides of the magnetopause was dominated by H^+ on average, although individual crossings did have significant and, on one occasion, dominant contributions from solar wind He^{2+} and magnetospheric O^+ . Similarly, the plasma pressure was dominated by H^+ on average, although individual crossings could have up to $\sim 25\%$ contributions from He^{2+} or O^+ . The constancy of the quantity $\rho(1-\alpha)$ across the magnetopause was checked for all crossings, some of which had accelerated plasma flows in the LLBL. This quantity was constant across only $\sim 25\%$ of the magnetopause crossings surveyed. In particular, $\rho(1-\alpha)$ was not constant across some magnetopause crossings when accelerated flows in the LLBL provided strong independent evidence that the magnetopause was indeed a rotational discontinuity. This discrepancy indicates that the time stationary and/or essentially one-dimensional nature of the magnetopause that is required for $\rho(1-\alpha)$ to be constant is rarely met at the dayside magnetopause.

1. 1992 Spring Meeting

2. 001025672

3 (a). S. A. Fuselier
Dept. 91-20, Bldg. 255
Lockheed Palo Alto Research
Laboratory
3251 Hanover St.
Palo Alto, CA 94304
(b). (415) 424-3334

4. (SM) Magnetospheric Physics

5 (a). SM04 Formation of
the Low Latitude Boundary Layer
(b). 2724 Magnetopause, Cusp
and boundary layers,
7835 Magnetic Reconnection

6. Oral

7. None

8. Invoice \$60 to
Lockheed Palo Alto Research
Laboratory
P. O. #ZAP24678-1X
(attached)
Inquiries to:
Technical Information
Dept 90-11, Bldg 201
Lockheed
3251 Hanover Street
Palo Alto, CA 94304
Attn: Janet Thomas

9. C (Contributed)

APPENDIX B: PUBLICATIONS

PRECEDING PAGE BLANK NOT FILMED

Mass Density and Pressure Changes Across the Dayside Magnetopause

S. A. FUSELIER E. G. SHELLEY AND D. M. KLUMPAR

Lockheed Palo Alto Research Laboratory, Palo Alto, CA

Plasma composition measurements from 27 magnetopause crossings are used to determine if mass density, ρ , modified by the anisotropic pressure term $(1-\alpha)$, is constant across the magnetopause. In the process of testing this relation across the magnetopause, several new properties of the discontinuity and its layers are presented. Pressure and mass density in the magnetosheath and low latitude boundary layer are found to be dominated by H^+ except on rare occasions when H^+ is a minor contributor to the total mass density in the low latitude boundary layer. Using these measurements, it is found that $\rho(1-\alpha)$ is not constant for almost all magnetopause crossings even when there is independent evidence for magnetic reconnection and an open magnetopause. This result indicates that even when reconnection is occurring at the magnetopause, this discontinuity is not described as a time stationary rotational discontinuity.

INTRODUCTION

One of the more elusive problems in solar wind-magnetospheric coupling has been determining how magnetosheath plasma crosses the Earth's magnetopause and populates the low latitude boundary layer. Clearly, some of the time this boundary layer as well as the boundary layer external to the magnetosphere (henceforth called the magnetosheath

boundary layer) are formed through the interconnection of magnetosheath and magnetospheric magnetic field lines referred to as magnetic reconnection [Dungy, 1961]. However, the difficulty has been to develop a definitive test that can be used on any magnetopause crossing to determine if the magnetosheath plasma in the low latitude boundary layer crossed an open magnetopause (i.e., a magnetopause where reconnection was occurring or had occurred sometime in the past).

One of the simplest tests to determine whether the magnetopause is open or closed at the time of a magnetopause crossing is to measure the component of the magnetic field normal to the magnetopause surface. An open magnetic field geometry will necessarily have a finite normal component. Practical application of this test is severely limited by the inability to determine the normal direction with sufficient accuracy [e.g., Cowley, 1982; Sonnerup et al., 1981]. The magnitude of the magnetic field tangent to the magnetopause is approximately ten times that of the normal component. Therefore even a small error in the normal direction can result in a large error in the magnitude of the normal magnetic field.

Another relatively simple but more restrictive test to determine whether the magnetopause is open or closed is to check the mass density, ρ , modified by the anisotropic plasma pressure, α (where, $\alpha = (P_{\parallel} - P_{\perp}) \mu_0 / B^2$) across the magnetopause [Hudson, 1970]. For a time-stationary, one-dimensional rotational discontinuity, the test entails determining if

$$\rho(1 - \alpha) = \text{constant} \quad (1)$$

across the discontinuity. Note that (1) is valid only across time-stationary rotational discontinuities and therefore would be valid only across the magnetopause itself. In the standard picture of an open magnetopause [e.g., Sonnerup et al., 1981;

Gosling et al., 1990; Fuselier et al., 1991c], (1) is valid only inside the separatrixes that separate the magnetosheath from the magnetosheath boundary layer and the low latitude boundary layer from the magnetosphere. For a closed magnetosphere represented by a tangential discontinuity, (1) does not hold in general but may appear to hold simply by accident.

Unfortunately, the use of (1) as a test for an open or closed magnetopause requires measurement of the total mass density and total pressure of the plasma including contributions from ions other than protons. The practical application of this test has been hampered by the lack of composition measurements of the thermal plasma at the magnetopause.

Given the difficulties in using the normal magnetic field and constancy of mass density as tests, attention has been focused on the plasma flow velocities in the magnetosheath and low latitude boundary layer. Without going into detail [see e.g., Hudson, 1970; Sonnerup et al., 1981; Paschmann et al., 1986], magnetohydrodynamic equations for the changes across a time-independent, one-dimensional rotational discontinuity in an anisotropic single fluid plasma predict the change in the plasma flow tangential to the magnetopause,

$$\Delta \mathbf{v} = \mathbf{v}_{2t} - \mathbf{v}_{1t}$$

as a function of relatively easily measured plasma and magnetic field parameters [see, Paschmann et al., 1986, equation 7].

$$\Delta \mathbf{v} = \pm \left(\frac{1 - \alpha_1}{\mu_0 \rho_1} \right)^{1/2} \left[\mathbf{B}_{2t} \left(\frac{1 - \alpha_2}{1 - \alpha_1} \right) - \mathbf{B}_{1t} \right] \quad (2)$$

Where the subscript 1 and 2 refer to the magnetosheath and magnetospheric sides of the magnetopause, respectively and the subscript t refers to the component of the magnetic field \mathbf{B} or the plasma bulk flow velocity \mathbf{V} tangential to the magnetopause. Part of the derivation of (2) assumes that (1) holds in order to eliminate the mass density on the

low latitude boundary layer side (ρ_2). It is also important to note that the derivation of (2) assumes a single fluid plasma. In a multi-fluid plasma like that at the Earth's magnetopause, (2) predicts the flow velocity changes of the center-of-mass of the plasma only [Paschmann et al., 1986; 1989].

Several magnetopause crossings observed by various spacecraft have been tested using (2) [see e.g., Sonnerup et al., 1981; Gosling et al., 1986; Paschmann et al., 1986]. Results indicate that many of these magnetopause crossings do appear to be consistent with a rotational discontinuity or open magnetopause. However, the use of (2) as a test for an open magnetopause assumes that (1) holds, an assumption that in fact has never been tested.

The purpose of this paper is to test (1) at the magnetopause using a set of magnetopause crossings from the AMPTE/Charge Composition Explorer (CCE) data. This test is subject to several restrictions discussed in the next section. In the process of testing (1), several new properties of the multi-component plasma in the magnetosheath boundary layer and low latitude boundary layer will be presented.

SURVEY

Observations from 27 magnetopause crossings will be used to test (1) at the magnetopause. These 27 magnetopause crossings were selected from the AMPTE/CCE data set from September to December, 1984, when the full complement of ion composition instruments was available. The actual number of magnetopause crossings in this four month interval was much larger than 27. However, time resolution restrictions discussed below limited the number of magnetopause crossings that could be studied. Contained in this set of 27 magnetopause crossings are 7 crossings discussed by Perroomian et al. [1992] which were selected for their relatively high O^+ content in the low latitude boundary layer. This present study is not restricted to specific features of the low latitude boundary

layer. In particular, the 27 magnetopause crossings span the entire range of possible shear angles for the magnetic field across the magnetopause.

Although no attempt has been made to limit this study to specific features of the low latitude boundary layer or magnetosheath, the AMPTE/CCE orbit and the nature of the spacecraft instrumentation do place important restrictions on the generality of the results. The apogee of the AMPTE/CCE orbit was only $8.9 R_E$, thus the spacecraft crossed the magnetopause only when the solar wind dynamic pressure was much larger than its typical value. Figure 1 shows the locations of the 27 magnetopause crossings rotated into the X-Y_{GSE} plane. (The AMPTE/CCE orbit was nearly in this plane.) Also shown in Figure 1 are the magnetopause position and shape for nominal and four times nominal solar wind dynamic pressures [Sibeck et al., 1991]. All AMPTE/CCE magnetopause crossings occurred when the solar wind dynamic pressure was at least four times the nominal pressure. The high solar wind dynamic pressure was most often the result of much higher than normal solar wind densities. Magnetosheath proton densities observed by CCE were typically larger than 100 cm^{-3} . The high solar wind dynamic pressure requirement also limits the local time coverage of this survey. Figure 1 shows that the magnetopause crossings all occurred in the local time range from 1000-1400 UT.

Observations of the thermal plasma including composition were made using the Hot Plasma Composition Experiment (HPCE) [Shelley et al., 1985]. In addition, the magnetic field measurements from the AMPTE/CCE magnetometer [Potemra et al., 1985] were used to determine the location of the magnetopause, the shear in the magnetic field across the magnetopause, and the magnetic field pressure. Many of the features of the HPCE instrument package have been discussed previously [e.g., Fuselier et al., 1991c] and will not be repeated here. However, the time resolution of the ion mass spectrometer (~ 2 min for a complete 2-dimensional angular and energy distribution of the four major ion species H^+ , He^{2+} , He^+ , and O^+) requires some discussion because it alone determined how the test of (1) across the magnetopause was conducted.

Ideally, to test (1) across the magnetopause, one should determine the time history of $\rho(1-\alpha)$ from the observations as the spacecraft transitioned from the magnetosheath across the magnetopause and its layers and into the magnetosphere. Such a time history of (1) may show abrupt changes across the separatrices between the magnetosheath and magnetosheath boundary layer and between the low latitude boundary layer and the magnetosphere. It may also show either no change or considerable change across the magnetopause depending on whether the magnetopause was open or closed.

The 2 min time resolution of the ion mass spectrometer portion of the HPCE limits the value of such a time history of (1). Typical magnetopause crossings were not smooth transitions between the various layers. Most of the crossings contained several transitions into or out of adjacent layers on time scales much faster than the time resolution of the ion mass spectrometer. In order to at least partially compensate for this severe time aliasing, the higher time resolution electron measurements (6 s for a complete 2-dimensional angular and energy distribution) from the electron spectrometer package of the HPCE were used to identify intervals in the low latitude boundary layer or in the magnetosheath boundary layer when the electron fluxes were relatively constant. Often, the magnetosheath boundary layer was either not present or very thin. In these cases, a magnetosheath interval as near to the magnetopause crossing as possible was chosen to represent the magnetosheath side in (1). Thus, instead of producing a time history of (1) for each magnetopause crossing, specific time intervals on either side of the magnetopause and as near to the crossing as possible were selected to represent the low latitude boundary layer and the magnetosheath boundary layer. Plasma moments (densities, velocities, and pressures) were computed for the major solar wind and magnetospheric ion species (H^+ , He^{2+} , He^{2+} , and O^+) from the angle-energy distributions. The partial pressures of each species required special consideration discussed in detail in the next section.

Finally, another possible limitation of the HPCE ion mass spectrometer is its 17.1 keV/q upper energy cutoff. The typical thermal energy of the hot H^+ distribution in the outer magnetosphere is in the energy range from 10-20 keV/q, or near the limit of the instrument. In order to estimate the effect of cutting off the hot magnetospheric proton distribution in the low latitude boundary layer and any part of this distribution that crosses the magnetosphere, the plasma moments (density and temperature) were computed for higher energy part of the proton distribution for several representative cases using the Charge- Energy-Mass (CHEM) spectrometer on CCE [Gloeckler et al., 1985], which had an energy range from 1 to 300 keV/q. It was found that in the low latitude boundary layer and the magnetosheath, the HPCE energy range was adequate for both the mass density and the plasma pressure determination and the contribution to these quantities from the portion of the energy distribution above 20 keV/q was negligible.

SURVEY RESULTS

Mass Density

Table 1 shows the contributions each species makes to the total mass density, and parallel and perpendicular pressures in the magnetosheath or magnetosheath boundary layer (if present). Table 2 shows these same contributions for the low latitude boundary layer. Considering first the mass densities, in Table 1 it is clear that H^+ makes up the bulk of the mass density on the magnetosheath side of the magnetopause. The next major contributor is He^{2+} , the second most abundant ion in the solar wind. Its contribution ranged from 1-23% of the total mass density. In terms of number density, He^{2+} was, on average, only 3.1% of the magnetosheath H^+ density. This is somewhat lower than the typical value of 4% often quoted as the solar wind He^{2+} concentration [e.g., Neugebauer, 1981]. Although data from solar wind monitors were not available for most

of these magnetopause crossings, the lower than average He^{2+} abundance in the magnetosheath was probably the result of the fact that the measurements were made near solar minimum and during very high solar wind density intervals. These conditions favor lower than average He^{2+} abundances [Neugebauer, 1981]. After He^{2+} , the magnetospheric species He^+ and O^+ contribute very little to the total mass density.

Contributions from the individual ion species to the total mass density in the low latitude boundary layer (Table 2) are somewhat different. The H^+ mass density contribution is somewhat lower than that on the magnetosheath side. However, H^+ still dominates on average, providing 82% of the total mass density. Unlike the magnetosheath side, the average contributions from the other species are almost equally split between He^{2+} of solar wind origin and O^+ of magnetospheric origin. Magnetospheric He^+ contributes very little to the mass density in the low latitude boundary layer on average and even under unusual conditions. The 7.9% average contribution from He^{2+} represents a ~25% reduction in its density relative to the proton density when compared to the densities on the magnetosheath side. Whether this actually represents an exclusion of He^{2+} relative to H^+ in the low latitude boundary layer or simply a larger contribution from H^+ of magnetospheric origin to the low latitude boundary layer requires an in depth study beyond the scope of this paper. It is interesting to note that a similar reduction in the $\text{He}^{2+}/\text{H}^+$ density ratio is observed in the central plasma sheet in the Earth's magnetotail [Lennartsson, 1992]. An important result in Table 2 is the range of the O^+ contribution to the total mass density. This magnetospheric ion can contribute nothing to the total mass density in the low latitude boundary layer or can be the dominant contributor.

In the set of 27 magnetopause crossings, O^+ was the dominant contributor to the total mass density for one crossing. Figure 2 shows this particular crossing on November 16, 1984 (84321). These data have been published previously for a different study [Perocmian et al., 1992]; however, the unusual nature of the low latitude boundary layer for

this magnetopause crossing warrants additional consideration. Plotted top to bottom in this figure are the electron number flux for four energies, the B_{GSE} component of the magnetic field, the H^+ number density, and the O^+ number density for 1 hour surrounding the multiple magnetopause crossings. The bar in the top panel has been used previously to identify regions [see, Fuselier et al., 1991a,c]. Clear bars indicate magnetospheric intervals, striped bars indicate boundary layer intervals on either side of the magnetopause, and solid bars indicate magnetosheath intervals. Brackets in the second panel show the intervals selected using the high resolution electron measurements to represent the low latitude boundary layer (0415:00 to 0417:19 UT) and the magnetosheath boundary layer (0425:30 to 0427:46 UT). During almost the entire low latitude boundary layer interval from 0404-0420 UT, the H^+ number density was about 10 cm^{-3} and the O^+ number density was over 1 cm^{-3} (or 10% of the H^+ number density), indicating that O^+ dominated the total mass density in this region. On the magnetosheath side from 0425-0428 UT and after 0432 UT, the O^+ number density dropped dramatically and the mass density was dominated by H^+ . The magnetosphere for this magnetopause crossing was highly disturbed, occurring when the AE index was ~ 1000 , just after a substorm where AE peaked at ~ 2000 [Perroomian et al., 1992]. In addition to the unusual circumstance of a low latitude boundary layer dominated by O^+ , part of the low latitude boundary layer contained counterstreaming kilovolt electron beams [Perroomian et al., 1992].

Pressure

The determination of the contribution each species makes to the total pressure in (1) requires some careful consideration. Equation (1) was developed for a single fluid plasma and therefore describes the center-of-mass properties (such as velocity and pressure) only. The pressure was determined from the second moment of the distribution for a given species, i , and in the center-of-mass frame, it is written as:

$$P_i \propto \int f(v) (v_i - U_{CM}) (v_i - U_{CM}) dv \quad (3)$$

Where the bulk flow velocity of the center-of-mass, U_{CM} , replaces the more familiar bulk flow velocity, U_i , of the individual species. Since protons are the dominant species most of the time on both sides of the magnetopause, the plasma pressure is affected greatest when the center-of-mass velocity differs substantially from the proton bulk flow velocity. Thus, it is important to determine when and where these differences are largest.

In the magnetosheath and in the magnetosheath boundary layer, Table 1 shows that the only other ion that contributes in a significant way to the total mass density is He^{2+} . Therefore, the only viable way the H^+ bulk flow velocity and the center-of-mass velocity can differ is if the H^+ and He^{2+} bulk flow velocities are substantially different. While there are systematic differences in these velocities along the magnetic field in the solar wind, these differences are small compared to the thermal velocities of the H^+ and He^{2+} distributions in the magnetosheath. In addition, observations of He^{2+} and H^+ distributions in the magnetosheath indicate that He^{2+} distribution slows less than the H^+ distribution across the bow shock. However, this differential velocity creates a He^{2+} shell distribution. By the time the distributions reach the magnetopause, the He^{2+} shell distribution has nearly the same velocity as the H^+ distribution [e.g., Fuselier et al., 1988]. Thus, solar wind and bow shock effects will not create a very large difference in the flow velocities of the He^{2+} and H^+ distributions and will result in a center-of-mass velocity that is nearly equal to the H^+ bulk flow velocity.

In the magnetosheath boundary layer during reconnection, H^+ streams out of the magnetosphere into the magnetosheath [e.g., Sonnerup et al., 1981]. This creates a second population of H^+ with no substantial He^{2+} counterpart and will thus change the H^+ bulk flow velocity relative to that of He^{2+} . However, this population has a very low density

relative to the total magnetosheath population and, although it can have a substantial velocity relative to the magnetosheath H^+ population, will not change the bulk flow velocity of the H^+ distribution very much.

On the magnetosheath side of the magnetopause, the above discussion indicates that there does not appear to be any way the center-of-mass velocity and the H^+ velocity can differ by a significant amount. Although not shown here, the actual center-of-mass and H^+ velocities for the 27 magnetosheath and magnetosheath boundary layer intervals in this study were found to differ by no more than 10 km/s. These velocities differences are on the order of 10 to 50 times smaller than the typical proton thermal velocities. Although the pressure calculations here were done in the center-of-mass frame, the total pressure along the magnetic field is not affected substantially by computing it in the rest frame of each individual species.

Table 1 shows the percent contribution each species makes to the parallel and perpendicular pressures in the magnetosheath and magnetosheath boundary layer. Like the mass density contribution, H^+ dominates the pressure contributions with He^{2+} as the next most important species. Magnetosheath He^{2+} contributes slightly more to the perpendicular pressure than the parallel pressure because the He^{2+} distribution is typically more anisotropic than the H^+ distribution in the magnetosheath [see also, Fuselier et al., 1991]. Also, the He^{2+} contribution to the total pressures is similar to its contribution to the total mass density. This result has a relatively simple explanation. Pressure is $n_s k T_s$, and the He^{2+} to H^+ temperature ratio in the magnetosheath was typically about 4, similar to the typical solar wind value [e.g., Neugebauer, 1981]. Thus, the factor of 4 temperature difference in the He^{2+} and H^+ pressures is equal to the factor of 4 mass difference in the mass densities, $m, n, .$

Unlike the magnetosheath side of the magnetopause, there are several ways the center-of-mass velocity can differ from the H^+ bulk flow velocity in the low latitude boundary layer. The most significant differences will be when reconnection is occurring at the

magnetopause and there are high speed flows of magnetosheath ions in the low latitude boundary layer. At other times, most ion species have little or no relative drift speed in the spacecraft or center-of-mass frame [see however, Fuselier et al., 1989]. During reconnection, the magnetosheath distributions in the low latitude boundary layer can have significantly different velocities along the magnetic field relative to the magnetospheric distributions [e.g., Cowley, 1982; Gosling et al., 1990; Fuselier et al., 1991]. Perpendicular flow velocities of the various species can be large but should be the same for all species during reconnection [Gosling et al., 1990; Fuselier et al., 1991]. Therefore substantial differences in the parallel flow velocities of the various species could lead to significant changes in the parallel pressure when it is computed in the center-of-mass frame, providing that the magnetospheric ion density is large enough relative to the magnetosheath H^+ density.

Differences in the flow velocities of the magnetosheath and magnetospheric ions in the low latitude boundary layer for several time intervals during five accelerated flow intervals are shown in Figure 3. Plotted are the magnetosheath H^+ and He^{2+} flow velocities parallel and perpendicular to the magnetic field in the rest frame of the incident cold magnetospheric ion distributions in the low latitude boundary layer [see Fuselier et al., 1990]. This figure clearly indicates that within the uncertainties of the measurements, the perpendicular flow velocities of all ion species are the same in the low latitude boundary layer. Furthermore, the parallel flow velocities of magnetosheath H^+ (solid squares) and He^{2+} (open triangles) are almost always the same for the accelerated flow events. This result was originally reported for one event [Paschmann et al., 1989] (also contained in this study) and from Figure 3 appears to be a common feature of accelerated flow events.

Figure 3 also shows that the flow velocities of the magnetosheath ion distributions can be substantially different from those of the magnetospheric ion distributions. However, this result does not guarantee significant differences in the center-of-mass

velocities and the H^+ (and He^{2+}) flow velocities because these differences also require a magnetospheric ion density that is a significant fraction of the magnetosheath ion mass density. As Table 2 shows, O^+ is the only magnetospheric ion that can possibly be a significant fraction of the total ion density. Although not shown here, the majority of the low latitude boundary layer intervals had center-of-mass velocities within 10 km/s of the H^+ velocities. Several events had very large differences of up to 100 km/s in the parallel component of the center-of-mass and H^+ velocities arising from the different parallel flow velocities such as in Figure 3 and relatively large magnetospheric O^+ densities, such as those in Figure 2.

Table 2 shows the relative contributions each species makes to the parallel and perpendicular pressures in the center-of-mass frame in the low latitude boundary layer. Again, H^+ dominates the average pressures but its contribution can be reduced significantly for special cases. One of these special cases is the magnetopause crossing in Figure 2, where O^+ dominated the mass density. However, even under these extreme conditions, the H^+ distribution still provided the majority of the pressure. Perpendicular pressure contributions for H^+ are slightly lower than parallel pressure contributions, reflecting the fact that other ion species such as He^{2+} and O^+ tend to have slightly more anisotropic distributions in the low latitude boundary layer. Similar to the magnetosheath side of the magnetopause, the He^{2+} contribution to the total pressure in the low latitude boundary layer is similar to the He^{2+} mass density contribution. This result indicates relatively little differential heating of the He^{2+} and H^+ distributions across the magnetopause. Contributions to the pressure and the mass density from He^+ are very minor for all magnetopause crossings, indicating that He^+ plays essentially no role in determining the structure and dynamics of the magnetopause and its boundary layers.

Mass Density Conservation

Figure 4 shows the ratio of $\rho(1-\alpha)$ in the magnetosheath or magnetosheath boundary layer (if present) and $\rho(1-\alpha)$ in the low latitude boundary layer as a function of the magnetic field shear angle between the two measurements. A ratio of 1 indicates that the magnetopause is consistent with a one-dimensional, time-stationary, single fluid MHD rotational discontinuity as discussed in the introduction. Figure 4 indicates that this is almost always not the case. In fact, (1) is not conserved across the magnetopause even for those crossings identified by filled squares when accelerated plasma flow signatures in the LLBL indicated that reconnection was occurring and the magnetopause was open. Reconnection signatures for two of these cases have been discussed in detail [Paschmann et al., 1989; Fuselier et al., 1991a].

The failure of (1) across the magnetopause requires some explanation. Figure 5 shows the $\rho(1-\alpha)$ ratio as a function of the LLBL to magnetosheath density ratio. These two ratios are strongly correlated, indicating that changes in α across the magnetopause have very little effect on keeping (1) constant. This is in direct contradiction to the effects on an anisotropic single fluid plasma at a one-dimensional time-stationary rotational discontinuity. Any change in the mass density across such a structure must be balanced by a corresponding change in the pressure anisotropy.

DISCUSSION AND CONCLUSIONS

Using thermal ion composition measurements from 27 magnetopause crossings of the AMPTE/CCE spacecraft, the mass density and plasma pressure of the multi-component plasma near the magnetopause were determined (see Tables 1 and 2) in order to test (1) across the magnetopause. Tables 1 and 2 show that the mass density and pressure on the magnetosheath side of the magnetopause and the pressure on the magnetospheric side are always dominated by H^+ . The second most important contributor to these quantities is

He^{2+} in a very predictable way. The He^{2+} contributions reflect the solar wind concentrations on the magnetosheath side and a $\text{He}^{2+}/\text{H}^+$ temperature ratio in the magnetosheath of about 4, also similar to that observed in the solar wind [Fuselier et al., 1991b,c]. The He^{2+} concentrations in the low latitude boundary layer drop by about 25% relative to the magnetosheath. The $\text{He}^{2+}/\text{H}^+$ temperature ratio does not change a great deal across the magnetopause so the contribution to the pressure by He^{2+} in the low latitude boundary layer is similar to that in the magnetosheath. The presence of magnetospheric ions does not affect the mass density and pressure on the magnetosheath side. In addition, the pressures on the magnetospheric side are not greatly affected by these ions. Contributions from magnetospheric He^+ to any of the parameters on either side of the magnetopause are negligible, making this ion an ideal tracer of essentially single particle motion in the vicinity of the magnetopause. Magnetosheath He^{2+} and Magnetospheric O^+ do contribute equally on average to the mass density in the low latitude boundary layer and in one magnetopause crossing (Figure 2), O^+ was observed to dominate the mass density in the low latitude boundary layer.

The relative contributions of the various species and the dominance of H^+ in all cases except for one low latitude boundary layer interval have important implications on previous studies of the low latitude boundary layer. These results indicate that by eliminating ρ_2 in the derivation of (2), the contributions from magnetospheric ions to the remaining parameters in (2) are negligible. Paschmann et al. [1986] assumed this to be true when they compared flow velocities changes across several magnetopause intervals. Their assumption of a 5% He^{2+} concentration is somewhat larger than the 3.1% average concentration obtained in this study but the higher concentration probably better reflects average solar wind conditions and not the unusual solar wind conditions in this study.

Although the contributions from magnetospheric ions is eliminated in the derivation of (2), the derivation of this equation assumes that (1) holds across the magnetopause.

Figure 4 shows that this is not the case for nearly all of the magnetopause crossings in this study. Furthermore, (1) changes by a factor of two or more across several magnetopause crossings in Figure 4 that had signatures consistent with reconnection and an open magnetopause. These results imply that the magnetopause cannot be considered a time stationary one dimensional rotational discontinuity even when reconnection is occurring there. Thus, one should not be surprised when observed velocity changes across the magnetopause compared with those changes predicted by (2) differ by a factor of two or more. This difference is an indication that the assumptions that were used to derive (2) are not valid at the magnetopause.

The correlation between the ratio of the mass densities and the ratio $\rho(1-\alpha)$ in Figure 5 shows that the reason why (1) does not hold across the magnetopause is that the equation is dominated by mass density changes across the magnetopause and the plasma pressure anisotropy has a negligible effect [see also *Paschmann et al.* [1986]]. As stated above, this result is in direct contradiction with MHD theory [*Hudson*, 1970] which indicates that any change in the mass density across a time stationary, one dimensional rotational discontinuity must be balanced by a corresponding change in the pressure anisotropy.

Probably the most important limitations of this study are the time resolution of the plasma measurements and the fact that representative time intervals sometimes separated by several minutes had to be selected on either side of the magnetopause in order to test (1) across the discontinuity. However, there is good reason to believe that (1) will not be found to be constant across the magnetopause even when much higher time resolution composition measurements at the magnetopause become available. As illustrated in Figure 5, the plasma pressure anisotropy plays a negligible role in (1) at the magnetopause. This result was also obtained by *Paschmann et al.* [1986] for several magnetopause crossings using much higher resolution data but without the benefit of ion composition measurements at the magnetopause. Their conclusion was that (1) could be con-

stant across the magnetopause only if the mass density changed through a change in ion composition across the discontinuity.

The change in ion composition from the magnetosheath to the low latitude boundary layer is nearly always determined by the ion composition in the outer magnetosphere. (On occasion, O^+ directly from the high latitude ionosphere is observed to increase the O^+ concentration in the low latitude boundary layer [Fuselier et al., 1989]) Ion composition changes in the outer magnetosphere occur on timescales much longer than the 2 min time resolution in this study. Therefore, the ion composition measurements in this study should be representative of the low latitude boundary layer. These measurements indicate that the average composition changes very little across the magnetopause.

In contrast, the change in mass density needed in order for (1) to be constant are extreme. Paschmann et al. [1986] concluded that O^+ concentrations in the low latitude boundary layer had to be on the order of 5% for (1) to be constant across the magnetopause. Table 2 shows that 5% concentrations of O^+ in the low latitude boundary layer are very rare. In fact, only one case of the 27 studied (Figure 2) had such high concentrations. These high concentrations (10% of the H^+ density) were the result of a very high O^+ density in the adjacent outer magnetosphere (see Figure 2). It is therefore concluded that much higher resolution ion composition measurements at the magnetopause probably will not show that (1) is constant across the discontinuity.

Another feature of this study that may result in errors in the determination of the mass density is the 2-dimensional nature of the plasma measurements. Plasma measurements were made in a plane nearly tangent to the magnetopause that contained the magnetic field. If the plasma had a large flow velocity along the Earth-Sun line, then the mass density could be severely underestimated. However, flow velocities along the Earth-Sun line would have to be unrealistically large (~few hundred km/s) for the mass density to be greatly effected in the low latitude boundary layer. Furthermore, in most

cases the low energy magnetospheric ions at near zero bulk flow velocity in the magnetosphere can be distinguished clearly in the low latitude boundary layer even when reconnection is occurring and the low energy ions pick up large transverse flow velocities [see Fuselier et al., 1991a]. The identification of these low energy ions coupled with the fact that flows parallel to the magnetic field were measured by the composition instrument indicate that very large flows along the Earth-Sun line are not common in the magnetopause crossings studied here and the 2-dimensional nature of the measurements probably does not affect the conclusions presented here.

Equation (1) is not constant across the magnetopause probably because the assumption of time stationarity is much too stringent. Another stringent assumption is that one is measuring the plasma on a magnetic field line in the magnetosheath that is simply connected to a region in the low latitude boundary layer that was sampled at some other time. This assumption implies that measurements are always taken inside the separatrixes in the reconnection geometry and on "connected" field lines, an assumption that is probably not valid most of the time. For example, if reconnection were occurring in the cusp region, then plasma from the magnetosheath outside the cusp would populate the low latitude boundary layer. In this case, (1) would not be expected to hold across the equatorial magnetopause (where the AMPTE/CCE measurements are made) since the plasma in the low latitude boundary layer came from a region of space that was not simply connected to the equatorial magnetosheath and magnetosphere.

For these reasons and probably others, (1) is not constant across the magnetopause. On average, (1) changes by about a factor of two across the discontinuity. Therefore, comparisons of observations and theory using the assumption that (1) is constant across the magnetopause should not be expected to agree by more than that factor.

Acknowledgments. The authors gratefully acknowledge discussions with G. Paschmann and C. Goodrich. Magnetometer data used in this study were from the CCE magnetometer and were provided by T. A. Potemra. Research at Lockheed was funded by NASA through contract NAS5-30565, the NASA Guest Investigator program through contract NAS5-31213, and through Lockheed Independent Research.

REFERENCES

- Cowley, S. W. H., The causes of convection in the Earth's magnetosphere: A review of developments during the IMS, *Rev. of Geophys. and Space Physics*, 20, 531-565, 1982.
- Dungey, J. W., Interplanetary field and the auroral zones, *Phys. Rev. Lett.*, 6, 47-48, 1961.
- Fuselier, S. A., E. G. Shelley, and D. M. Klumpar, AMPTE/CCE observations of shell-like He^{2+} and O^{6+} distributions in the magnetosheath, *Geophys. Res. Lett.*, 15, 1333-1336, 1988.
- Fuselier, S. A., D. M. Klumpar, W. K. Peterson, and E. G. Shelley, Direct injection of ionospheric O^+ into the dayside low latitude boundary layer, *Geophys. Res. Lett.*, 16, 1121-1124, 1989.
- Fuselier, S. A., D. M. Klumpar, and E. G. Shelley, Ion reflection and transmission during reconnection at the Earth's subsolar magnetopause, *Geophys. Res. Lett.*, 18, 139-142, 1991a.
- Fuselier, S. A., O. W. Lennartsson, M. F. Thomsen, and C. T. Russell, He^{2+} heating at a quasi-parallel shock, *J. Geophys. Res.*, 96, 9805-9810, 1991b.
- Fuselier, S. A., D. M. Klumpar, E. G. Shelley, B. J. Anderson, and A. J. Coates, He^{2+} and H^+ dynamics in the subsolar magnetosheath and plasma depletion layer, *J. Geophys. Res.*, 96, 21095-21104, 1991c.
- Gosling, J. T., M. F. Thomsen, S. J. Bame, and C. T. Russell, Accelerated plasma flows at the near-tail magnetopause, *J. Geophys. Res.*, 91, 3029-3041, 1986.

- Gosling, J. T., M. F. Thomsen, S. J. Bame, R. C. Elphic, and C. T. Russell, Cold ion beams in the low latitude boundary layer during accelerated flow events, *Geophys. Res. Lett.*, 17, 2245-2248, 1990.
- Hudson, P. D., Discontinuities in an anisotropic plasma and their identification in the solar wind, *Planet. Space Sci.*, 18 1611-1622, 1970.
- Lennartsson, O. W., A scenario for solar wind penetration of the Earth's magnetic tail based on ion composition data from the ISEE-1 spacecraft, *J. Geophys. Res.*, submitted, 1992.
- Neugebauer, M., Observations of solar-wind helium, in *Fundamentals of Cosmic Physics*, Vol. 7, 131-199, 1981.
- Peroomian, V., M. Ashour-Abdalla, S. A. Fuselier, D. Schriver, W. K. Peterson, and R. J. Strangeway, Electrostatic waves due to field-aligned electron beams in the low-latitude boundary layer, *J. Geophys. Res.*, 97, 3169-3183, 1992.
- Paschmann, G., I. Papamastorakis, W. Baumjohann, N. Sckopke, C. W. Carlson, B. U. Ö. Sonnerup, and H. Lühr, The magnetopause for large magnetic shear: AMPTE/IRM observations, *J. Geophys. Res.*, 91, 11099-11115, 1986.
- Paschmann, G., S. A. Fuselier, D. M. Klumpar, High speed flows of H^+ and He^{++} ions at the magnetopause, *Geophys. Res. Lett.*, 16, 567-570, 1989.
- Potemra, T. A., L. J. Zanetti, and M. H. Acuna, The AMPTE CCE magnetic field experiment, *IEEE Trans. Geosci. Remote Sens.*, GE-23, 246-249, 1985.
- Shelley, E. G., A. Ghielmetti, E. Hertzberg, S. J. Battel, K. Altwegg-Von Burg, and H. Balsiger, The AMPTE CCE Hot-Plasma Composition Experiment (HPCE), *IEEE Trans. Geosci. Remote Sens.*, GE-23, 241-246, 1985.
- Sibeck, D. G., R. E. Lopez, and E. C. Roelof, Solar wind control of the magnetopause shape, location and motion, *J. Geophys. Res.*, 96, 5489-5495, 1991.

Sonnerup, B. U. Ö., G. Paschmann, I Papamastorakis, N. Sckopke, G. Haerendel, S. J.

Bame, J. R. Asbridge, J. T. Gosling, and C. T. Russell, Evidence for magnetic field reconnection at the Earth's magnetopause, *J. Geophys. Res.*, *86*, 10049-10-67, 1981.

Fig. 1. Location of 27 magnetopause crossings rotated into the ecliptic plane. All magnetopause crossings occurred in the local time range from 1000-1400 UT when the magnetopause was compressed by about a factor of 4 from its nominal position.

Fig. 2. (Top to bottom) Electron number flux at four energies centered on 0.151 (squares), 0.342 (triangles), 1.748 (stars), and 8.927 (pentagons) keV, B_{GSE} , H^+ and O^+ densities for one hour centered on a magnetopause crossing on 16 November, 1984 (84321). At 10% of the total density, O^+ dominated the mass density in the low latitude boundary layer. Brackets identify time intervals chosen to represent the low latitude boundary layer and magnetosheath boundary layer.

Fig. 3. Parallel and perpendicular flow velocities for magnetosheath ions computed in the rest frame of the incident cold magnetospheric ion populations in the low latitude boundary layer. All species have the same perpendicular velocity. He^{2+} and H^+ have significant parallel flow velocities in this frame but these flow velocities are almost always equal.

Fig. 4. Magnetosheath to low latitude boundary layer ratio of $\rho(1-\alpha)$ versus magnetic field rotation angle. A ratio of 1 would indicate that the magnetopause is consistent with a time-stationary rotational discontinuity.

Fig. 5. $\rho(1-\alpha)$ ratio (from Figure 3) versus the magnetosheath to low latitude boundary layer mass density ratio. The mass density and $\rho(1-\alpha)$ ratios are highly correlated, indicating that $(1-\alpha)$ does not play a significant role in Equation 1.

Table 1

Magnetosheath and "Outer Boundary Layer" mass density and pressure contributions by species for 27 magnetopause crossings observed by AMPTE/CCE

	ρ		$P_{ }$		P_{\perp}	
	average	range	average	range	average	range
H^+	88.3 \pm 4%	77-99%	87.6 \pm 5%	79-99%	85.6 \pm 5%	76-99%
He^{2+}	10.9 \pm 5%	1-23%	12.0 \pm 5%	9-21%	13.9 \pm 6%	1-24%
He^+	00.2 \pm 1%	0-3%	00.1 \pm 1%	0-0.5%	00.1 \pm 3%	0-1%
O^+	00.7 \pm 2%	0-6%	00.4 \pm 1%	0-4%	00.5 \pm 1%	0-6%
Mass> H^+	11.7 \pm 4%	1-23%	12.5 \pm 5%	1-21%	14.4 \pm 5%	1-24%
Total	100%		100%		100%	

ψ

Table 2

**Low Latitude Boundary Layer mass density and pressure
contributions by species for 27 magnetopause crossings observed by
AMPTE/CCE**

	ρ		P_{\parallel}		P_{\perp}	
	average	range	average	range	average	range
H^+	$82.4 \pm 13\%$	34-97%	$85.6 \pm 8\%$	65-99%	$83.6 \pm 8\%$	62-99%
He^{2+}	$7.9 \pm 4\%$	1-19%	$9.3 \pm 4\%$	0.5-17%	$12.4 \pm 7\%$	1-38%
He^+	$0.9 \pm 1\%$	0-5%	$0.6 \pm 1\%$	0-5%	$0.6 \pm 0.5\%$	0-1%
O^+	8.8 ± 12	0-60%	$4.5 \pm 6\%$	0-23%	$3.4 \pm 5\%$	0-22%
Mass> H^+	17.6 ± 13	3-66%	$14.4 \pm 8\%$	1-35%	$16.4 \pm 8\%$	1-38%
Total	100%		100%		100%	

251

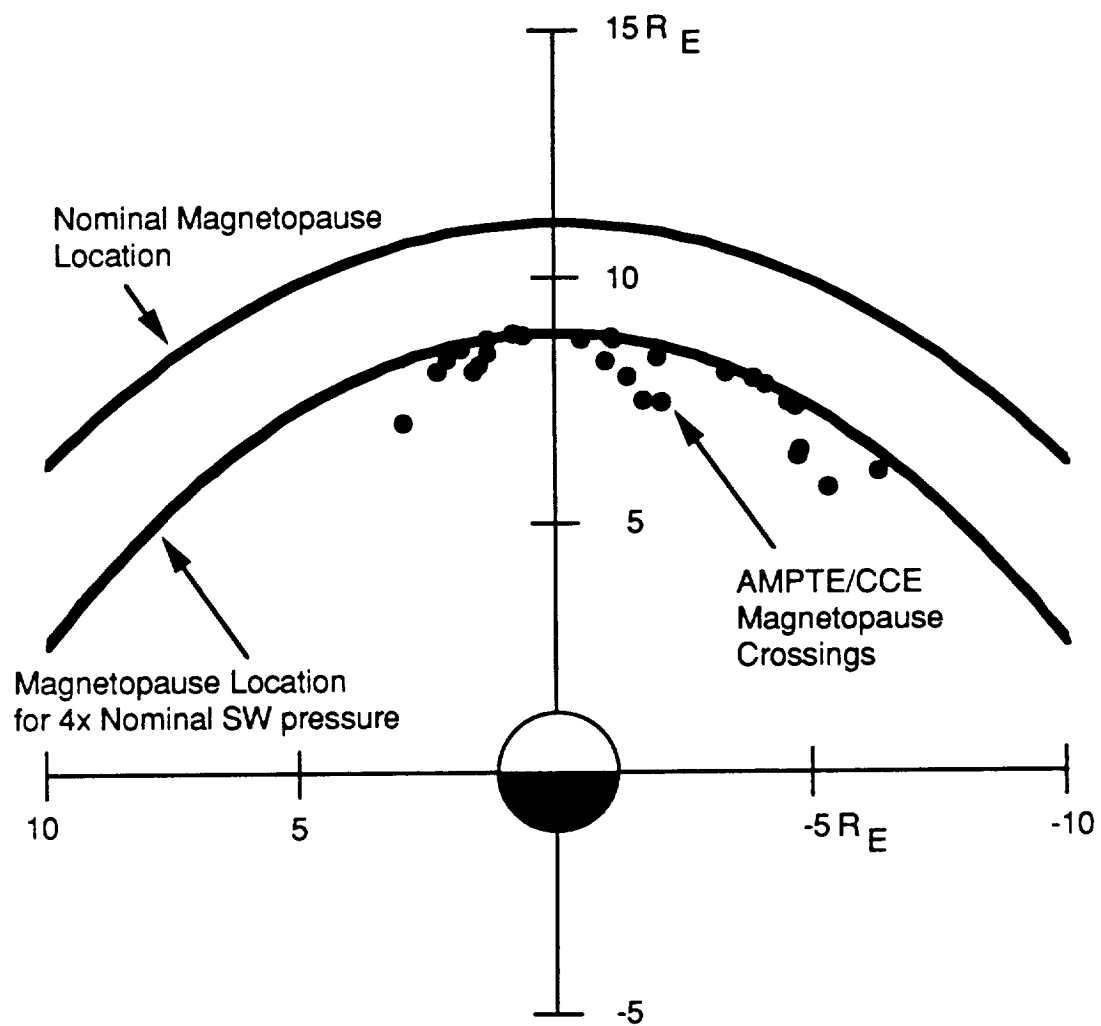


Figure 1

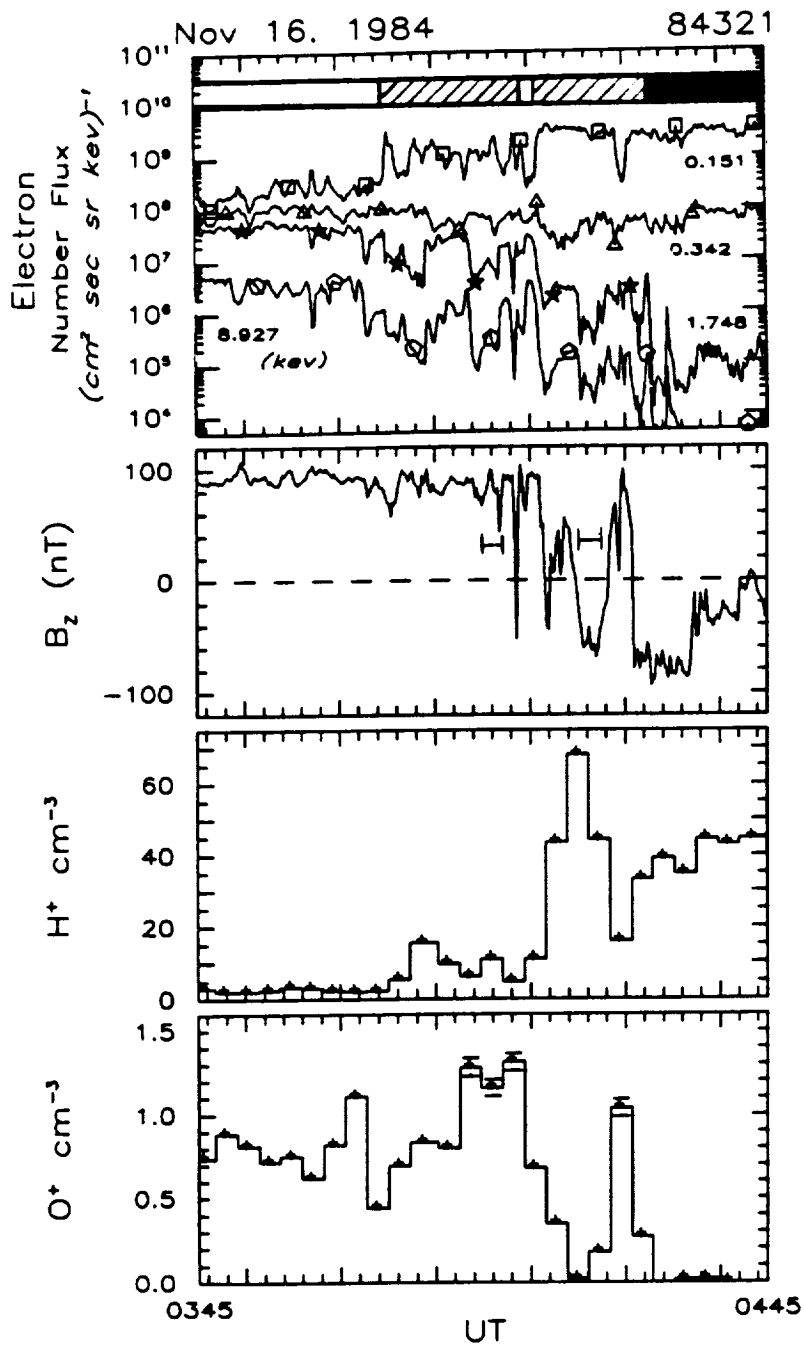


Figure 2

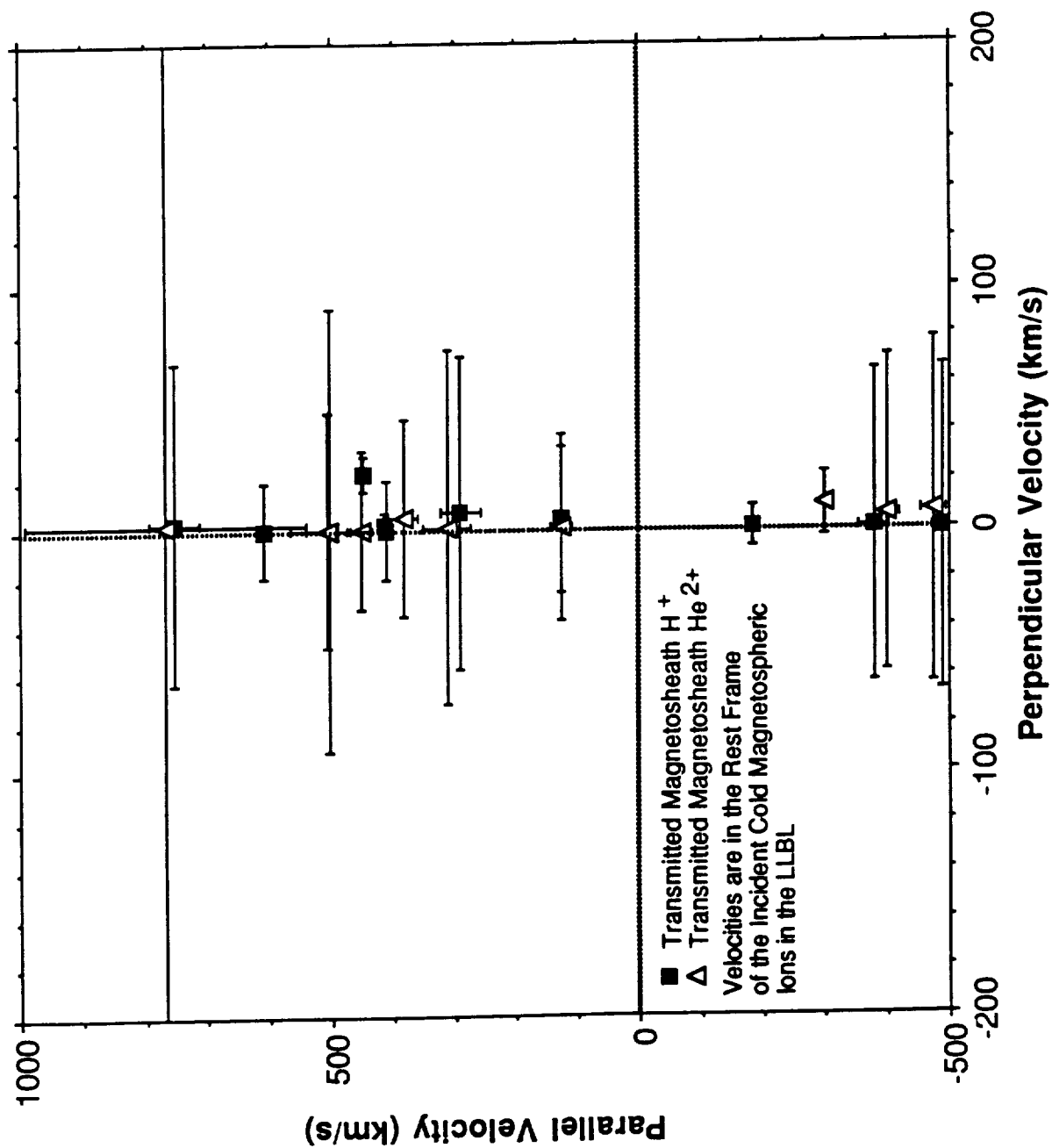


Figure 3

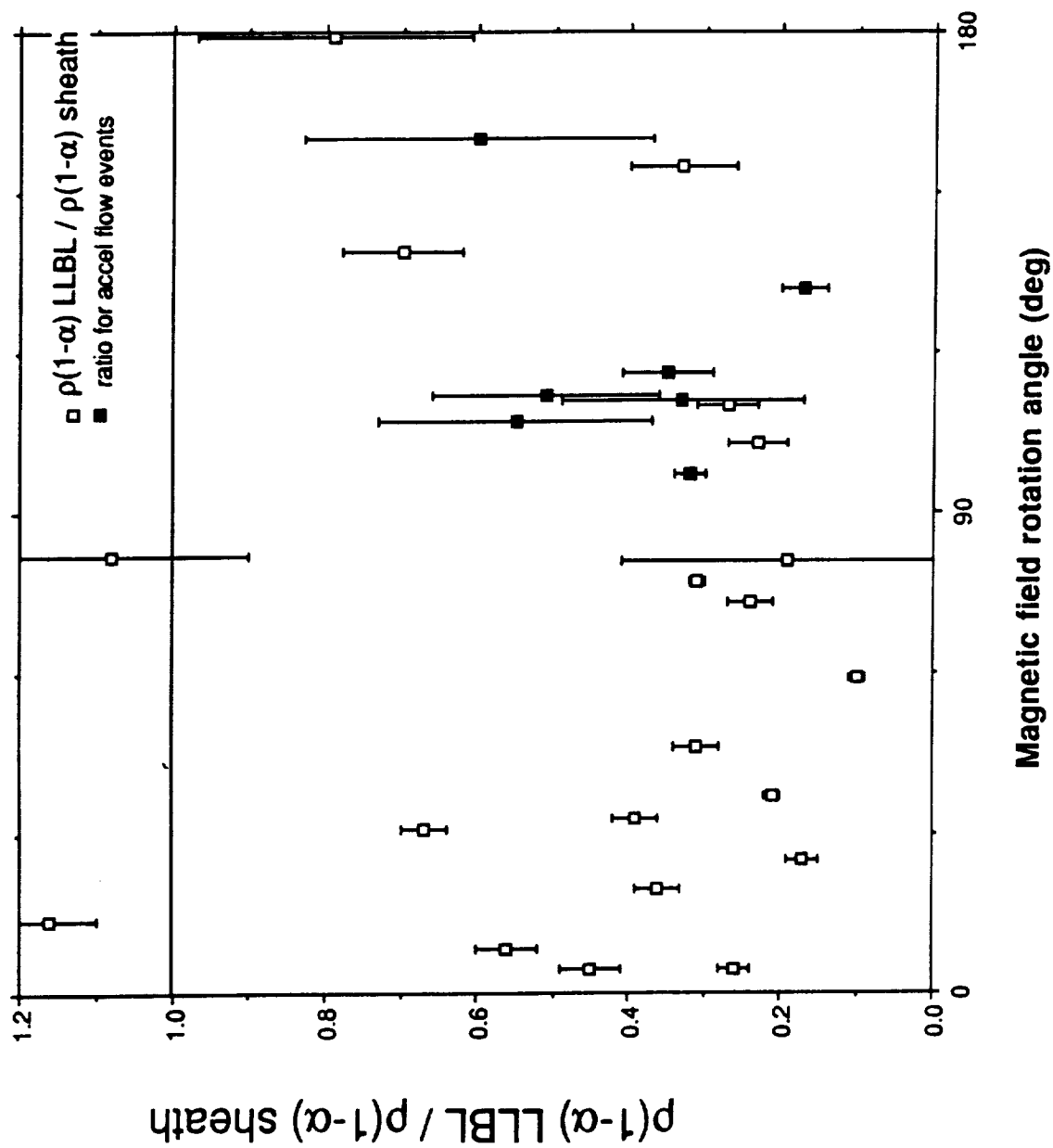


Figure 4

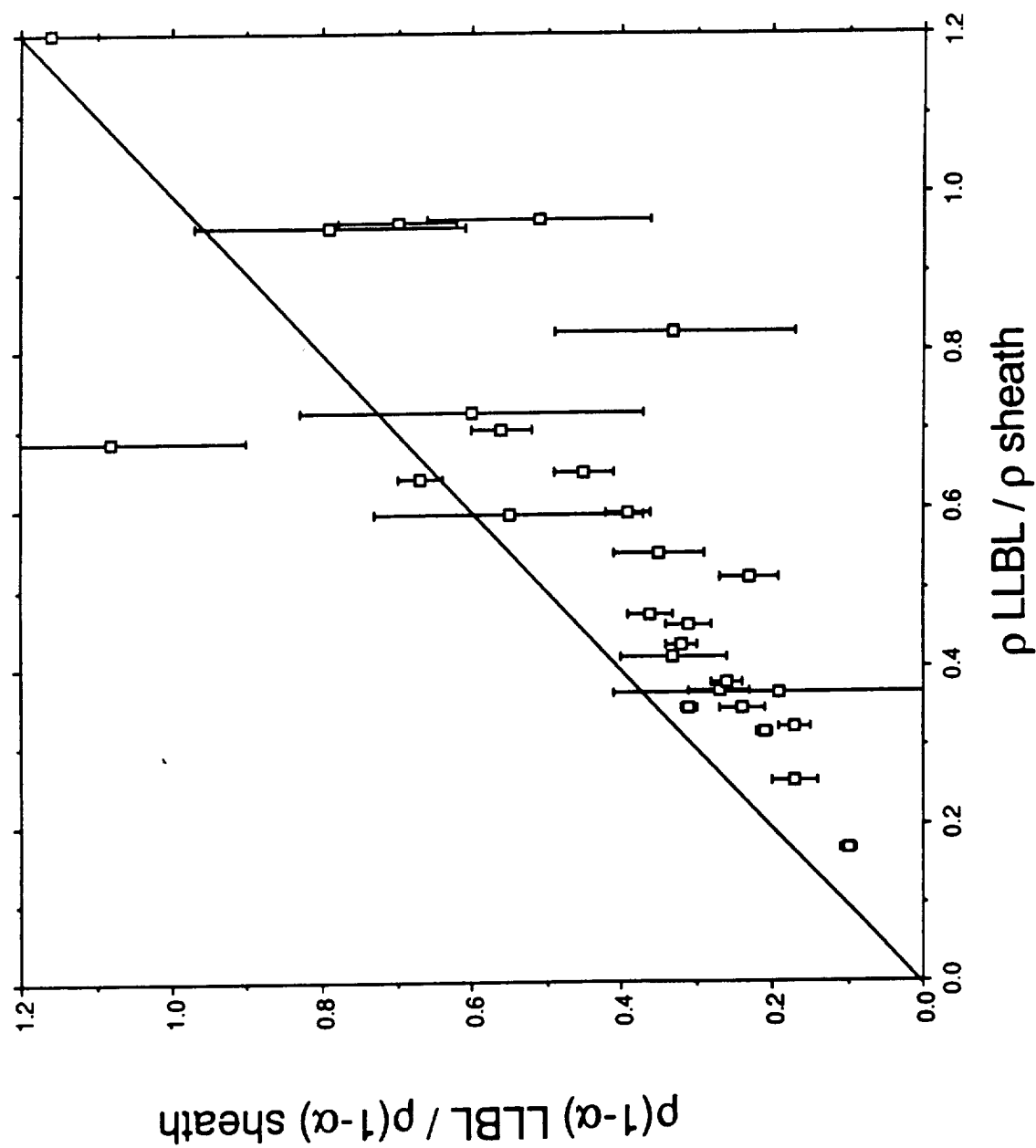


Figure 5

JGR April 29, 1992

Energetic Magnetospheric Protons in the Plasma Depletion Layer

STEPHEN A. FUSELIER

Lockheed Palo Alto Research Laboratory, Palo Alto, California

Interplanetary magnetic field draping against the Earth's dayside subsolar magnetopause creates a region of reduced plasma density and increased magnetic field called the plasma depletion layer. In this region, leakage of energetic ions from the Earth's magnetosphere onto magnetic field lines in the plasma depletion layer can be studied without interference from ions accelerated at the Earth's quasi-parallel bow shock. Active Magnetospheric Particle Tracer Experiment/Charge Composition Explorer (AMPTE/CCE) observations for 13 plasma depletion layer events are used to determine the characteristics of energetic protons between a few keV/e and ~ 100 keV/e leaked from the magnetosphere. Results indicate that the leaked proton distributions resemble those in the magnetosphere except that they have lower densities and temperatures and much higher velocities parallel (or anti-parallel) and perpendicular to the magnetic field. Compared to the low energy magnetosheath proton distributions present in the depletion layer, the leaked energetic proton distributions typically have substantially higher flow velocities along the magnetic field but similar flow velocities perpendicular to the magnetic field. The higher flow velocities along the magnetic field indicate that the leaked energetic proton distributions do contribute to the energetic proton population seen upstream and downstream from the quasi-parallel bow shock. However, their contribution is small compared to the contribution from acceleration of protons at the bow shock because the leaked proton densities are on the order of 10 times smaller than the energetic proton densities typically observed in the vicinity of the quasi-parallel bow shock.

INTRODUCTION

Soon after the discovery of energetic ions (~ 10 - >100 keV/e) adjacent to the magnetopause, in the magnetosheath, and in the region upstream from the Earth's quasi-parallel bow shock, it was recognized that these ions had two probable sources [West and Buck, 1976]. (The quasi-parallel region of the bow shock is defined as the region where the angle between the average upstream magnetic field direction (averaged over several minutes) and the shock normal, θ_{Bn} , is less than 45° .) These ions can be the result of leakage of energetic ions from the Earth's magnetosphere and/or the result of first order Fermi acceleration of solar wind ions in the turbulent regions upstream and downstream from the Earth's quasi-parallel bow shock. Quantifying the relative contributions of these two sources as a function of energy, location, etc. continues to be an important but difficult to solve problem.

One of the primary difficulties has been that although the two sources act independent of one another, in most instances they contribute to the energetic ion population in the same regions outside the magnetosphere [e.g., Luhmann et al., 1984]. This is particularly true for protons in the energy range from a few keV/e to ~ 150 keV/e. Another difficulty related to this is that while there are well developed theories for Fermi acceleration, there are no similar theories for magnetospheric leakage. For example, Monte Carlo simulations of the acceleration process at the Earth's bow shock have been used successfully to predict the energy spectrum for protons as well as other solar wind ions near the bow shock [Ellison et al., 1990]. These simulations and analytic theory [e.g., Lee, 1982] show that solar wind ions (H^+ , He^{2+} , O^{6+} , etc.) can be accelerated up to energies on the order of 150 keV/e by scattering in the turbulent region in the vicinity of the quasi-parallel bow shock. However, no similar predictions exist for the energy spectrum or composition of ions leaked from the magnetosphere.

Even if predictions existed for ion leakage from the magnetosphere, these predictions would be difficult to test because, as stated above, in most instances the energetic ion

population in the magnetosheath and upstream region is composed of ions from both the magnetospheric and bow shock sources. However, the two sources have been effectively separated in some special instances. Composition measurements have played a key role in identifying and distinguishing the two sources. Observations of tracer ions such as energetic He^{2+} (of solar wind origin) and O^+ (of magnetospheric origin) have been used previously to determine the relative contributions of the two sources for ions heavier than protons [e.g., Möbius et al., 1986; Scholer et al., 1989]. In some cases, these tracer ions have been used to infer the relative contributions from the two sources to the dominant energetic proton distribution in the energy range from a few keV/e to ~ 150 keV/e [e.g., Möbius et al., 1986; Ellison et al., 1990; Fuselier et al., 1991a].

Special orientations of the magnetic field and/or special spacecraft locations have also been used to separate the bow shock and magnetospheric sources. For example, near radial Interplanetary Magnetic Field (IMF) conditions coupled with particular locations of a spacecraft near the bow shock were used to effectively eliminate the magnetospheric source from the proton energy spectrum [Gosling et al., 1989]. Also, energetic ions from the magnetosphere were studied in magnetosheath directly adjacent to the magnetopause when magnetic reconnection was apparently taking place [Scholer et al., 1981]. However, these observations and others near the magnetopause [e.g., Sibeck et al., 1987, and references therein] suffer from the ambiguity that the proximity of a spacecraft to the magnetopause is not sufficient to rule out the presence of bow shock accelerated ions [see e.g., Luhmann et al., 1986].

In this paper, a unique IMF geometry and spacecraft location is proposed for the study of energetic ions leaked from the magnetosphere without interference from bow shock accelerated ions. Figure 1 shows the desired nominal magnetic field orientation as well as the region of interest. When the angle between the IMF and the X_{GSE} direction (ϑ_{Bz}) is greater than 45° , the quasi-parallel region of the bow shock is located on the flanks. The larger the value of ϑ_{Bz} , the further around the flanks of the bow shock the

quasi-parallel region is located. This effect was illustrated by *Luhmann et al.* [1986] although they selected streamlines with $\vartheta_{Bn} < 30^\circ$ for the quasi-parallel region of the bow shock. For $\vartheta_{Bn} = 60^\circ$ in Figure 1, the quasi-parallel bow shock region (defined here as streamlines with $\vartheta_{Bn} < 45^\circ$) and therefore the region where bow shock acceleration of solar wind ions occurs is located well away from the subsolar point. This same geometry produces significant draping of the IMF in the subsolar region as illustrated in Figure 1. The slowing of the plasma in the subsolar region combined with the draping of the IMF produces a region of depressed plasma density and increased magnetic field strength near the magnetopause called the Plasma Depletion Layer [*Zwan and Wolf*, 1976]. This layer is immediately adjacent to the magnetopause and extends about $0.5 R_E$ into the magnetosheath. Other properties of this layer include large temperature anisotropies of magnetosheath ion distributions [*Crooker et al.*, 1979; *Anderson et al.*, 1991; *Fuselier et al.*, 1991b]. These large temperature anisotropies provide a free energy source for electromagnetic ion cyclotron waves observed in this region [*Anderson et al.*, 1991].

The draping of the magnetic field against the magnetopause also satisfies the single condition for magnetospheric ion leakage [*Sibeck et al.*, 1987 and references therein] i.e., that a magnetic field line pass sufficiently close to the magnetopause for the magnetospheric ions to scatter onto it. Indeed, energetic protons of magnetospheric origin were recently reported in the plasma depletion layer [*Anderson et al.*, 1991; *Fuselier et al.*, 1991b]. Thus, as illustrated in Figure 1, the plasma depletion layer is an excellent region to study magnetospheric ion leakage into the magnetosheath without interference from the bow shock acceleration source. The elimination of the bow shock source is particularly important because it allows the study of the leaked energetic protons in the energy range from a few keV/e to ~ 150 keV/e, which in the past was not necessarily studied without interference. The presence of the depletion layer is critical to this study because it implies large values of ϑ_{Bn} effectively removing of the bow shock acceleration region from the subsolar region of the magnetosheath and

also implies that the spacecraft is not far ($\sim 0.5 R_E$ according to *Zwan and Wolf* [1976]) from the magnetopause. In this respect, this study differs from previous studies of energetic ions adjacent to the magnetopause [e.g., *Sibeck et al.*, 1987; and references therein] because previous studies were not confined to the depletion layer and therefore could not claim to effectively eliminate the bow shock acceleration source.

Plasma depletion layer intervals were selected from the AMPTE/CCE data set primarily for the period from September to December 1984. Observations in this paper were from two of the ion mass spectrometers on the CCE spacecraft. The Hot Plasma Composition Experiment (HPCE) [*Shelley et al.*, 1985] covered the energy range from the spacecraft potential (\sim few eV) to 17.1 keV/e. The Charge-Energy-Mass Spectrometer (CHEM) [*Gloeckler et al.*, 1985] covered the energy range from about 1.5 to 300 keV/e. Both of these ion mass spectrometers have been discussed in detail previously [e.g., *Fuselier et al.*, 1991a,b; *Gloeckler and Hamilton*, 1987]. In addition to the ion observations, magnetic field measurements from the CCE magnetometer [*Potemra et al.*, 1985] as well as electron measurements from the electron spectrometer part of the HPCE were used to confirm the location of the spacecraft either in the magnetosphere or the plasma depletion layer [see for example, *Anderson et al.*, 1991; *Fuselier et al.*, 1991b].

OBSERVATIONS

Using the HPCE and magnetic field data, the plasma depletion layer was identified by a plasma density decrease, magnetic field increase, and an increase in the solar wind proton and He^{2+} temperature anisotropies when compared to the adjacent magnetosheath. As an additional check, electromagnetic ion cyclotron (EMIC) waves in dynamic spectra from the CCE magnetometer [see, *Anderson et al.*, 1991] were identified in the candidate plasma depletion layer intervals. Thirteen such intervals were identified and are listed in Table 1. In most cases, there were no spacecraft upstream from the Earth's

bow shock to directly confirm the presence of a plasma depletion layer. However, during four of the events in this study (see Table 1), the AMPTE/Ion Release Module (IRM) spacecraft was monitoring the magnetic field and plasma changes in the solar wind directly upstream from the subsolar region of the Earth's bow shock. Two of these four events have been discussed in detail previously [Anderson et al., 1991; Fuselier et al., 1991b]. The other two events with upstream monitors and all events that did not have this benefit show characteristics in the magnetic field and plasma similar to the two plasma depletion layer intervals discussed previously. The similar aspects of the observations provides confidence that all intervals considered here were indeed in the plasma depletion layer. For the four events when upstream magnetic field data was available, these data show θ_{Bz} ranged from 60 to 90° consistent with the schematic illustration in Figure 1.

In order to determine the characteristics of magnetospheric energetic ions, the energetic ions spectrum in the plasma depletion layer must be compared to the energetic ions found in the magnetosphere as well as the thermal ions in the plasma depletion layer. In principal, this comparison should be done for all major ion species found in the magnetosphere. However, this paper is limited to the study of the proton component because it is typically the most abundant ion in the outer magnetosphere and because it cannot be readily studied in other regions outside the plasma depletion layer without interference from the bow shock accelerated protons. Furthermore, the study is limited to the energy range from a few keV/e to ~100 keV/e because of counting statistics limitations discussed below. However, this energy range is exactly the range of greatest overlap of the leaked protons from the magnetosphere and the protons accelerated at the bow shock when both sources contribute to the energetic proton spectrum.

To facilitate the comparison between the magnetosphere and plasma depletion layer, proton distribution functions with 45° angular resolution in the spacecraft spin plane were produced for both the HPCE and CHEM data for selected intervals inside the plasma

depletion layer and inside the magnetosphere (using the nearest available magnetopause crossing) for the 13 events. In order to further improve counting statistics at energies above 20 keV/e, the 32 energy channel CHEM data were averaged over 3 energy channels and typical time averages were on the order of 5 min. Even with 3 channel averages and relatively long time averages, energetic proton fluxes in the plasma depletion layer were low and comparison with magnetospheric spectra was limited to energies below 100 keV/e.

The magnetic field direction for these events was always nearly in the plane of the 2-dimensional plasma measurements (i.e., the spacecraft spin plane) for both the plasma depletion layer and magnetosphere intervals selected. Therefore, cuts parallel and perpendicular to the magnetic field for the energetic proton distribution functions in the plasma depletion layer and magnetosphere were fit using drifting two-temperature maxwellians. In all cases, the maxwellian distributions fit the data reasonably well for energies up to ~ 100 keV/e. Densities, velocities, and temperatures of distributions in the plasma depletion layer and magnetosphere were determined from these fits.

Figure 2 shows an example of the parallel (top panel) and perpendicular (bottom panel) cuts in the depletion layer and magnetospheric proton distributions for one of the events. Positive velocities in the top panel of this and the next figure show velocities parallel to the local magnetic field. Solid squares show the HPCE data, extending to 17.1 keV/e and open squares show the CHEM data extending in this case from 2 keV/e to ~ 80 keV/e. The two instruments have an overlapping energy range from about 2 to 17 keV/e or from about 850 to 1800 km/s in Figure 2. In this range of overlap, phase space density measurements from the two instruments show quite good agreement. In both panels, the magnetospheric distribution was shifted in velocity and reduced in phase space density to demonstrate the similarities between it and the energetic portion (above 1500 km/s) of the plasma depletion layer distributions. The very low velocity magnetospheric distribution below about 300 km/s in Figure 2 would be effectively dominated in the plasma

depletion layer by the magnetosheath protons. For this particular event, the drift velocities (V_{drift} in Figure 2) perpendicular and parallel to the magnetic field for the energetic proton distribution in the plasma depletion layer are below about 100 km/s. These drift velocities are slightly higher than those of the lower energy distribution in the plasma depletion layer and also higher than those for the magnetospheric distribution.

Parallel and perpendicular cuts in the distributions from a second event are shown in Figure 3. Wave observations for this event were discussed in detail by Anderson et al., [1991]. For this event, the anti-parallel velocity of the energetic ion distribution was over 200 km/s. This is significantly higher than the anti-parallel bulk flow velocity of the low energy magnetosheath protons and is also significantly higher than the bulk flow velocity of the distribution in the magnetosphere. Despite these higher flow velocities, the energetic proton distribution in the plasma depletion layer in Figure 3 resembles that in the magnetosphere except that its density is significantly less and its temperature is somewhat less.

RESULTS

For the events in Figures 2 and 3, the energetic ion density in the plasma depletion layer was less than that in the magnetosphere. Figure 4 shows that this is true for all events in this study. This figure shows the magnetospheric proton density above several keV/e (i.e., excluding the very low velocity component seen in Figures 2 and 3 below ~300 km/s) versus the density of the energetic proton component in the plasma depletion layer (i.e., excluding the contribution from magnetosheath proton distribution at velocities below 1500 km/s in Figures 2 and 3). Equal densities would lie along the horizontal line. Energetic proton densities in the plasma depletion layer averaged about a factor of ten below energetic proton densities in the magnetosphere.

Because there is typically a velocity difference between the energetic proton distributions in the magnetosphere and the plasma depletion layer, the density decrease may be the result of proton loss in the magnetopause region and/or simply conservation of flux across the magnetopause. Figure 5 compares the total energetic proton flux (density times bulk velocity) in the magnetosphere with that in the plasma depletion layer.

In order to reduce the statistical uncertainty in the proton velocity in the magnetosphere, the low and high energy components (see Figures 2 and 3) were assumed to be flowing at the same velocity. (Note that this assumption was not made for the low and high energy distributions in the plasma depletion layer.) Several events in Figure 5 are consistent with approximate total flux conservation across the magnetopause. Among the other events, some have what appears to be an excess total flux in the plasma depletion layer while others appear to have the opposite.

For the two events in Figures 2 and 3, the energetic proton distributions in the magnetosphere and plasma depletion layer had similar temperatures. This is also true for the other 11 events. Figure 6 compares the energetic proton temperatures in the magnetosphere with those in the plasma depletion layer. The perpendicular and parallel temperatures in the plasma depletion layer are similar to but typically about a factor of 2 lower than the magnetospheric temperatures. Not shown here are the temperature anisotropies. These also tended to be similar in the plasma depletion layer and magnetosheath with the anisotropies in the plasma depletion layer typically on the order of 1 to 1.5 and somewhat lower than the temperature anisotropies in the magnetosphere.

The energetic proton distributions in the plasma depletion layer for one of the events (Figure 3) discussed in the observations section had very large anti-parallel flow. This flow was significantly higher than the proton bulk velocity for the lower energy magnetosheath protons in the plasma depletion layer. Several other events had high flow velocities parallel or anti-parallel to the magnetic field when compared to the flow velocities of the low energy (thermal) protons in the plasma depletion layer. Figure

7 compares the parallel flow velocities of the thermal (0-6 keV/e) and energetic protons in the plasma depletion layer. Bulk flow velocities for the thermal population are typically less than 50 km/s. This is consistent with the fact that these observations were made near the subsolar region, where magnetosheath flow velocities are usually small. Flow velocities for the energetic ions are quite large, often over 200 km/s either parallel or anti-parallel to the magnetic field with no apparent direction preference. Figure 8 is a similar comparison of the perpendicular flow velocities. Although there are some events that have significantly different perpendicular flow velocities and there is no apparent direction preference, the perpendicular flow velocities of the two components in the plasma depletion layer are typically the same.

Finally, Figure 9 compares the thermal and energetic proton densities in the plasma depletion layer. With the exception of one event, typical energetic proton densities are on the order of 0.1% of the total density in the plasma depletion layer. This is significant because densities for energetic protons in the upstream region and in the magnetosheath downstream from the quasi-parallel bow shock are typically on the order of 1% of the total proton density [Thomsen, 1985] or about a factor of 10 higher than the energetic proton densities observed in the plasma depletion layer.

DISCUSSION

In this paper, it was argued that large angles between the IMF and the X_{GSE} direction ($\vartheta_{Bz} > 60^\circ$) effectively remove the bow shock acceleration region from the subsolar region of the Earth's magnetopause. These large ϑ_{Bz} angles also result in significant magnetic field draping against the subsolar magnetopause and the formation of a plasma depletion layer. Draping of the magnetic field line against the magnetopause satisfies the single condition for leakage of ions from the magnetosphere. Using observations from the AMPTE/CCE spacecraft in the plasma depletion layer, the characteristics of the leaked magnetospheric protons were discussed (see Figures 4 through 9).

In general, the energetic proton distributions observed in the plasma depletion layer are similar to those found in the magnetosphere except: 1) they have lower densities (Figure 4), 2) they have higher parallel (or anti-parallel) and perpendicular velocities, and 3) they have somewhat lower parallel and perpendicular temperatures (Figure 6). In several events, the velocity increase and density decrease across the magnetopause are simply consistent with total flux conservation (see Figure 5).

In several respects, it is surprising that total flux is conserved across the magnetopause for any of the events. Magnetospheric leakage is thought to occur through essentially a diffusive process [e.g., Sibeck et al., 1987]. Under these conditions, only the flux normal to the magnetopause surface is conserved. This flux is essentially unrelated to the total flux in Figure 5 since the AMPTE/CCE plasma instruments measure only in a plane essentially tangent to the magnetopause. For total flux to be conserved, measurements must be made along an interconnected streamline such as those found near the magnetopause when the magnetopause is open. Table 1 shows that the events are almost evenly distributed between southward and northward magnetosheath magnetic fields. Although not shown, there is no correlation between events with apparent total flux conservation (Figure 5) and events with southward magnetosheath fields (Table 1) as might be expected if total flux conservation is indicative of an open magnetopause where magnetic reconnection is taking place. Thus, it is concluded that although total flux may be conserved for several events, this conservation does not necessarily indicate how the protons escaped the magnetosphere.

In addition to a comparison between the energetic proton distributions in the plasma depletion layer and magnetosphere, the velocities and densities of the high and low energy distributions in the plasma depletion layer were compared in Figures 7 through 9. Velocities along the magnetic field of the energetic proton distributions in the plasma depletion layer were usually significantly higher than those of the thermal distributions in that region (Figure 7). In general, perpendicular velocities were the same for

the low and high energy distributions (Figure 8). These comparisons indicate that the magnetospheric proton distributions that have crossed the magnetopause and entered the plasma depletion layer have significant velocities parallel (or anti-parallel) to the magnetic field relative to the magnetosheath protons but pick up the $\mathbf{E} \times \mathbf{B}$ convection of the plasma. Thus, as the magnetic field line convects away from the magnetopause, the leaked magnetospheric plasma and the magnetosheath plasma convect with it but the magnetospheric plasma flows along the field at a velocity that is considerably different from that of the bulk of the plasma. No preference for dawnward or duskward flow is observed. This is probably because the flow direction is determined by properties of the plasma depletion layer and not indicative of preferred leakage directions.

As pointed out in the introduction, determination of the contribution to the total energetic proton distribution by energetic protons from the magnetosphere in the energy range from a few keV/e to 100 keV/e has been hampered by the presence of bow shock accelerated protons. By removing the bow shock source, the relative contribution of the leaked magnetospheric ions to the total energetic proton population in the region upstream and downstream from the quasi-parallel bow shock can be estimated. It is important to realize that magnetospheric ion distributions in the plasma depletion layer do contribute to the energetic ion population near the quasi-parallel bow shock. As illustrated in Figure 1, the magnetic field line threading the plasma depletion layer is ultimately connected on one end to the energetic ion region upstream from the quasi-parallel bow shock. Leaked magnetospheric proton distributions on these field lines have large (up to 300 km/s, see Figure 7) flow velocities along the magnetic field and therefore will exit the magnetosheath both well downstream on the dusk side and in the quasi-parallel bow shock region on the dawn side for the magnetic field configuration illustrated in Figure 1.

Figure 9 shows the contribution the leaked magnetospheric protons in the few keV/e to 100 keV/e energy range make to the plasma depletion layer when compared to the total proton density in that layer. Expressed as a percentage of the total thermal plasma density, leaked protons in this study account for only about 0.1% of the total density. This percentage will either not change much or will decrease as the leaked protons leave the plasma depletion layer and expand into the magnetosheath and upstream region. Typically, the energetic proton densities in the range from a few keV/e to ~100 keV/e are on the order of 1% of the total solar wind density in the region upstream from the Earth's quasi-parallel bow shock [e.g., *Thomsen, 1985*]. This is about 10 times higher than the densities for the leaked magnetospheric protons in the plasma depletion layer. Thus, it is concluded that, on average, magnetospheric leakage provides only about 10% of the energetic proton distribution in the energy range from a few keV/e to 100 keV/e in the region upstream from the Earth's bow shock when the IMF has orientations similar to that illustrated in Figure 1. The other 90% comes from the bow shock accelerated source.

Acknowledgments. Research at Lockheed was funded through the NASA Guest Investigator program under contract NAS5-31213. Hot Plasma Composition Experiment data was provided by E. G. Shelley, Charge-Energy-Mass Spectrometer data was provided by G. Gloeckler, and Magnetometer data was provided by T. A. Potemra. The author also acknowledges several useful discussions with B. J. Anderson.

REFERENCES

- Anderson, B. J., S. A. Fuselier, and D. Murr, Electromagnetic ion cyclotron waves observed in the plasma depletion layer, *Geophys. Res. Lett.*, **18**, 1955-1958, 1991.
- Crooker, N. U., T. E. Eastman, and G. S. Stiles, Observations of plasma depletion in the magnetosheath at the dayside magnetopause, *J. Geophys. Res.*, **84**, 869-874, 1979.

- Ellison, D. C., E. Möbius, and Götz Paschmann, Particle injection and acceleration at the Earth's bow shock: Comparison of upstream and downstream events, *Ap. J.*, 352, 376, 1990.
- Fuselier, S. A., D. M. Klumpar, and E. G. Shelley, On the origins of energetic ions in the Earth's dayside magnetosheath, *J. Geophys. Res.*, 96, 47-56, 1991a.
- Fuselier, S. A., D. M. Klumpar, E. G. Shelley, B. J. Anderson, and A. J. Coates, He^{2+} and H^+ dynamics in the subsolar magnetosheath and plasma depletion layer, *J. Geophys. Res.*, 96, 21095-21104, 1991b.
- Gloeckler, G., F. M. Ipavich, W. Studemann, B. Wilken, D. C. Hamilton, G. Kremser, D. Hovestadt, F. Gliem, R. A. Lundgren, W. Reick, E. O. Tums, J. C. Cain, L. S. Masung, W. Weiss, and P. Winterhof, The Charge-Energy-Mass Spectrometer for 0.3-300 keV/e ions on the AMPTE CCE, *IEEE Trans. Geosci. Remote Sens.*, GE-23, 234-240, 1985.
- Gloeckler, G., and D. C. Hamilton, AMPTE ion composition results, *Physica Scripta*, T18, 73-84, 1987.
- Gosling, J. T., M. F. Thomsen, S. J. Bame, and C. T. Russell, On the source of diffuse, suprathermal ions observed in the vicinity of the Earth's bow shock, *J. Geophys. Res.*, 94, 3555-3563, 1989.
- Lee, M. A., Coupled hydromagnetic wave excitation and ion acceleration upstream of the Earth's bow shock, *J. Geophys. Res.*, 87, 5063-5080, 1982.
- Luhmann, J. G., R. J. Walker, C. T. Russell, J. R. Spreiter, S. S. Stahara, and D. H. Williams, Mapping the magnetosheath field between the magnetopause and the bow shock: Implications for magnetospheric particle leakage, *J. Geophys. Res.*, 89, 6829-6834, 1984.
- Luhmann, J. G., C. T. Russell, and R. C. Elphic, Spatial distributions of magnetic field fluctuations in the dayside magnetosheath, *J. Geophys. Res.*, 91, 1711-1715, 1986.

- Möbius, E., D. Hovestadt, B. Klecker, M. Scholer, F. M. Ipavich, C. W. Carlson, and R. P. Lin, A burst of energetic O^+ ions during an upstream particle event, *Geophys. Res. Lett.*, 13, 1372-1375, 1986.
- Potemra, T. A., L. J. Zanetti, and M. H. Acuna, The AMPTE CCE magnetic field experiment, *IEEE Trans. Geosci. Remote Sens.*, GE-23, 246-249, 1985.
- Scholer, M., F. M. Ipavich, G. Gloeckler, D. Hovestadt, and B. Klecker, Leakage of magnetospheric ions into the magnetosheath along reconnected field lines at the dayside magnetopause, *J. Geophys. Res.*, 86, 1299-1304, 1981.
- Scholer, M., E. Möbius, L. M. Kistler, B. Klecker, and F. M. Ipavich, Multispacecraft observations of energetic ions upstream and downstream of the bow shock, *Geophys. Res. Lett.*, 16, 571-574, 1989.
- Shelley, E. G., A. Ghielmetti, E. Hertzberg, S. J. Battel, K. Altwegg-Von Burg, and H. Balsiger, The AMPTE CCE Hot-Plasma Composition Experiment (HPCE), *IEEE Trans. Geosci. Remote Sens.*, GE-23, 241-246, 1985.
- Sibeck, D. G., R. W. McEntire, A. T. Y. Lui, R. E. Lopez, S. M. Krimigis, R. B. Decker, L. J. Zanetti, and T. A. Potemra, Energetic magnetospheric ions at the dayside magnetopause: Leakage or merging?, *J. Geophys. Res.*, 92, 12,097-12,114, 1987.
- Thomsen, M. F., Upstream suprathermal ions, in *Collisionless Shocks in the Heliosphere: Reviews of Current Research*, *Geophys. Monogr. Ser.*, vol. 35, pp. 253-270, edited by B. T. Tsurutani and R. G. Stone, AGU, Washington, D. C., 1985.
- West, H. I., and R. M. Buck, Observations of >100 keV protons in the Earth's magnetosheath, *J. Geophys. Res.*, 81, 569-584, 1976.
- Zwan, B. J., and R. A. Wolf, Depletion of solar wind plasma near a planetary boundary, *J. Geophys. Res.*, 81, 1636-1648, 1976.

JGR April 29, 1992

Table 1. Plasma Depletion Layer Intervals

Year/Day	Time	Bz	Upstream
	hhmm-hhmm	(+/-)	Confirmation
84263	0830-0837	+	No
84279	1450-1500	+	Yes
84280	0414-0421	+	No
84280	0626-0635	+	No
84280	1900-1904	+	No
84281	1224-1231	-	Yes
84292	1320-1326	-	Yes
84319	0942-0947	+	Yes
84320	0020-0027	+	No
84320	1758-1807	-	No
84335	0310-0320	-	No
84348	0401-0405	+	No
85333	1245-1255	+	No

S. A. Fuselier, Dept. 91-20 Bldg 255, Lockheed Palo Alto Research Laboratory, 3251
Hanover Street, Palo Alto, CA 94304.

(Received March 5, 1992;
revised August 13, 1992;
accepted August 13, 1992.)

Copyright 1992 by the American Geophysical Union.

Paper number 92JA02145.

0148-0227/91/91JA-02145\$05.00

FUSELIER: ENERGETIC PROTONS IN THE PLASMA DEPLETION LAYER

FUSELIER: ENERGETIC PROTONS IN THE PLASMA DEPLETION LAYER

FUSELIER: ENERGETIC PROTONS IN THE PLASMA DEPLETION LAYER

FUSELIER: ENERGETIC PROTONS IN THE PLASMA DEPLETION LAYER

FUSELIER: ENERGETIC PROTONS IN THE PLASMA DEPLETION LAYER

FUSELIER: ENERGETIC PROTONS IN THE PLASMA DEPLETION LAYER

FUSELIER: ENERGETIC PROTONS IN THE PLASMA DEPLETION LAYER

FUSELIER: ENERGETIC PROTONS IN THE PLASMA DEPLETION LAYER

FUSELIER: ENERGETIC PROTONS IN THE PLASMA DEPLETION LAYER

FUSELIER: ENERGETIC PROTONS IN THE PLASMA DEPLETION LAYER

FUSELIER: ENERGETIC PROTONS IN THE PLASMA DEPLETION LAYER

Fig. 1. Schematic of the magnetic field draping when the IMF angle $\theta_{Bz}=60^\circ$. Under this condition, the energetic ion region upstream and downstream from the quasi-parallel bow shock is located on the flanks of the dawnside bow shock. Also, draping of the magnetic field against the magnetopause results in the formation of a plasma depletion layer in the subsolar region. Magnetospheric energetic ions scatter across the magnetopause onto magnetic field lines into the plasma depletion layer.

Fig. 2. Parallel (top panel) and perpendicular (bottom panel) cuts in the proton distribution in the plasma depletion layer (solid lines) for one of the events in the study. Solid and open squares are measurements from the HPCE and CHEM instruments, respectively. Dashed lines show the magnetospheric proton distribution which has been shifted in velocity and reduced in phase space density to illustrate the similarity between it and the energetic proton distribution in the plasma depletion layer. The thin solid line shows the maxwellian fit to the energetic ion distribution in the plasma depletion layer.

Fig. 3. Same format as in Figure 2, except for another event in the study. In this event, the energetic ion distribution in the plasma depletion layer is flowing at a significant velocity (V_{drift}) parallel to the magnetic field.

Fig. 4. Comparison between the energetic proton densities in the plasma depletion layer and the magnetosphere. Magnetospheric energetic proton densities average about 10 times higher than those in the plasma depletion layer.

Fig. 5. Comparison between the energetic proton total fluxes in the plasma depletion layer and the magnetosphere. Total fluxes in the plasma depletion layer are consistent with total flux conservation across the magnetopause for several events.

Fig. 6. Comparison between the parallel (closed squares) and perpendicular (solid squares) temperatures of the energetic proton distributions in the plasma depletion layer and the magnetosphere. Temperatures in the two regions are similar except that temperatures in the plasma depletion layer tend to be lower than those in the magnetosphere.

Fig. 7. Comparison between the parallel velocities of the energetic and thermal proton distributions in the plasma depletion layer. Parallel velocities of the thermal proton distributions in the plasma depletion layer are small while velocities of the energetic proton distributions in that region can be quite large.

Fig. 8. Comparison between the perpendicular velocities of the energetic and thermal proton distributions in the plasma depletion layer. Unlike the parallel velocities of these two distributions, the perpendicular velocities tend to be the same.

Fig. 9. Comparison between the thermal and energetic proton densities in the plasma depletion layer. Energetic proton densities average about 0.1% of the thermal densities in the plasma depletion layer. This is about a factor of 10 below typical densities of energetic protons found upstream from the Earth's bow shock.

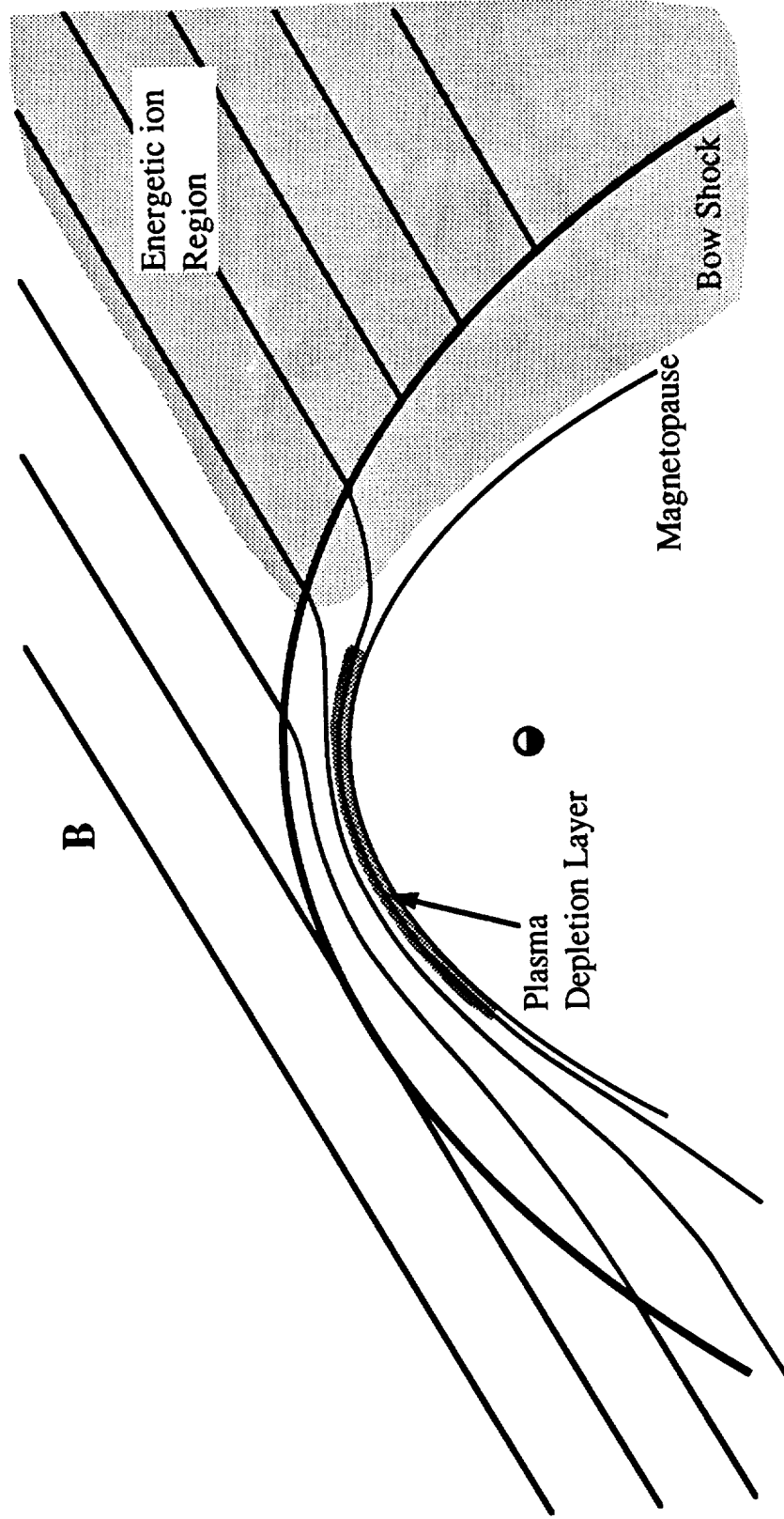


Figure 1

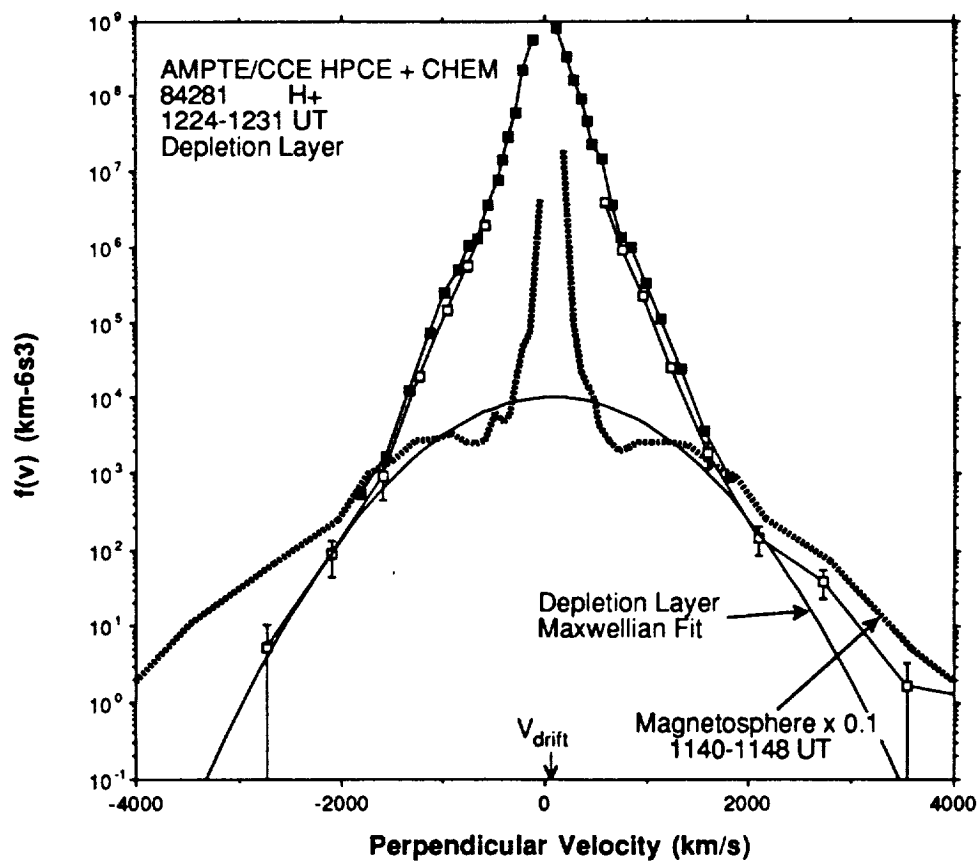
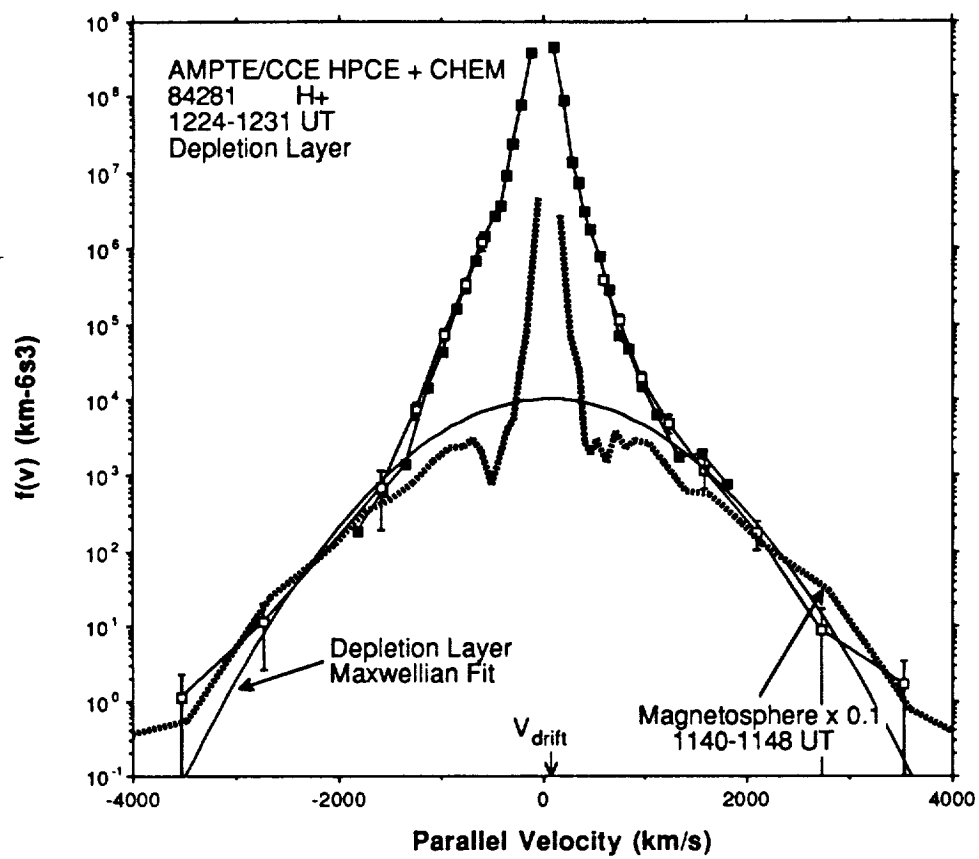


Figure 2

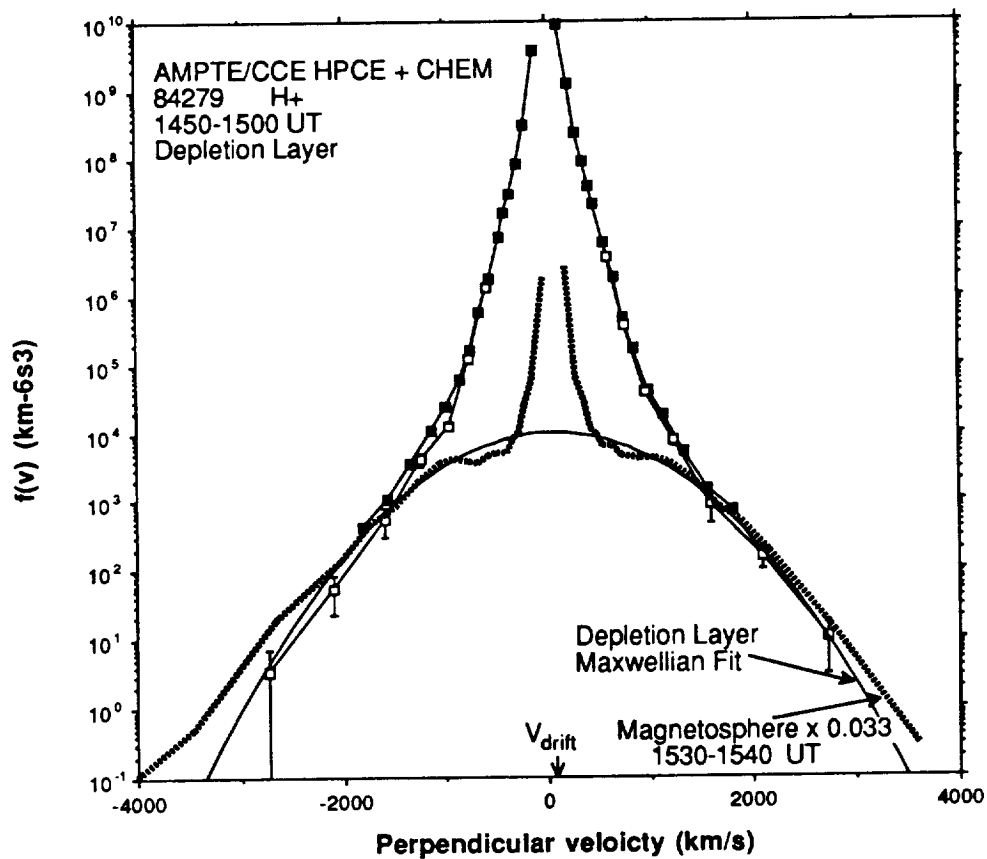
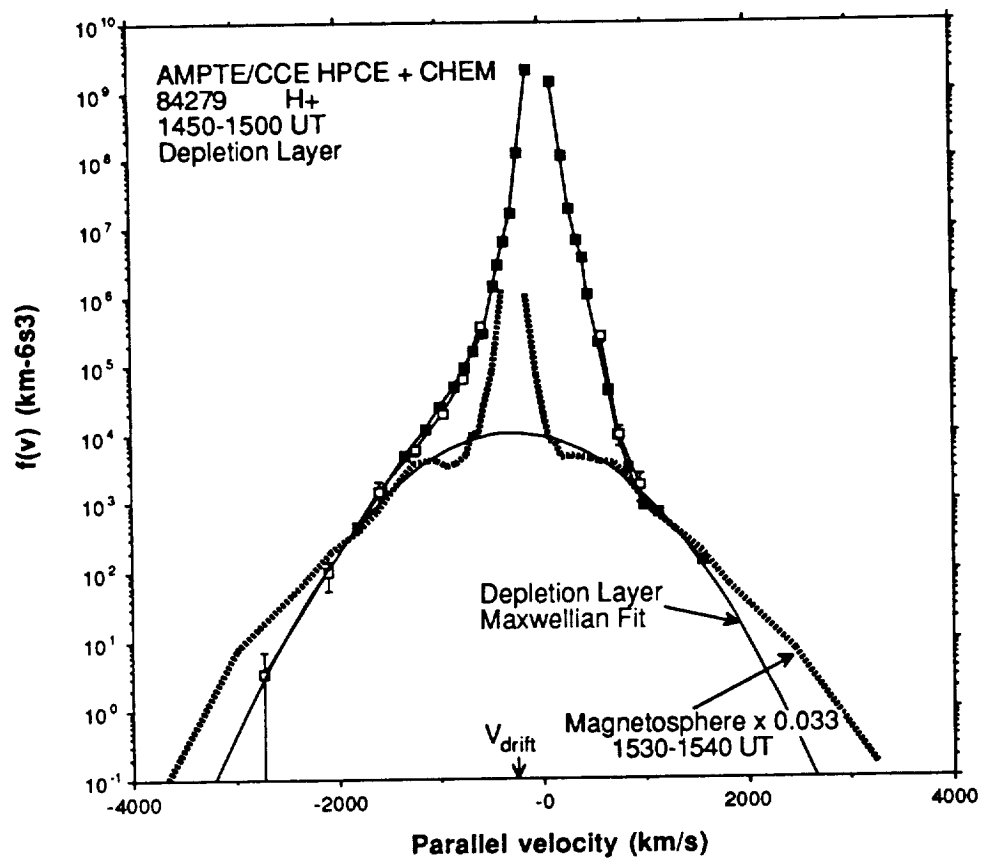


Figure 3

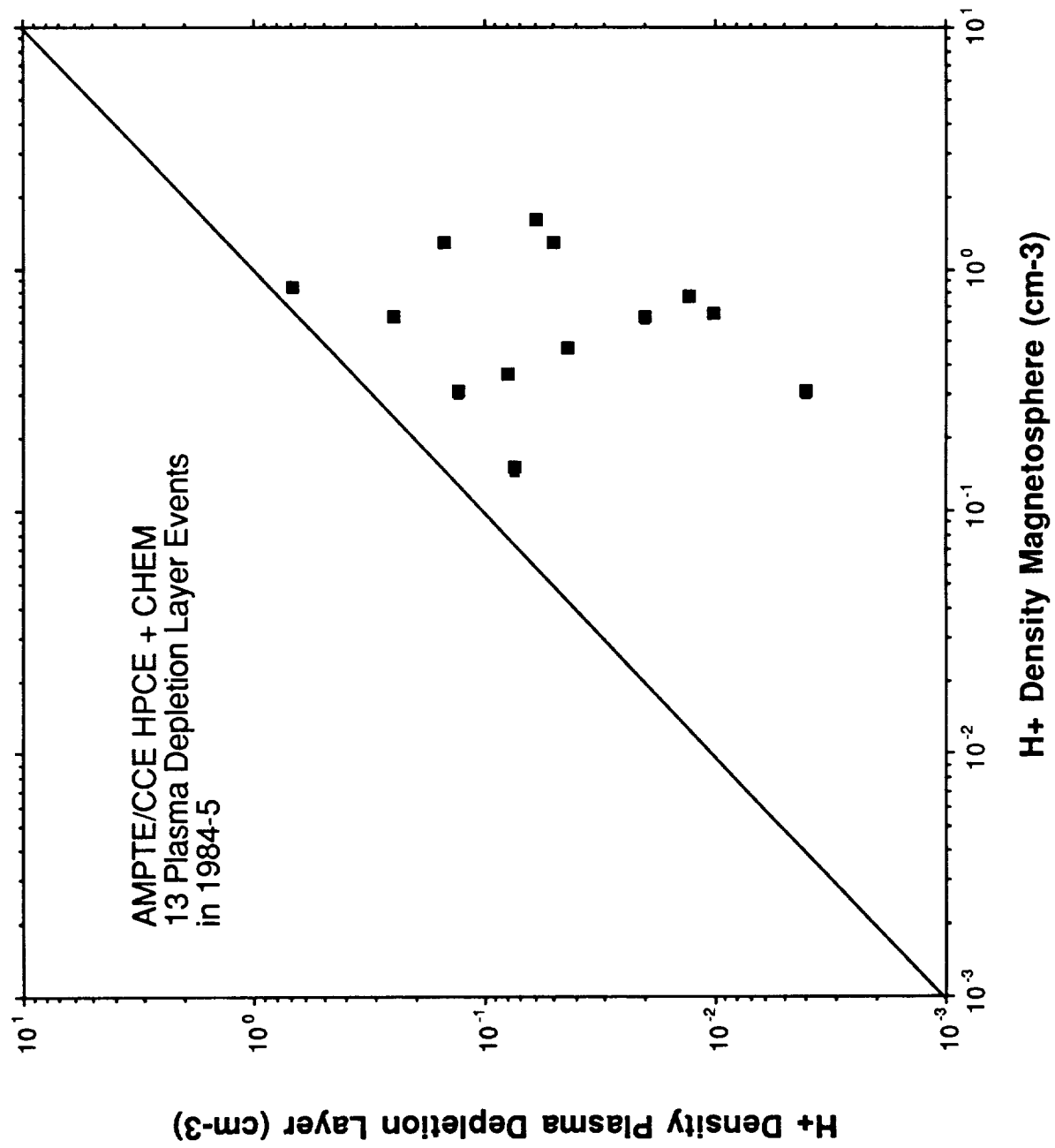


Figure 4

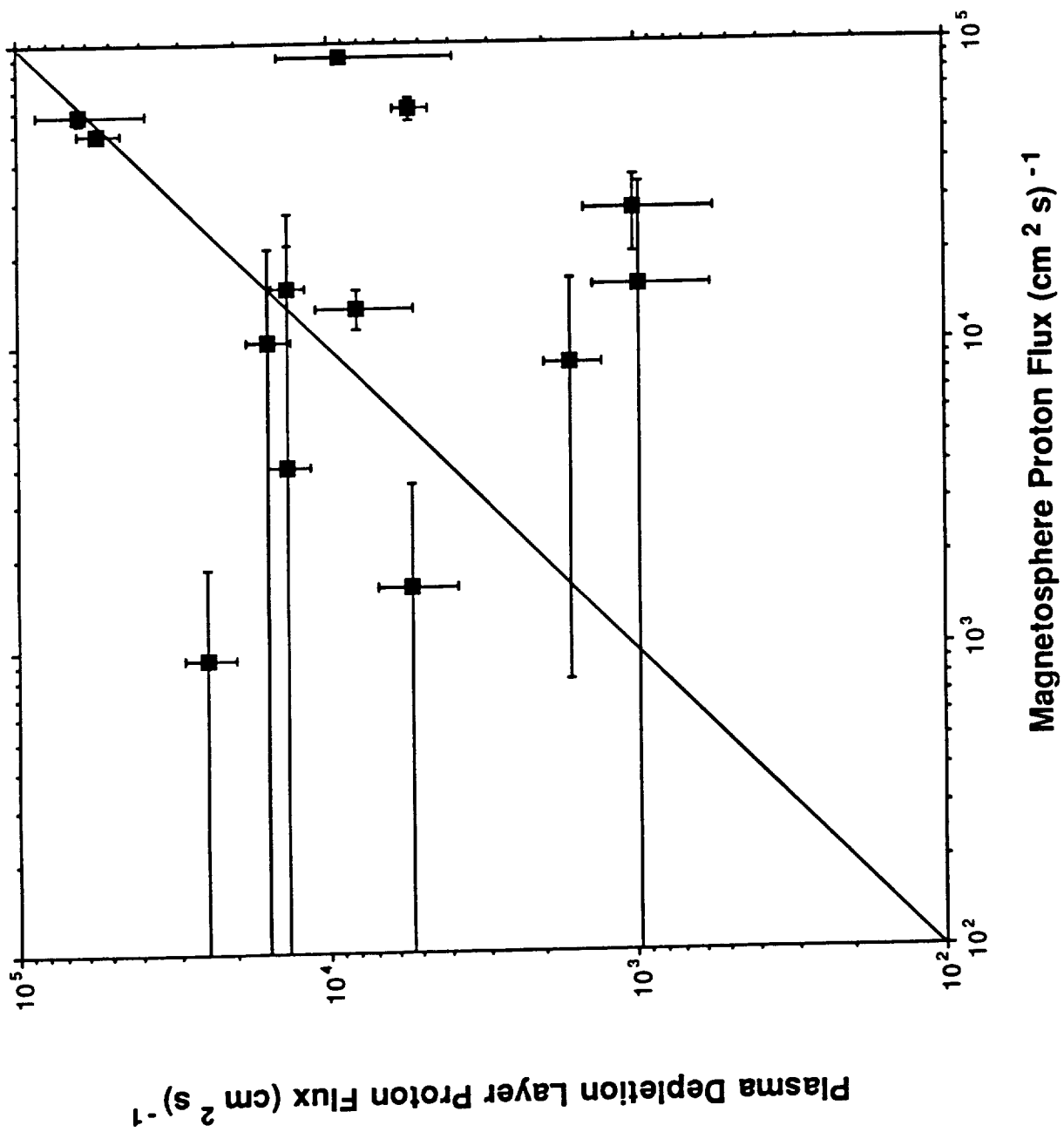


Figure 5

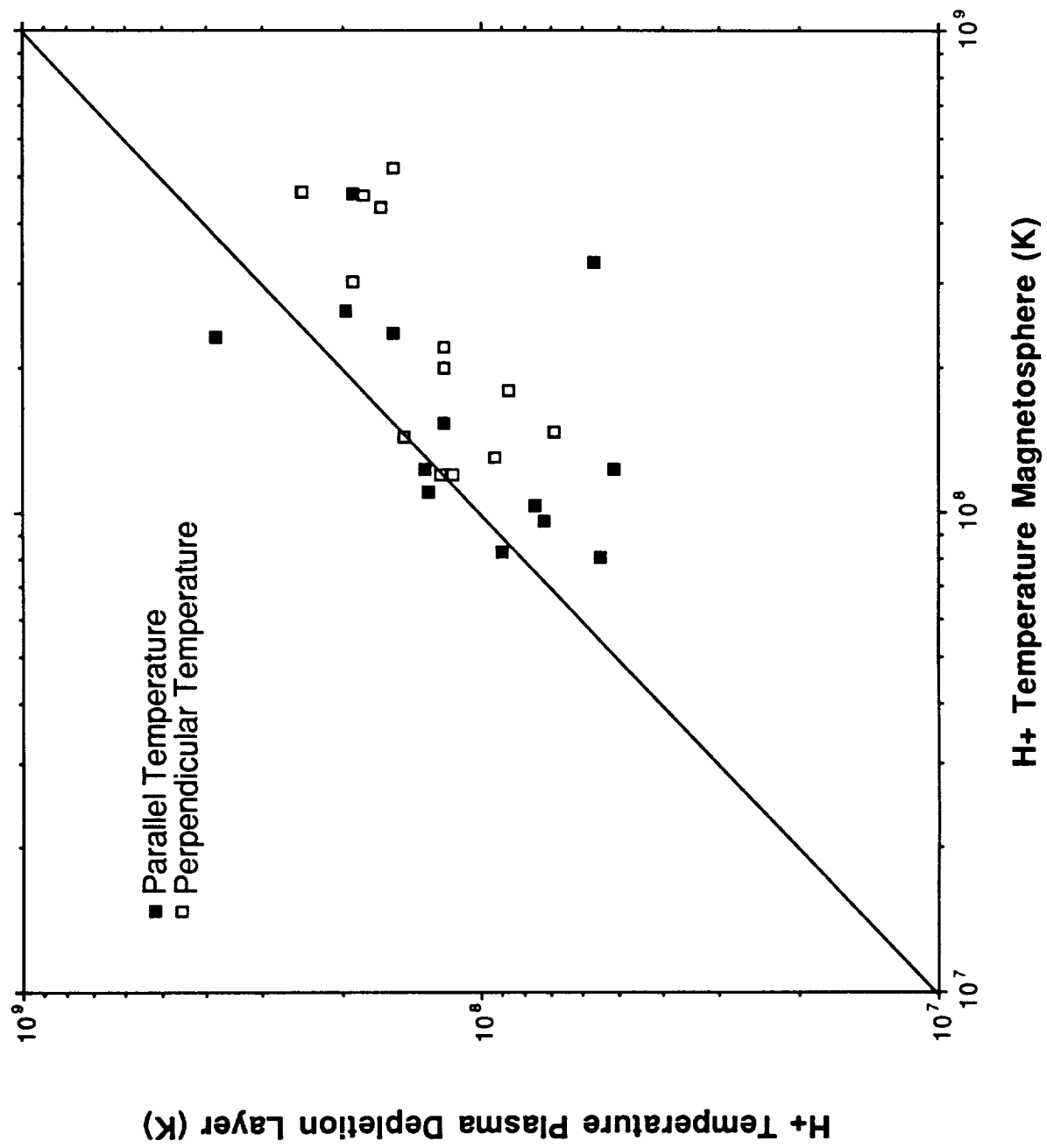


Figure 6

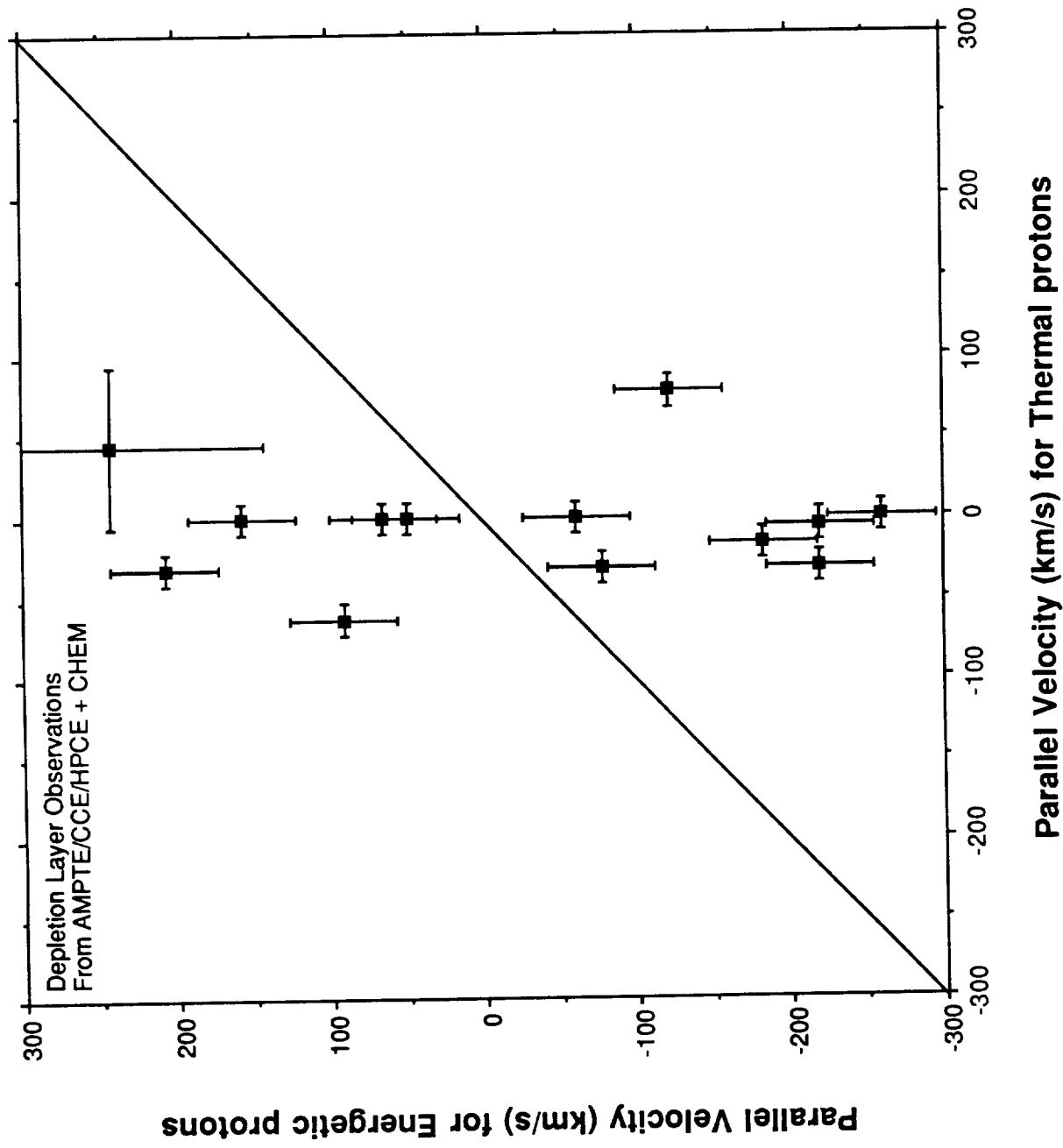
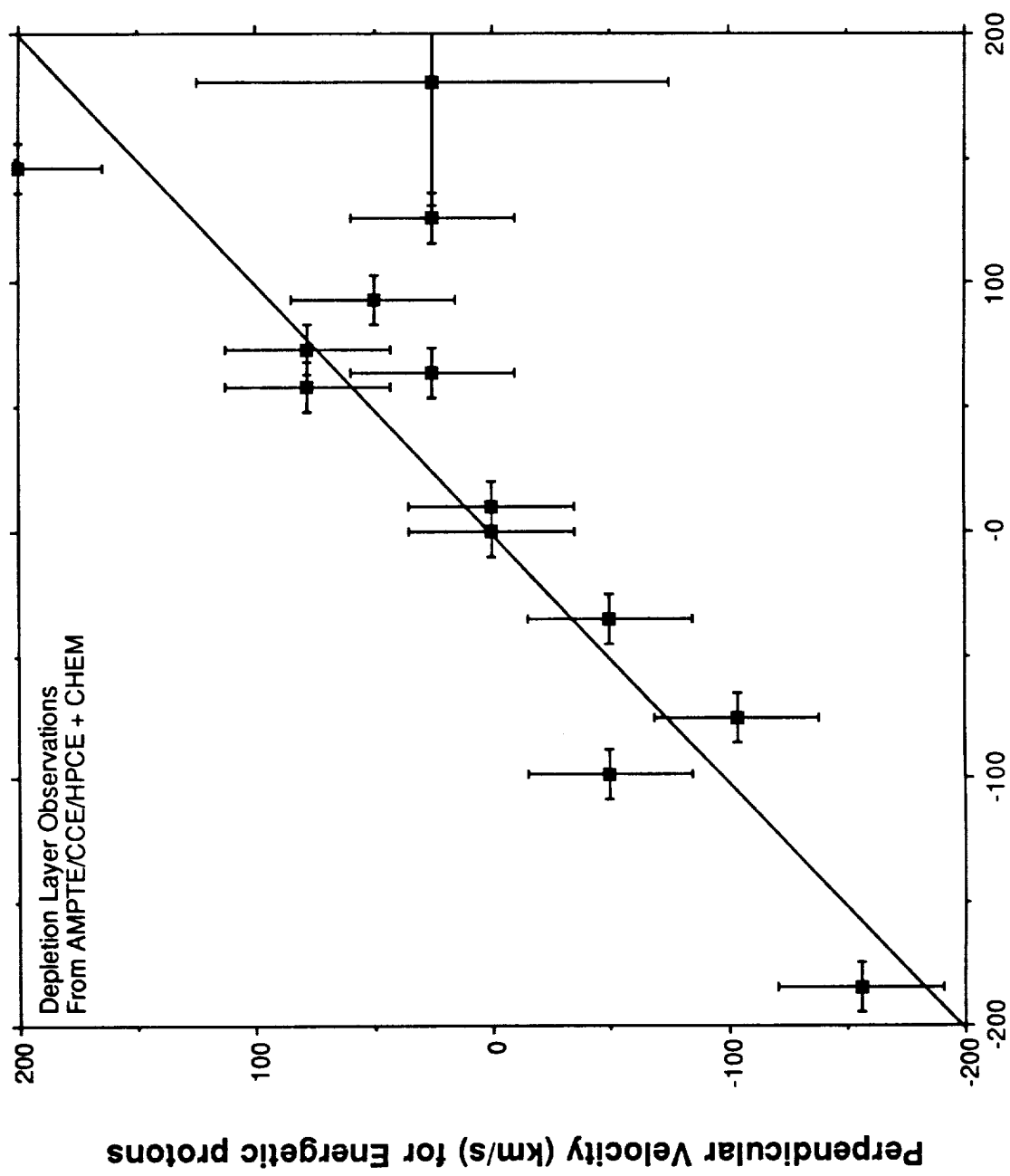


Figure 7



Perpendicular Velocity (km/s) for Thermal protons

Figure 8

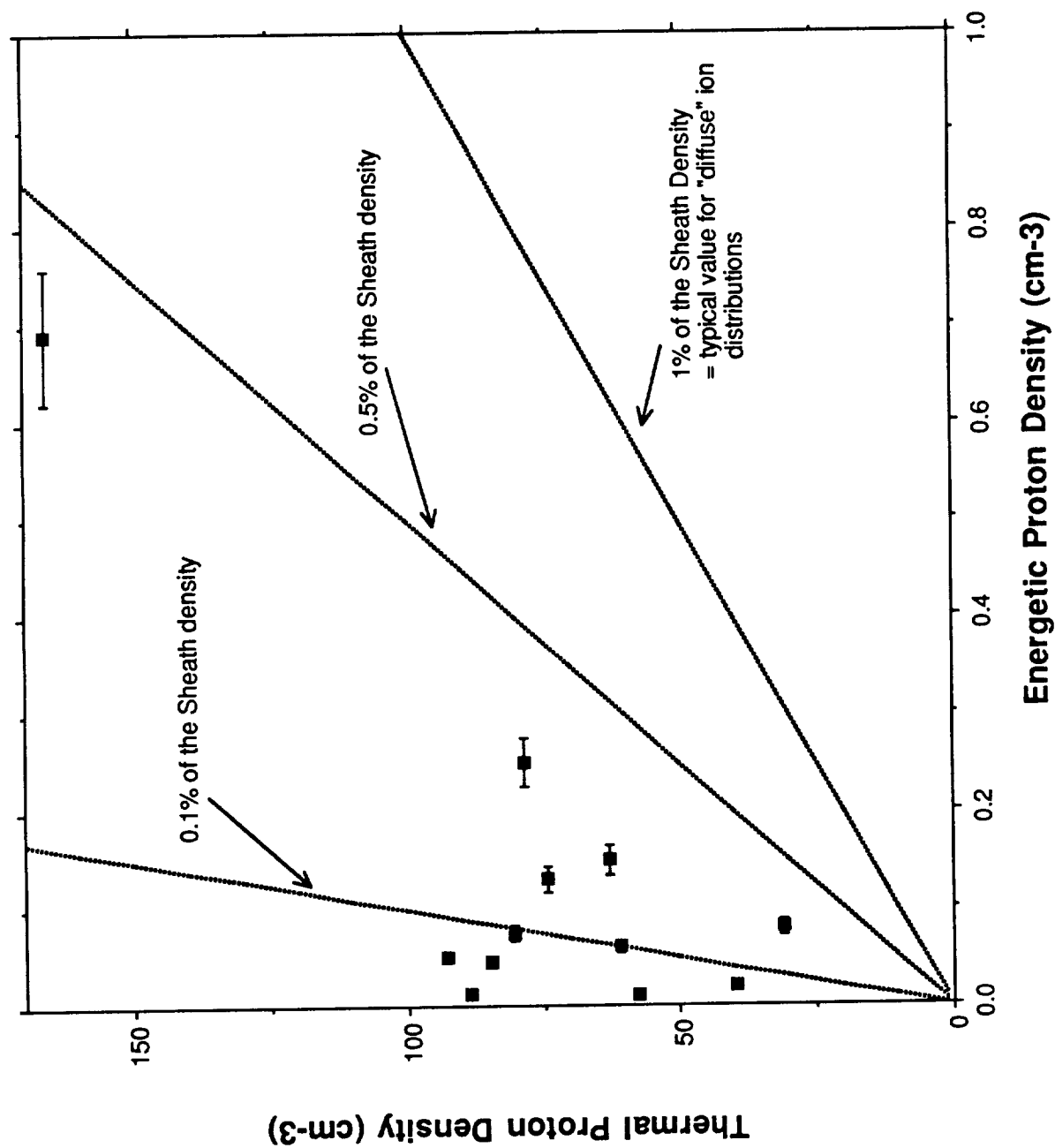


Figure 9

THE SPATIAL EXTENT OF RADIAL MAGNETIC PULSATION EVENTS

OBSERVED IN THE DAYSIDE NEAR SYNCHRONOUS ORBIT

M. J. Engebretson¹, D. L. Murr¹, K. N. Erickson¹,
R. J. Strangeway², D. M. Klumpar³, S. A. Fuselier³, L. J. Zanetti⁴, and T. A. Potemra⁴

revised version of April 10, 1992

submitted to the JOURNAL OF GEOPHYSICAL RESEARCH

¹ Augsburg College, Minneapolis, Minnesota 55454

² Institute for Geophysics and Planetary Physics, UCLA, Los Angeles,
California, 90024

³ Lockheed Palo Alto Research Laboratory, Palo Alto, California 94304

⁴ The Johns Hopkins University Applied Physics Laboratory, Laurel,
Maryland 20723

ABSTRACT

We have used simultaneous observations from the AMPTE CCE satellite, in an elliptical orbit with apogee at $8.8 R_E$, and GOES 5 and GOES 6, in geostationary orbit at $6.6 R_E$, to investigate the radial and longitudinal extent of magnetic pulsation events with predominantly radial polarization. Twenty one events were selected by visual inspection of color-coded Fourier spectrograms produced from data from all three satellites during a several month interval in fall 1984 when the apogee of AMPTE CCE was on the dayside; sixteen events were observed at all three satellites. Local time of the observed events ranged from 9 to 19 MLT, but the apparent longitudinal extent of the oscillation region varied considerably from event to event, ranging from the minimum resolution of 1.5 hours MLT (the local time separation of GOES 5 and GOES 6) to 8 hours MLT. Plasma wave data from AMPTE CCE indicated the waves occurred in regions of density characteristic of the outer plasmasphere ($\sim 10 \text{ cm}^{-3}$), and quite far outside the L shell region where densities reached 400 cm^{-3} . These events occurred during magnetically quiet times usually after magnetic storms; IMF data, when available, indicated an either roughly radial or northward orientation during the events. Wave onset often (but not always) occurred within one hour after sharp drops in the AE index to values of 100 or below. There was no apparent correlation of wave onset or amplitude with plasma beta, which ranged from 0.23 to 1.09 during the nine events presented here. Our frequent observation of the simultaneous onset of waves at different local times with considerably different frequencies reinforces the belief that the onset of these pulsations is determined by an instability that covers some longitudinal extent, but that the frequencies are determined by local Alfvén resonance conditions, not by the bandwidth of an external source. The data suggest that

local plasma density increases associated with plasmaspheric refilling are the immediate cause of local instabilities leading to wave onset; the increase in density may alter the field line resonance conditions to allow the free energy of ~ 100 keV trapped ions to drive waves via the drift-Alfven-ballooning-mirror mode instability.

1. INTRODUCTION

Significant progress has taken place in the past several years in determining the energy source of a variety of long-period ULF waves (Pc 3 to Pc 5) in the earth's magnetosphere. Multistation and multisatellite studies have helped confirm earlier suggestions that dawnside Pc 5 pulsations appear to be driven by the relative velocity shear between the dawnside magnetopause/boundary layer and the outer magnetosphere; increased solar wind velocity correlates well with increased amplitude/occurrence of these pulsations [see Anderson et al. 1990, 1991 and references therein]. "Storm-time Pc5" pulsations, observed predominantly in the dusk and afternoon sectors, have similarly been linked to the injections of ring current plasma during geomagnetic storms [e.g., Barfield and McPherron, 1972, 1978; Kokubun, 1985; Pangia et al., 1990]. A third class of pulsations, harmonically structured dayside pulsations, occurring typically in the Pc 3 but occasionally in the Pc 4 period ranges, have been shown to occur when the interplanetary magnetic field (IMF) is nearly radial [Engebretson et al., 1987; Anderson et al., 1991]. This IMF orientation has been shown to be the condition for the existence of a quasi-parallel shock geometry near the nose of the earth's bow shock; such a shock is now known to produce upstream waves in the Pc 3-4 frequency range [Russell and Hoppe, 1983] and very strong, more broadband fluctuations in the subsolar magnetosheath [Engebretson et al., 1991, Lin et al., 1991].

Our understanding of the extent and source of radially polarized pulsations is much more limited. Although numerous studies at synchronous orbit have provided information on the morphology of such waves [cf. Cummings et al., 1969; Hughes et al., 1978; Arthur and McPherron, 1981; Takahashi and McPherron, 1984; and Takahashi et al., 1985], the lack of ground signatures for most such waves and the paucity of observations at other than synchronous orbit has made it difficult to determine their extent in latitude and/or L shell or to confirm their source.

Many studies of radially polarized Pc 4 pulsations at synchronous orbit have determined that they are second-harmonic Alfvén waves resonant along a magnetic flux tube [Cummings et al., 1969; Singer et al., 1982; Takahashi et al., 1984, 1985; 1990; Engebretson et al., 1988]. Arthur and McPherron [1981] further noted that the occurrence of radially polarized Pc 4 pulsations at synchronous orbit was sharply peaked near dusk, with nearly all events occurring between 1100 and 2300 UT. In contrast to the rather narrow frequency range of nighttime Pc 4 pulsations they observed, the radially polarized daytime pulsations exhibited a nearly uniform distribution of frequencies over the Pc 4 band, with no evident dependence of frequency on local time. They suggested that possible sources of these radially polarized waves could be localized effects such as bounce resonances and drift mirror instabilities.

Rostoker et al. [1979] found from studies of ground-based data that Pg (or giant) pulsations, a rather rare subset of Pc 4 pulsations which are observed on the ground primarily in the pre-noon sector, are highly localized in latitude, but may be quite extended in longitude. They suggested that Pg pulsations accompany suddenly reduced levels of magnetospheric convection, and that they might be due to field line resonances at the plasmapause in the region where the electric field changes its azimuthal direction from westward to eastward. They

noted that the pulsations occurred on quiet days and normally after a sustained period of low magnetospheric activity, and occasionally exhibited a tendency toward daily recurrence under sufficiently favorable conditions, namely sustained quiet conditions during a state of recovery from prior geomagnetic activity. They noted that the Pg events occurred in a rather narrow region in L, and suggested that a large density gradient, such as that found at the plasmopause, might be a necessary feature in conjunction with a shear in the electric field convection pattern.

Takahashi et al. [1985] used 4 geosynchronous satellites, 3 with particle detectors and one with a magnetometer, to study the relations between pulsations in fluxes of 30 - 300 keV particles and all classes of magnetic pulsations in the Pc 4-5 range. Over 60% of the electron flux pulsations they observed had corresponding magnetic pulsations. Their Pc 4 band events were almost exclusively radially polarized, and had a local time distribution which maximized between 1200 and 1800. The frequency distribution was much more spread out than that for pulsations with other polarizations, scattered from 2 to 19 mHz with a mean of 9 mHz. They saw no phase shift between electron and magnetic oscillations for this class of pulsations.

Kokubun et al. [1989] used particle detectors and magnetometers on board the ATS 6 satellite in geosynchronous orbit to examine the dawn-dusk asymmetry of Pc 4-5 pulsations. According to Kokubun et al. [1989], radially polarized Pc 4 pulsations are almost never observed near the subsatellite point on the ground, the exception being Pg pulsations observed in the early morning. Radially polarized Pc 4 waves were found to occur at all local times, but with greatest probability in the afternoon, and tended to be the dominant wave type in the afternoon sector under quiet magnetic conditions. Kokubun et al. also studied the statistical dependence of radially polarized Pc 4 pulsations on

selected solar wind and geomagnetic activity parameters. They found that Pc 4 waves tend to appear during conditions of lower solar wind velocity and quiet magnetic conditions ($AE < 200$ nT) and exhibited a strong preference for $B_z > 0$. They attributed the lack of ground-magnetosphere correlation to the limited longitudinal scale of the radially polarized waves in space (based mostly on the large azimuthal wave numbers observed).

Studies of data from the elliptically orbiting satellites ISEE 1 and 2 [Singer et al., 1982] and AMPTE CCE [Engelbreton et al., 1988, Takahashi et al., 1990, Anderson et al., 1990, 1991] have suggested a complex spatial distribution for radially polarized Pc 4 pulsations, which is somewhat dependent upon local plasma conditions. Singer et al. [1982] looked at three dayside Pc 4-5 pulsation events between $L = 4$ and 7 and within 10° of the geomagnetic equator. The width of the resonant region for these events ranged from 0.2 to 1.6 L shells. Two of the three events appeared to be associated with plasmopause density gradients; in one of these events waves disappeared at one of the satellites as it encountered a region of depleted plasma density.

The most recent single-satellite data set available for studies of these waves comes from the AMPTE CCE satellite. In a statistical survey of the first 1-1/2 years of AMPTE CCE data Anderson et al. [1990] noted an increased probability of occurrence for radially polarized pulsations at evening and later dayside local times, and at L shells roughly between 5 and 8. Because of the elliptical nature of the AMPTE CCE orbit, they were able for the first time to detect a statistical tendency for the radial pulsations to occur at slightly higher L shells as local time shifted from local noon through evening to premidnight. This trend is roughly consistent with the local time variation of the equatorial distance to the plasmopause and/or low latitude convection boundary. Anderson et al. [1990] also found that periods of radially polarized

wave activity did not appear to be associated with freshly injected particle populations, but that spatial inhomogeneities, perhaps resulting from evolution of the previously injected ion distributions, might be a factor in the occurrence of such waves.

In a followup study Anderson et al. [1991] compared their AMPTE CCE pulsation data base, which includes the events at AMPTE CCE presented here, with various geomagnetic indices and solar wind parameters. Comparisons of all wave types to AE (auroral electrojet) indices and average solar wind velocities indicated associations of these waves with quieter than average conditions. Comparisons with D_{st} , however, indicated a tendency for radial pulsations to occur during intervals of moderate to enhanced ring current. In contrast to dayside azimuthally polarized pulsations, which correlated with low cone angles, radial pulsations occurred preferentially for cone angles upward of 60 degrees (IMF vectors tending toward being perpendicular to the sun-earth line). Superposed epoch analysis revealed a sharp drop in AE of ~ 100 in the ~ 4 hours preceding wave onset, a similarly rapid recovery of ~ 50 in AE during the first 2 hours after wave onset, and a shift from IMF $B_z < 0$ to $B_z > 0$ from 2 to 10 hours before the events.

When wave events were separated into two intensity categories, the sharp minimum in AE at wave onset was found to be common to both sets, but AE for stronger events fell from >350 to ~ 200 , and for weaker events it fell from ~ 230 to ~ 130 . There was a large increase in AE from 5 to 15 hours before the onset of stronger events, but a decrease during the corresponding interval before weaker events. Their analysis also showed a generally strong ring current during, and an extended interval of southward IMF B_z prior to, the more intense events. They concluded that ions injected during substorms might provide energy for these waves, but that the convection electric field plays an

important role in establishing conditions for conversion of energy from particles to waves: the sharp drop in AE and positive IMF B_z suggested that radial pulsations were evident only for sufficiently low convection electric fields.

In an earlier paper using AMPTE CCE data [Engebretson et al., 1988], we used magnetic field measurements, plasma wave observations, and hot plasma data (both ions and electrons) to characterize radially polarized pulsations, and found that large amplitude pulsations of this type observed within two degrees of the geomagnetic equator were always associated with large fluxes of warm, equatorially trapped light ions (with temperatures of ~ 10 – 50 eV). In this study we extend our observations of radially polarized pulsations by adding data from the GOES 5 and 6 satellites, situated in synchronous orbit at $6.6 R_E$. Unfortunately, the GOES satellites were positioned in the appropriate local time sector for only one of the events studied (but not presented) by Engebretson et al. [1988]. The events observed at AMPTE CCE used in this study do form a subset of the events used in the statistical studies of Anderson et al. [1990, 1991] and exemplify the conclusions of those studies, but the complex spatial and temporal characteristics of these events cannot be readily determined from single-satellite measurements. Because of our event selection criteria (detailed below), our data set is biased toward long-lasting pulsation occurrences. Although in five of the six cases presented here a sharp drop in AE occurs within one hour of wave onset at at least one of the three satellites, we present two examples where AE remains very low for many hours after onset, as well as three others during which waves continued while AE returned to higher levels.

2. INSTRUMENTATION

The AMPTE CCE satellite was launched August 16, 1984, into a near-equatorial highly elliptical orbit with a period of 15.6 hours and an apogee of $8.8 R_E$. The orbit of AMPTE CCE allowed long residence time near local noon during the first six months of the mission and again during the first six months of 1986. A thorough description of the AMPTE mission and instrumentation can be found in the May 1985 issue of the IEEE Transactions on Geoscience and Remote Sensing. This issue contains descriptions of the AMPTE CCE magnetometer [Potemra et al., 1985], plasma wave instrument [Scarf, 1985], and hot plasma composition experiment [Shelley et al., 1985]. Magnetic field data from AMPTE CCE used in this paper are 6.2-s median samples of data originally obtained at 0.124-s resolution.

The GOES 5 and 6 satellites were positioned in geostationary orbits above the western hemisphere. GOES 5 was positioned at -75° east longitude (with a variation of less than 3°), and thus had a nominal magnetic latitude of 11.4° at $L = 6.9$. GOES 6 was positioned at -110° east longitude (with a variation down to $\sim -98^\circ$), and thus had a magnetic latitude ranging from 9.0 to 10.0° at $L = 6.8$. The fluxgate magnetometers on board the GOES 5 and 6 satellites obtained vector samples of the local magnetic field at a rate of one sample every 3 seconds [Grubb, 1975].

3. OBSERVATIONS

3.1 Data Selection

The period of data studied was from September 1 to December 31, 1984, the first extended interval when the orbit of AMPTE CCE intersected geostationary orbit on the dayside. For each of these days magnetic field data from GOES 5

and 6 were averaged to 6-s averages and used to create color spectrograms covering 0000 to 1200 UT and 1200 to 2400 UT. These spectrograms were then compared to find correlated radially polarized pulsation events. Color spectrograms routinely produced from AMPTE CCE data were independently scanned for evidence of pulsations with predominantly radial power and compared with the GOES events list. As a result we identified sixteen events observed at all three satellites. Each selected event demonstrated a clear oscillation in the radial magnetic field component, with frequency from 5 to 20 mHz. The radial extent of the oscillation regions was quite narrow, varying in L value from 0.2 to 3.1, with a mean of 1.2. Local time of the observed events ranged from 9 to 19 MLT, but the apparent longitudinal extent of the oscillation region varied considerably from event to event, ranging from the minimum resolution of 1.5 hours MLT (the local time separation of GOES 5 and GOES 6) to 8 hours MLT.

Although individual events were scattered widely throughout the four month interval studied, two extended sequences of events were also observed. During each of these sequences, in early and late September 1984, pulsation events were observed on three or more successive passes of the satellites through dayside local times. In all other respects these pulsation events were typical of the larger population of events observed. In the following section we present selected events during each of these two sequences.

3.2 Sequence 1: September 2 - 6, 1984

Figure 1 shows magnetic field data from AMPTE CCE from 1700 to 1900 UT September 2, 1984 (84246) after removal of a 299 point (~30 minute) sliding average. During this interval the satellite traveled outbound from 5.0 to 7.3 R_E and from 11.3 to 12.6 magnetic local time (MLT), and the satellite's magnetic latitude varied slowly from 13.3° to 11.0° . The onset of the

radially polarized pulsations near 1744 UT was very sudden. Although this could be either a spatial or a temporal feature, the similarity of this event to those of Singer et al. [1982] and to others in our data set suggests strongly that the sudden onset is related to satellite's crossing of the spatial boundary of a pulsation region. Pulsations of the same period but with lower amplitude and with many sharp phase changes are evident in both the azimuthal and compressional components at the same time as the radial components. Pulsation activity stopped near 1825 UT with the onset of longer period perturbations including a moderate field compression peaking at 1835 UT, but data to be shown later suggests this is only coincidental.

These radially polarized pulsations occurred during a prolonged interval of low geomagnetic activity. D_{st} remained above -20 for over a day prior to this event, although the K_p index averaged near 2 during the wave event and the AE index (shown in Figure 2) ranged from 100 to slightly over 500 during this same period. AE decreased from 500 at 1530 UT to ~ 50 at 1710 UT, the time of wave onset at GOES 5. AE increased again to 250 at 1900 UT as the waves disappeared, but D_{st} continued to rise toward 0.

We show in Figure 3 a magnetic local time—L value plot of the AMPTE CCE, GOES 5, and GOES 6 satellite orbits from 1600 to 2200 UT September 2, 1984. GOES 5 (dashed line) is located at 74.8° west longitude, approximately 1.5 hours of local time duskward (eastward) of GOES 6 (solid line), located at 98.2° west longitude and at a slightly larger L value ($L = 6.9$ rather than 6.8). The region of pulsations observed by AMPTE CCE shown in Figure 1 is highlighted in this figure, as are the regions of simultaneous radially polarized oscillations observed by GOES 5 and GOES 6. At 1815 UT AMPTE CCE crossed synchronous orbit ($6.6 R_E$) at 91.5° west longitude, between the locations of GOES 5 and 6.

Figure 4 shows the radial component pulsations from GOES 5, GOES 6, and AMPTE CCE for this event from 1700 to 1900 UT. The period of the pulsations observed by AMPTE CCE increased from 55 s near 1750 UT ($\sim 6.2 R_E$) to 62 s near 1815 UT ($\sim 6.6 R_E$). The period observed by GOES 6 remained fairly constant near 57 s from 1735 to 1835 UT, and the period observed by GOES 5 was approximately 60–65 s from 1710 to 1815 UT. The pulsation event had a rather sharp onset at GOES 6, but at GOES 5 the pulsations appeared to occur over a more extended range of times with lower amplitude. Pulsations persisted at both GOES 5 and 6 during the interval of large, longer period pulsations from 1830 to 1900 UT, and to well after the end of pulsation activity at AMPTE CCE. AMPTE CCE passed between GOES 5 and GOES 6 near 1800 UT; note there are some temporal similarities between the pulsations observed at GOES 6 and AMPTE CCE, for example the simultaneous weakening of wave power near 1805, and similar wave packet structure from 1807 to 1818 UT. Waves observed by GOES 6 and AMPTE CCE from 1735 to 1803, however, showed no such correlation. The longitudinal extent of this oscillation appeared to be relatively narrow, between 1100 and 1300 MLT (or it was temporally limited). The radial extent of the oscillation, as inferred from the AMPTE CCE observations, was $\sim 0.8 R_E$.

Localized radial wave activity, often with a duration of one hour or less, was observed by AMPTE CCE on each successive orbit, on either the inbound or the outbound pass or both and usually near geosynchronous orbit, for the next thirteen passes over a period of eight days, with the exception of the immediately succeeding pass. Simultaneous or nearly simultaneous radial wave activity was observed by GOES 5 and/or GOES 6 during nearly all of these events when the geosynchronous satellites were situated at local times ranging from slightly prenoon through dusk. The duration of wave activity was also often one hour or less at these satellites. This repetitive, extended progression of

radial events was unique in our data set.

On September 4-5, 1984 (days 84248-84249) the GOES 5 and GOES 6 satellites observed a temporally and longitudinally extended oscillation region (over 4 hours UT at both satellites) centered at approximately 1500 MLT (Figure 5). The onset of this pulsation event coincided with a return to relatively more quiet geomagnetic conditions after a brief interval of strong activity. After having been quiet for several days, Dst dropped rapidly to -60 four hours before, but recovered to -40 one hour before the onset of wave activity. Simultaneously, the K_p index rose to over 7 during the period of strong geomagnetic activity 3-6 hours prior to wave onset, but returned to ~ 3 during the wave event. The AE index (shown in Figure 6) exhibited a dramatic drop, however. After reaching nearly 1900 at 1500 UT, it fell rapidly from 1250 to below 250 between 1600 and 1620 UT, and remained below 100 from 1815 to 2340 U. All three indices showed rising activity beginning the next day, but with a slight diminution from 0130 to 0330 UT.

As Figure 5 shows, the event began slightly earlier, and extended slightly longer, at GOES 5 than at GOES 6, even though these satellites were offset 1.5 hours in MLT. The pulsation was seen at both satellites from 1915 UT to 2345 UT. AMPTE CCE passed through the pulsation region near 1530 MLT several hours later, from 0130 to 0240 UT the following day, and observed radially polarized wave activity at a much higher frequency. The frequencies observed at the GOES satellites ranged from 5 to 6 mHz (Figure 7), while the frequency observed 6 hours later but in the same local time region by AMPTE CCE ranged from 15 to 20 mHz. The radial width of the pulsation region was again narrow (~ 0.9 R_E) when AMPTE CCE traversed it.

A third wave event September 6, 1984 (day 84250) was also extended in local time (~ 6 hours) and duration, as indicated in Figure 8. In this case AMPTE CCE crossed a narrow pulsation region on both its outbound and inbound passes, separated by almost 9 hours UT, while GOES 5 and GOES 6 (at longitudes of 74.7° west and 97.7° west) observed repeated wave activity for 5 and 4 hours, respectively. Figure 9 shows stacked dynamic power spectra from each satellite. Each panel shows power vs. frequency and UT for the radial components (BV for GOES 5 and GOES 6 and BR for AMPTE CCE) for the same 12 hr UT range, from 1400 September 6 to 0200 September 7. Magnetic local time, magnetic latitude (MLAT) and L shell are listed every two hours for each satellite.

This event again occurred during quiet (but not uniformly quiet) magnetic conditions. D_{st} retreated from near -80 one day before the wave event to ~-30 throughout the event, and K_p fell from ~ 5- one day before the event to near 2+ during the wave event. Except for a short rise to 1000 near 0850 UT, the AE index varied between 100 and 500 during the sixteen hours prior to the wave event (Figure 10). It reached its minimum of ~80 near the observed onset of wave activity at AMPTE CCE (1500 UT), but then gradually increased to 250 at 1700 UT, jumped rapidly to 700 and fluctuated between 500 and 900 from 1700 to 1800 UT. It then declined steadily to below 100 at 2000 UT, and remained at 300 or below for the next 45 hours. Although the wave activity at GOES 6 would suggest a second pulsation onset as the AE index declined and remained low after 1830 UT, the sustained activity at GOES 5 beginning at 1630 UT indicates either that GOES 5 moved into a region of existing wave activity (previously seen by AMPTE CCE) or that the onset of radial wave activity need not always occur as AE drops sharply.

The locations of wave observations by AMPTE CCE and the GOES satellites provide possible evidence for either a local time effect in the radial location and extent of the region of wave activity or an outward movement of that region during the nearly 9 hours between times AMPTE CCE encountered it on its outbound and inbound passes (Figure 8). Pulsations were seen from $L \sim 5.2$ out to $L \sim 6.8$ on the outbound leg of the AMPTE CCE orbit, and from $L \sim 7.7$ in to $L \sim 6.9$ on the inbound leg. The locations of wave observations by the GOES satellites provide possible evidence of movement of the oscillation region in local time as well. The first oscillations were detected at GOES 5 ($L = 6.9$) near 1630 UT and 1130 MLT. Weak oscillations were detected at GOES 6 ($L = 6.8$) at 1800 UT and 1130 MLT, but strong pulsations were not evident until 1930 UT at 1300 MLT. The onset of wave activity at both satellites at 1130 MLT, but shifted by 1.5 hours in UT (because of the 1.5 hour MLT separation of the satellites in longitude) suggests the existence of a pulsation region stable in local time; the delay of 3 hours in UT and shift of 1.5 hours of MLT in the observation of strong wave power by GOES 6, however, suggests that the region of strong wave growth was not spatially fixed, but may have moved slowly in the direction of corotation during this interval.

Figure 11, a stacked plot of the radial components observed by the three satellites from 1500 to 2000 UT, gives evidence that individual radially polarized waves or wave packets are strongly localized, in sharp contrast to the more widespread nature of longer period perturbations shown in this figure: although many large amplitude, longer period structures appear simultaneously with nearly identical amplitude, period, and phase in all three traces, Pc 4 pulsations are evident at one or at most two of the satellites at any given time. For example, from 1500 to 1600 UT Pc 4 pulsations appear only at AMPTE CCE; from ~1640 to 1800 UT they appear only at GOES 5, and from 1800 to 2000 UT

they appear at both GOES 5 and GOES 6. Plots of all three components (not shown) indicate some coordination between the longer period structures and compressional pulsations but little or no signal in the azimuthal component, whereas the Pc 4 pulsations were weakest in the compressional component and at times had comparable radial and azimuthal amplitude. We will consider the implications of this evident localization later in the paper.

3.3 Sequence 2: September 26-28, 1984

The three pulsation events in this sequence also occurred during periods of low to moderate geomagnetic activity, but none provided the close spatial conjunctions between AMPTE CCE and the GOES satellites shown in the first or third events.

In contrast to the events shown above, the first event in this sequence exhibited simultaneous pulsation activity at widely separated locations. Figure 12 shows the locations of the GOES satellites from 2000 to 2400 UT September 26, 1984 (day 84270) and of AMPTE CCE from 2000 UT September 26 to 0800 UT September 27, 1984 (84271). Radially polarized pulsations with a period of ~60 s (increasing slightly with increasing L shell) were observed at AMPTE CCE from ~2140 to 2330, as the satellite traveled outbound from L = 6.7 at 11.1 MLT to L = 8.2 at 11.9 MLT. On the inbound pass of AMPTE CCE waves with period ~85-90 s were observed from 0445 UT September 27 at L = 8.0 and 13.8 MLT to 0700 UT at L = 6.1 and 14.8 MLT. In this case there was very little change of period with L shell.

Bursts of radially polarized pulsations appeared at GOES 6 at 2000 UT (1340 MLT), 2110, 2200, 2310, and 2345 UT (1720 MLT). A burst also appeared at GOES 5 at 2000 UT, when the satellite was at ~1512 MLT, and more sustained waves appeared between 2110 UT (~1620 MLT) and 2300 UT, when the satellite was at

~1810 MLT. Azimuthally polarized waves at higher frequencies (Pc 3) were also evident in the GOES 6 spectrogram beginning slightly before 1400 UT, and continuing to 2300 UT. Predominantly azimuthally polarized wave activity was also evident in the 12-hour spectrogram of GOES 5 data from slightly before 1400 UT to 2100 UT. (We attribute the difference in Pc 3 cutoff time to local time effects: Pc 3 pulsations rarely extend to the dusk terminator [Anderson et al., 1990].)

Although there was strong geomagnetic activity several hours before this wave event, with Dst dropping to below -60 and AE exceeding 1500 three times during the previous 14 hours (Figure 13), magnetic activity shown in all three indices (D_{st} , K_p , and AE) had fallen by the time of wave onset at 2000 UT and remained moderately low for the next several hours.

During this event the pulsation period was much shorter at GOES 6 (60-66 s) than at GOES 5 (100-125 s). Because GOES 5 was located at a later local time and at a slightly larger L shell than GOES 6, the difference in pulsation frequency between these two locations could be due to either radial or local time variations in plasma density along the flux tubes sampled by the satellites. In addition to the frequency differences with local time in this event, however, it is notable that the onset of radial pulsations occurred at nearly the same universal time at both geosynchronous satellites, despite their different positions in local time. In this case radial wave occurrence was best correlated in UT, not MLT. The roughly simultaneous observation of waves by AMPTE CCE in this case may or may not be fortuitous, but the combined observations of wave onset and duration at the three satellites suggest that conditions for wave growth were simultaneously "turned on" over a wide range of local times. The observations also clearly indicate a large local time extent for this event, as well as the (apparently typical) limitation in L shell (in

this case, a range of 1.5 outbound and 1.9 inbound).

Figure 14 shows the locations of observations of radial pulsations by AMPTE CCE, GOES 5, and GOES 6 the following day, September 27, 1984 (84271). Waves were observed at GOES 5 from 1530 UT (1040 MLT) to 2145 UT (1655 MLT) and at GOES 6 from ~1730 UT (1105 MLT) to 2200 UT (1535 MLT). Wave onset at AMPTE CCE was less distinct during this event, but radial pulsations were clearly observed between 2045 UT (1350 MLT, $L = 7.8$) and 2205 UT (1425 MLT, $L = 6.7$). Cutoff of wave activity at the inner edge was again sharp, as in event 1. In this case each satellite saw waves at nearly identical frequencies, 17–19 mHz, throughout the interval. Comparison of the wave durations at the three satellites suggests that the cutoff of waves at AMPTE CCE could be either temporal or spatial.

Shortly before the beginning of this pulsation event the AE index (Figure 13) declined sharply from a relative maximum of 1000 at 1430 UT to 300 at 1500 UT and ~200 at 1600 UT. It remained near or below 100 from 1620 to 1720, and then returned to roughly 500 for the remainder of the day.

Pulsations were seen for a third successive day on September 28, 1984 (84272), as shown in Figure 15. AMPTE CCE passed inbound through the midafternoon sector from 1200 to 1600 UT, well before the GOES satellites traversed this local time sector. AMPTE CCE observed three strong but short, clearly separated packets of radially polarized pulsations: a ~10 min burst near 1300 UT (1400 MLT, $L = 7.4$); a ~30 min series of waves from 1400 to 1440 UT (1430 to 1500 MLT, $L = 6.4$ to 5.7); and a final packet from 1510 to 1525 UT (1525 to 1535 MLT, $L = 5.0$ to 4.5). During its subsequent outbound pass AMPTE CCE again observed a narrow region of weak radially polarized pulsations from 1925 to 1945 UT (1015 to 1030 MLT, $L = 5.3$ to 5.8). Waveform plots of the

pulsation activity at GOES 5 and GOES 6 (not shown) during the latter part of this event showed a variation of frequency with local time opposite that of the September 26 event: higher frequency wave activity was observed at GOES 5, located duskward of GOES 6.

Geomagnetic conditions were moderate during most of this day. D_{st} rose gradually from -40 to -20 before wave onset and fell slightly during the next 12 hours, while K_p ranged from 2 to 4 during this same period. The AE index (Figure 13) was steady near 200 from 0500 to 1130 UT, and rose to a level of near 500 from 1200 to 1900 UT, with drops from 1230 to 1430, near 1500, and near 1800 UT. It rose to over 700 at 1915, but declined again quickly and dropped to 200 by 2200 UT, roughly the time the pulsation event ended. Although the pattern of wave onsets at AMPTE CCE appears to roughly coincide with slight drops in the AE index, only the second wave onsets at GOES 5 and 6, near 2000 UT, agree with this pattern.

These three events, on September 26, 27, and 28, also demonstrate the variable frequency of pulsations observed simultaneously but at different local times. On September 26 (day 84270) the frequency of the oscillation at GOES 5 was 8–10 mHz and at GOES 6 was 15 mHz. On September 27 (day 84271) all three satellites observed a frequency of 18 ± 1 mHz. On September 28 (day 84272), two days later, the frequency observed at GOES 5 was 12 mHz and that observed at GOES 6 was 8 mHz, exhibiting a variation essentially opposite that of September 26.

On day 270 pulsations occurred simultaneously (to within ~ 30 min) at all three satellites, despite their six hour separation in local time. More intriguing simultaneity was observed on day 272: the event at 1515 was simultaneous at AMPTE CCE and GOES 5 (but not GOES 6), and the event at 1925 was

simultaneous at AMPTE CCE and GOES 6 (but not at GOES 5). The frequency observed at GOES 5 ranged from 7 mHz near 1515 UT to 16 mHz near 1615 UT, and back down to 12 mHz near 2130 UT. At GOES 6 the observed frequencies were 16 mHz at 1630 UT (the same as at GOES 5) and 8 mHz from 2000 to 2200 UT (much lower than at GOES 5). This suggests again that local plasma conditions affect both the frequency and the onset of wave activity, but that onset can occur at widely separated locations, with different frequencies, if instability conditions are otherwise satisfied.

3.4 Plasma Environment

The frequently sharp spatial boundaries observed for these events in both the radial and longitudinal directions suggest that some local property of the plasma or magnetic field configuration may be responsible for their occurrence, either as an energy source or as a medium with a favorable growth rate. Because the pulsations also exhibit clear temporal synchronization at times, we consider it likely that both spatial and temporal factors govern the occurrence of these waves.

In order to determine whether specific bulk plasma properties are important for the onset of these wave events, we have examined electron data in the energy range 50 eV — 25 keV from the AMPTE CCE Hot Plasma Composition Experiment (HPCE) [Shelley et al., 1985], ion data in the energy range 29 eV/e to 300 keV/e from the HPCE instrument and the AMPTE CCE Charge Energy Mass Spectrometer (CHEM) [Gloeckler et al., 1985], and in situ plasma densities estimated using data from the AMPTE CCE plasma wave experiment (PWE) [Scarf, 1985]. Both the HPCE and CHEM instruments view perpendicular to the satellite spin axis, which was roughly sunward; thus radial motion of the plasma is not observable to first order. Proton data from the HPCE and CHEM instruments were used to estimate the

plasma beta at the highest available temporal resolution (three minutes). Comparison with sample beta values calculated using all ion species in the energy range from 29 eV/e to 300 keV/e indicated that using only the energetic proton data (from 1 to 300 keV/e) caused an underestimate of the true beta value by typically ~10%.

In Table 1 we summarize wave and plasma density data obtained by AMPTE CCE for each event shown. The date and time of the wave observation is noted in the first column, along with an indication whether the pass was inbound or outbound. The second column contains the L shell ranges in which pulsations were observed. The third column lists the amplitude of the radial component of the pulsation. The fourth and fifth columns contain estimates of the ratio of the amplitudes of the pulsations in the radial and compressional components, B_r/B_n , at each of the satellites, and the range of plasma beta observed during the wave events. The last two columns list the approximate locations of the 400 cm^{-3} and 10 cm^{-3} density levels, as inferred from signals in the 178 kHz channel and the 30 kHz channel, respectively, of the plasma wave experiment. Timing accuracy for these inferred locations is at best within ± 5 minutes, or roughly 0.2 L shells near $L = 3$. We give a range of times for the 30 kHz channel since the signal often lasted around 30 minutes.

The ratio of B_r/B_n wave components was often very high, and appeared to be independent of amplitude of the radial wave component; our limiting estimate of >5 primarily reflects uncertainty in detecting weak compressional wave signals in the presence of background noise. When a range of values is shown, it indicates that compressional waves of clearly larger amplitude appeared during part of the wave interval. There was no apparent correlation between amplitude of the compressional component and local time or magnetic latitude (in the range $\pm 15^\circ$), but in many cases we noted a trend

toward lower ratios of B_r/B_n in the GOES data as time progressed during the events.

The plasma beta value for the nine events shown ranges from 0.23 to 1.09, and shows no evident correlation with pulsation amplitude or B_r/B_n ratio. Beta also appears to have little to do with the spatial onset of wave activity: in two of the nine cases the plasma beta showed a modest (~20%) increase during the wave events as compared to times immediately before and after the waves, but in the other seven cases the beta value either remained roughly constant before, during and after the wave event, or changed monotonically with L value.

Because the particle pressure perpendicular to the magnetic field is significant for some wave instabilities, we also examined the perpendicular and parallel beta values separately. During these AMPTE CCE passes the perpendicular to parallel temperature anisotropy was never more than 2, and typically about 1.5. We found that the perpendicular beta values were never more than 50% higher than the beta values shown in Table 1, and the parallel beta values never less than 50% lower; typical values were often much closer. For example, during the first two events the ratios of perpendicular beta to parallel beta were $1.25 \pm .10$ and $1.42 \pm .09$, respectively. Once again, we found no evident difference between these beta values, or their ratio, before, during, or after the wave events.

Electron flux observations from the HPCE instrument also revealed no consistent signatures. In two of the nine events electron flux modulations were observed in antiphase with the B_r oscillations; both cases corresponded to times when the amplitude of compressional pulsations was nearly 50% of the radial pulsation amplitude. Weak modulations of ~20% were observed during the

September 2 event (84246), and strong modulations of from 50% to 150%, at times with strong counterstreaming flows, were observed during the 0600 UT September 27 event (84271). In both cases modulations were strongest in the lowest energy electron channel (67 eV), but during the September 27 event (which had the largest pulsation amplitude of all the events presented), modulations of over 50% were evident in all electron channels. No noticeable electron flux modulations were evident in the other seven events listed; these corresponded to weak or negligible amplitude in the compressional magnetic field component. In general, electron fluxes responded much more strongly to longer period fluctuations, such as those noted in Figure 1 after 1830 UT, than to the Pc 4 events that are the focus of this study. We also attempted to observe ion flux variations during these wave events using data from the AMPTE CCE Medium Energy Plasma Analyzer (MEPA) [McEntire et al., 1985], but no wave-associated variations were observed, possibly because of limitations in wave amplitudes and instrument sensitivity (K. Takahashi, personal communication, 1991). It is also important to note that the event studied by Takahashi et al. [1990] was the only one in the AMPTE CCE data set with period long enough to allow the sort of analysis of particle data presented in that paper.

In each case shown the 400 cm^{-3} density level was inside $L = 4$, considerably removed from the region of pulsation activity, and in three cases it was inside $L = 3$. These locations are consistent with those found for similar radially polarized pulsations near the geomagnetic equator by Engebretson et al. [1988]; those pulsations also occurred well outside the observed 400 cm^{-3} region. As the table indicates, however, the location of the 10 cm^{-3} density level, when observed at all, was much more variable, including even some multiple signatures.

PWE plasma wave data for the three most complex plasma wave events are shown in Figure 16. The figure indicates that there was probably additional density structure outside of the nominal 10 cm^{-3} level on days 251 and 270, and possibly also on day 272. The 30 kHz waves were polarized perpendicular to the ambient magnetic field, indicating that the waves were Upper Hybrid Resonance waves, which correspond to a density of 10 cm^{-3} when the electron gyrofrequency is much less than the electron plasma frequency.

The locations of both density levels are consistent with the distributions found by Horwitz et al. [1990] in their statistical survey of plasmaspheric structure. They found that a multiple-plateau plasmasphere was common on the dayside, especially during quiet times. When such a multiple-plateau structure was observed, Horwitz et al. found that the location of a sharp inner gradient (which usually crossed the 400 cm^{-3} density level) averaged near or below $L = 4$ on the dayside. Furthermore, they found that the L value of the low energy ion transition (LEIT), an indicator of the plasmopause based on measurements of cold, light ions, exhibited no consistent relation to the L value of the region or regions where the number density was still at or above 10 cm^{-3} , differing by up to 3 L shells during early afternoon local times.

During the first three passes no plasma wave signal characteristic of the 10 cm^{-3} density level was observed, but on each of the other passes the 10 cm^{-3} density level was observed either within and/or at the inward edge of the region of radial pulsations. Near 1400 UT September 28 (84272), the 10 cm^{-3} level coincided with the middle one of the three distinct packets of pulsations observed, and the PWE signal suggested a rather complex radial density structure during this interval.

3.5 Density Estimation Based on Pulsation Frequencies

Although the limited frequency resolution of the AMPTE CCE PWE instrument prevents us from obtaining any more direct information about plasma densities in the regions where waves were observed, it is possible to estimate equatorial densities from the observed pulsation periods, provided certain assumptions about the plasma density distribution along a field line are valid.

We have based our estimation on the formula used by Orr and Matthew [1971] for calculating the eigenperiod of a fundamental toroidal resonant oscillation,

$$T = 0.05881 L^4 (n_0/kC)^{1/2}, \quad (1)$$

and scaled it to fit the second poloidal harmonic according to an empirical factor derived from the results of Cummings et al. [1969]. We used the resulting modified formula,

$$n_0 = T^2 kC / (0.02606 L^4)^2 \quad (2)$$

to calculate the equatorial mass density n_0 for each of the wave events presented, using the observed periods T at the respective L shell. Here kC is calculated using the formulas Taylor and Walker [1984] developed for toroidal fundamental mode oscillations in a dipolar geomagnetic field with infinite ionospheric conductivity boundary conditions. The plasma density distribution along a field line is assumed to be $n = n_0(r_0/r)^m$, where r_0 is the geocentric distance to the equatorial crossing point of the field line, and r is the geocentric distance to a point on the field line. The value of m is usually taken to be 4 outside the plasmapause (corresponding to a collisionless distribution) and 3 inside (corresponding to diffusive equilibrium). Because in the cases shown here the satellite was clearly outside the steep inner plasmapause density gradient, we have assumed $m = 4$. Although the validity of either plasma distribution model is uncertain during times of plasmaspheric

refilling, Orr and Matthew [1971] have shown that the period depends only weakly upon which of these two values of m is chosen. In particular, kC is a slowly varying function of L and m , varying less than 5% from $L = 5$ to $L = 8$ and less than 10% from $m = 3$ to $m = 4$.

The resulting equatorial densities are listed in Table 2. In every case when the 10 cm^{-3} density level was observed by the AMPTE CCE PWE instrument near a region of wave activity, the density level determined from equation (2) was consistently near but somewhat lower than the value inferred from the PWE data. We make mention especially of the agreement during events 4 and 6. During the inbound portion of event 4, AMPTE CCE observed waves with roughly constant period (85–90 s) from $L = 8.0$ to $L = 6.1$, while the PWE instrument observed 30 kHz wave activity, indicative of a density of 10 cm^{-3} , near $L = 7.2$. Using equation (2) and a period of 87.5 s we infer equatorial densities of 2.4 at $L = 8.0$, 5.6 at $L = 7.2$, and 21.7 at $L = 6.1$. During the inbound portion of event 6, AMPTE CCE observed three regions of radially polarized wave activity; the second one had a period near 50 s over the range $L = 6.4$ to $L = 5.7$. The PWE instrument observed 30 kHz wave activity, indicative of a density near 10 cm^{-3} , from $L = 6.3$ to $L = 5.8$. Using equation (2) and a period of 50 s we infer equatorial densities of 5.5 cm^{-3} at $L = 6.3$ and 10.7 cm^{-3} at $L = 5.8$, respectively.

The good agreement between densities inferred independently from ULF wave periods and from plasma wave signals appears to support the approximate validity of this time-of-flight method, even though the pulsations occur during periods of flux tube refilling, when the plasma distributions are not well characterized. The absence of clear plasma wave signals at 30 kHz (corresponding to a density of 10 cm^{-3}) on the outbound legs of the first and third events, while the equatorial densities calculated from wave periods

were below 10 cm^{-3} near synchronous orbit, however, makes it prudent to treat these density values with some caution.

The equatorial densities at synchronous orbit listed in Table 2 cover a substantial range, from 2.8 to 46.9 cm^{-3} . These are elevated over typical $\sim 1 \text{ cm}^{-3}$ levels for this region, but consistent with regions of plasmaspheric refilling or detached plasma [Chappell et al. [1971]. This suggests that whatever instability is operative in generating these waves must be able to function over a broad range of densities (and wave frequencies).

3.6 AMPTE IRM Observations

In order to rule out the influence of interplanetary field fluctuations or bow shock-related upstream waves as a source for the observed pulsations, we surveyed the AMPTE IRM data set before and during each wave interval we identified. In all cases available when AMPTE IRM was in the solar wind, the IMF was either northward or close to radial, consistent with a quiet magnetosphere, and there were no significant solar wind density or velocity perturbations. In contrast to the case for Pc 3-4 pulsations, there was no significant correlation with IMF cone angle. These results are consistent with the earlier observations of Kokubun et al. [1989], and as expected, are also consistent with the superposed epoch analysis of Anderson et al. [1991], whose set of events observed by AMPTE CCE includes those presented here.

During the September 28 event AMPTE IRM was tracked deep into the magnetosphere on the inbound portion of its orbit as it followed AMPTE CCE with about one hour's delay from 13 to 16 UT. The AMPTE IRM magnetometer detected packets of radially polarized Pc 4 magnetic pulsations near 1440 UT ($L \sim 7.4$), 1520 UT ($L \sim 6.6$), and 1600 UT ($L \sim 5.1$). The periods observed by AMPTE IRM corresponded closely to those observed at similar L shells by AMPTE CCE slightly earlier. The event from 1510 to 1525 also coincided temporally but not spatially with an event at AMPTE CCE, and had a longer period. Plasma and plasma wave data from AMPTE IRM indicated a greatly increased plasma density coincident with the first two pulsation events; unfortunately, no data from these instruments were available inside $L = 6.6$. Based on the available evidence, we may infer that the Pc 4 events observed by AMPTE CCE coincided with regions of increased plasma density, either in a highly structured outer plasmasphere or as detached plasma regions. Either of these could be created by irregular variations in the plasmopause boundary, with each outward excursion

followed by an interval of plasmopause refilling.

4. DISCUSSION

The examples presented here, from the two longest sequences of radial pulsation events in our data set, share many features of events studied earlier by various authors. We have found, as did Kokubun et al. [1989] and several others, that radially polarized Pc 4 pulsations are primarily an afternoon sector phenomenon, and occur under quiet to very quiet geomagnetic conditions. We have also verified for specific events the close temporal association of wave onsets with dropping of the AE index to low levels found statistically by Anderson et al. [1991], although this is by no means true for all the events studied. The primary new contributions of this study are 1) the determination of the spatial extent of the wave region in local time, L shell, and relative to thermal plasma boundaries; and 2) the lack of correlation of wave onset, amplitude, or B_r/B_n ratio with plasma beta, which ranged from 0.23 to 1.09 (Table 1). In conjunction with recent studies of plasma boundaries in the inner magnetosphere, this information provides further clues to the origin of this class of pulsations.

Our observations are consistent with the results of Rostoker et al. [1979] in having a narrow extent in L, but we have found no cases for which the events coincide with a simple, sharp plasmopause boundary. They occur far outside regions of large densities of cold plasma, and instead appear to coincide with, or are embedded within, an outer plasmasphere that is evidently the site of (sometimes complex) expansion and refilling processes such as would be expected during relatively quiet times. Horwitz et al. [1990] found that the most common kind of plasmaspheric profile observed during low K_p conditions ($K_p \leq 2$) was of the "multiple plateau" type, and that this profile was also

strongly dominant in the afternoon sector.

Our observations are also supportive of an association with an electric field reversal boundary, although not in the sense suggested by Rostoker et al. [1979], who considered an association with an electric field reversal region localized in azimuth near local noon. Instead, during times of plasmaspheric refilling (periods of recovery after geomagnetic storms) the boundary between corotation and convection electric fields lies at an L shell beyond the previous plasmopause density gradient. A preliminary comparison between wave occurrence and increases in the latitude of the DMSP auroral boundary index [Gussenhoven et al., 1981; Madden and Gussenhoven, 1990] has revealed a generally good correlation. Also, as mentioned above, we have found generally good agreement in the cases shown here between the onset of radially polarized ULF pulsations and low to very low levels of the AE index, consistent with the earlier statistical results of Anderson et al. [1991]. Both of these indices are related to the level of magnetospheric convection; the good correlation implies that greatly reduced convection, and the consequent expansion of the convection/corotation boundary to larger L shells, may be a necessary condition for wave onset.

The statistical profile of Pc 4 occurrence reported by Anderson et al. [1990], which as noted above includes the events reported here, appears to track the local time — L dependence of the low energy ion transition (LEIT), defined by Horwitz et al. [1990] as the location in L at which detectable fluxes of ions disappear from the retarding ion mass spectrometer (RIMS) instrument on the DE 1 satellite. Horwitz et al. [1986] suggested that the LEIT may be a more sensitive signature of the boundary between open and closed convection trajectories than the steep gradient "plasmopause" signature of electric field probe saturation. In their data set the LEIT was located roughly at or slightly

earthward of the 10 cm^{-3} ion density boundary, as determined from an electric field measurements. Horwitz et al. [1990] found that the large, multiple plateau region often observed in noon/afternoon local times spanned geosynchronous orbit, and was usually $2 - 4 R_E$ wide. The LEIT was often just inside $6.6 R_E$ prenoon, and was often well outside $6.6 R_E$ postnoon. The low-energy ion transition expanded for low K_p in the afternoon sector (12-18 MLT) to typically $> 7 R_E$ for $K_p < 2$.

Until recently, attempts to find the free energy source of radially polarized Pc 4 pulsations have focused on energetic particles rather than on thermal plasma. Because energetic ring current ions are insensitive to the convection electric field, ions injected during magnetic storms can penetrate deep into the inner magnetosphere and remain there until their numbers are depleted by processes that include charge exchange and various wave-particle interactions. Unstable distribution functions or concentration gradients of these energetic particles have been considered to be a possible energy source for a variety of localized and/or convecting (non-propagating) ULF instabilities.

Several theoretical studies have suggested a bounce resonance interaction of energetic protons as a possible excitation mechanism for radially polarized Pc 4 waves [Southwood, 1976; Southwood and Kivelson, 1981; Tamao, 1984]. According to Southwood [1976], an antisymmetric pulsation driven by bounce resonance is possible for a location at the inner edge of the ring current (i.e., in a region with an outwardly directed energetic particle density gradient). Southwood was the first to note that an enhanced background cold plasma is a destabilizing influence for bounce resonance interactions, because it reduces the frequency of free oscillations of the plasma such as Alfvén waves. He also pointed out, however, that because the pulsation growth rate is

proportional to beta, the growth should be slow in a low beta region so that other effects, such as ionospheric wave damping, might be adequate to stop weakly growing instabilities.

Recent work by Takahashi et al. [1990] using both magnetic field data and energetic particle measurements has suggested that drift-bounce resonance instabilities are likely to be responsible for at least some radially polarized pulsations. In the case they studied, they observed an inward gradient of ion fluxes with energies above ~50 keV, indicating the wave was observed at the outer edge of the proton ring current rather than at the inner edge, and they suggested a high energy bounce resonance with ~100 keV ions. Although they used AMPTE CCE satellite data in this study, the ion head on the HPCE instrument had stopped working by the time of their event, so no lower energy ion data were available.

As Horwitz et al. [1986] pointed out, however, energetic particles and perhaps also low-energy ions in the equatorial dayside magnetosphere are primarily the result of the history of injection and convection over the previous 24 hours or longer, whereas the boundaries of the low-energy and thermal plasma and the corotation electric field boundary are more responsive to the instantaneous convection pattern and the current level of magnetic activity. The fact that pulsation onsets often occurred shortly after AE dropped to very low values leads us to infer, then, that while energetic particles may play a necessary role in generating these waves, some property of the low energy or thermal plasma, or of the magnetospheric configuration associated with rapid expansion of the outer plasmasphere, may be the trigger of wave onset in localized regions. The suggestion in our data set of simultaneous wave onset in a longitudinally extended but radially narrow region also argues in favor of a thermal plasma contribution to the wave instability.

We suggest two possible localized plasma effects. First, there have been several reports of trapped warm light ions near the geomagnetic equator during times of plasmaspheric refilling [Olsen, 1981; Olsen et al., 1987; Engebretson et al., 1988. Olsen et al. [1987] found using DE 1 data that equatorially trapped plasma was most likely to be found in the mid-afternoon sector (out to the $L = 5$ limit of the DE 1 measurements), centered at the magnetic equator, and at and/or outside the plasmopause. Observations by Engebretson et al. [1988] from AMPTE CCE showed that these populations could extend out to beyond $L \sim 8$ in the afternoon sector. No means has been suggested, however, as to how these ion populations might drive ULF waves.

Second, as Kokubun et al. [1989] noted, these pulsations appear to be associated with the afternoon bulge in the outer plasmasphere, and no theory has yet succeeded in explaining this distribution in local time. We have already remarked that the statistical profile of Pc 4 occurrence presented by Anderson et al. [1990] also indicated dominant activity in this region. Horwitz et al. [1986, 1990] pointed out that the convection reversal boundary (or, equivalently, the plasmopause) appears to extend considerably beyond synchronous orbit in the afternoon sector under quiet geomagnetic conditions, and refilling flux tubes circulate on closed (almost corotating) convection trajectories, which bow outward in the afternoon sector [Horwitz et al., 1990].

Several authors have studied the possibility of onset of ballooning modes, which might become unstable near a plasmapauselike boundary. Ballooning is basically an MHD fluid instability that is driven by the presence of a pressure gradient in a region of favorable magnetic field curvature. Both Vinas and Madden [1986] and Lakhina et al. [1990] considered ballooning modes at the plasmopause under high beta conditions, Lakhina et al. using a more general field line and curvature geometry. Both considered the effect of shear flow,

such as that between cold plasma in the plasmasphere (corotating) and hot/warm plasma in the outer magnetosphere (convecting sunward), on wave stability. Unfortunately, until very recently most studies (including those of Miura et al. [1989] and Ohtani et al. [1989a,b]) have focused on storm time pulsation conditions, and on the fundamental mode instabilities which are observed to occur under high beta conditions, mostly in the evening sector, rather than on the second harmonic modes observed during quiet times mostly in the afternoon sector.

Miura et al. [1989] considered a magnetotail geometry with greatest curvature at the magnetic equator, and found the fundamental mode, the only mode they claimed to be unstable, to be sharply localized in this region. Chen and Hasegawa [1991], however, pointed out that trapped particles localized at the equator will damp the fundamental mode, and argued that the second harmonic mode is the most unstable to coupled drift-Alfven-ballooning-mirror instabilities. Lee and Cahill [1975] noted that during storm recovery periods the trapped particles are more localized near the equator than is the case during disturbed periods.

Cheng et al. [1991] found that radially polarized Pc 4 waves were associated with pressure gradients in regions of enhanced field line curvature, and were found to satisfy conditions for ballooning instabilities. They found such waves most likely to occur under low beta conditions ($\sim 0.1 - 0.3$), consistent with the lower half of the beta values observed in this study.

Chen [1991] reviewed two possible instabilities which involved ballooning modes. Both of these, the reactive ballooning-mirror instability and the drift Alfven ballooning-mirror instability, are expected to have coupled compressional and transverse polarized components, with the radial component stronger than the

azimuthal, and to have a second-harmonic antisymmetric structure along the magnetic field.

Chen and Hasegawa [1991] used a kinetic approach to describe the drift Alfvén ballooning-mirror (DABM) instability. This instability, which leads to primarily second harmonic radially polarized pulsations, is the low-beta analog of the more well-known drift mirror instability, which is invoked as the cause of the "storm-time Pc 5" pulsations often observed under high-beta conditions. Both are driven by wave-particle interactions, with pulsation frequency determined by local field line resonance conditions, but their calculations indicate that the DABM mode is more likely to be destabilized by ~ 100 keV ions and stabilized by ~ 1 keV ions; hence it is expected to be more likely to occur from one to several days after ring current injections, by which time the lower energy peak of the ring current population will have decayed away (and hence after the beta of the magnetospheric plasma has been reduced).

Our observations suggest that wave onset is probably not caused by a ballooning mode instability alone. Although plasmaspheric refilling will increase the local plasma density significantly inside the instantaneous plasmapause boundary, the impact of these cold particles on plasma pressure is negligible. In addition, we have found no correlation between field line curvature at AMPTE CCE and the presence or absence of these wave events under similar storm recovery conditions.

Our observations do, however, appear to favor some sort of coupled ballooning mode / bounce resonance instability, such as discussed by Cheng et al. [1991] and Chen and Hasegawa [1991]. We suggest that increases of local plasma density associated with plasmaspheric refilling affect instability conditions more indirectly, perhaps in the way outlined by Chen and Hasegawa

[1988] by reducing the frequency of resonant Alfvén oscillations of the local flux tube, the bounce-resonance stabilization of the plasma is reduced, and the growth rate is increased. Studies of plasmaspheric refilling processes reviewed by Singh and Hwang [1987] and Horwitz et al. [1991] have suggested that during the initial stages of plasmaspheric refilling during quiet or storm recovery times, when the convection/corotation boundary suddenly moves outward, plasma tubes refill first at the magnetic equator; the less than 1 hour delay between drops in AE and many wave onsets is qualitatively consistent with the time needed to accumulate cold plasma close to the magnetic equator, where it will have the greatest impact on the resonant frequency of the local flux tubes, but not at significantly higher magnetic latitudes.

In addition to the sharp average drop in AE index by ~100 1–2 hours before the onset of Pc 4 wave activity, the superposed epoch results of Anderson et al. [1991] showed that there was a clear increase of the AE index by about ~130 during the interval from 15 to 5 hours before the onset of large amplitude Pc 4 events, but a gradual drop by about ~50 during this same interval before the onset of lower amplitude events. Because rises in the AE index correlate well with substorm injection activity, these results suggest that, in the longer term, the amplitude of Pc 4 wave activity does depend on the density of the relevant energetic particle populations. Even under quiet magnetospheric conditions, and especially during storm recovery conditions, however, there are likely to be sufficient densities of ~ 100 keV ring current ions to drive bounce resonances or drift modes: Lee and Cahill [1975], observing near the magnetic equator on Explorer 45, found that protons with energy above 100 keV appeared to be sufficient to produce the quiet time magnetic field inflation they observed. Their study also reaffirmed earlier findings that the distribution of ring current particles was more confined to equatorial latitudes during quiet times

than during disturbed times. The magnetic field inflation might also increase the curvature of field lines close to the magnetic equator throughout the storm recovery period. Although as noted above we could not find any significant correlation between curvature and wave occurrence in our data set, consistently increased curvature might still play a necessary role in creating the conditions for wave growth.

We have noted a trend for the ratio of radial wave power to compressional wave power observed at synchronous orbit to decrease during most events (Table 1). Unfortunately, the available data do not allow us to clearly separate UT from MLT effects: In almost every case wave onset was associated with high ratios of radial pulsation amplitude at all three satellites, regardless of whether the satellites were at the same local time and/or L shell. The first event is a clear exception; in it the ratio of B_r to B_n is clearly ordered by local time, with the ratio decreasing as local time increases. In addition, the Q value of the resonant oscillations also decreases with satellite position in local time for this event. Based on available data, and using the first event as an example, we speculate that wave growth and/or instability might be enhanced when this ratio is high, i.e., when the coupling of radially polarized waves to compressional modes is minimized.

The calculations of Chen and Hasegawa [1991] indicated that both the growth rate and the ratio of compressional to radial wave amplitudes excited by these wave-particle interactions should decrease as beta decreases. This may explain the association of IMF $B_z > 0$ with the radially polarized waves we observed: conditions must be quite stable in order for waves to grow to reasonable levels when the growth rate is low. Our observation that the ratio of compressional to radial components increases during wave events, however, is hard to explain using this model, as is the apparent lack of correlation between beta value

(within the observed ranges) and wave onset, amplitude, or B_r/B_n ratio.

Because AMPTE CCE particle instrumentation was not adequate to allow us to perform a more detailed analysis of ions in the ~ 100 keV energy range thought to be the source of free energy in this model, however, a definitive test of this and other wave excitation models must await a future observational study.

The evident localization of the observed waves, exemplified by Figures 1 and 10, can be interpreted to mean either that (1) the waves simply do not propagate in either azimuth or L shell (except possibly in a frame of reference moving with the wave source), or (2) that the waves have a short wavelength and low coherence over the region of generation. In case (2) waves might propagate away from an extended source region, but decay rapidly because of incoherent superposition effects.

Earlier studies have often found azimuthal wave numbers m for such waves to be ~ 100 , and have had good success in associating them with bounce-resonant energetic ions (e.g., Takahashi et al., [1990]). The azimuthal drift of these ions would then suggest a necessary azimuthal motion of the wave region, and the bounce-resonance interaction is expected theoretically to have a wave number in this range. On the other hand, the observation of frequently sharp radial boundaries around wave regions with nearly constant amplitude (e.g., Figure 1) can be used to place a constraint on the radial wavelength of these waves. If we assume $m \sim 100$ and consider a wave region near $L = 7$, the azimuthal wavelength $\sim 0.4 R_E$. If the radial wavelength is similar to the azimuthal wavelength, we would expect waves to decay exponentially in radial distance with a roughly similar scale length; instead, Figure 1 indicates a spatial onset with a scale length near $L = 6.4$ that is roughly $1/10$ as large. In addition, as noted above, Singer et al. [1982], in the only other study of such events to comment on the radial structure of the events, found a sharp wave cutoff in

association with a plasma density boundary. A more complete determination of wave propagation characteristics, including radial wave numbers and/or wave lengths, must await further study using a set of more closely spaced satellites such as those in the forthcoming CLUSTER program.

As to the spatial pattern of waves that is observed, we speculate that radially polarized Pc 4 pulsations occur between the "inner plasmopause" and the corotation/convection boundary, in the region of plasmaspheric refilling many hours after a ring current injection. A scenario for wave onset is presented in Figure 17, which shows conditions both before and after an expansion of the corotation/convection boundary to beyond synchronous orbit. Increased densities of thermal plasma associated with refilling of the outer plasmasphere will destabilize the marginally stable local ring current population, and cause some of the free energy of the hot particles to be transferred to ULF wave motion. Occurrence in local afternoon/evening might be aided by the often-observed bulging of the corotation/convection boundary during these local times, and by the increased dayside ionospheric/plasmaspheric densities associated with solar illumination. The combination of these factors would expose ring current plasmas trapped at these L shells to the highest concentrations of cold plasma in precisely the regions where Pc 4 pulsations are observed.

Instabilities might also occur outside of the instantaneous plasmopause, in regions of detached cold plasma, as they convect sunward. These regions, like highly structured regions in the outer plasmasphere, are likely to occur on the dayside as a result of variations in the location of the convection/corotation boundary. Our observation on day 84272 of three radially separated wave regions may be an example of this situation. We cannot distinguish between these two possibilities in this study, however, because of the limited frequency resolution of the AMPTE CCE plasma wave instrument: it would not be able to

detect such regions unless they had the large cold plasma densities characteristic of a true inner plasmaspheric distribution. Further, even if flux tubes with detached plasma were to start with rather high density, as they convect sunward with a fixed plasma population the density would decrease because the flux tube volume expands. Because there is at present no means by which to measure the location of the corotation/convection electric field boundary using AMPTE CCE, this matter cannot be explored further using only this data set.

5. SUMMARY AND CONCLUSIONS

Our multi-satellite study has shown that 1) radially polarized pulsations in the equatorial dayside outer magnetosphere occur in radially narrow and often sharply bounded strips extending typically from late morning to dusk; 2) the frequencies of these waves appear to be determined by local conditions; 3) based on the available evidence, waves appear to be confined to the outer plasmasphere (or possibly detached plasma regions as well), and 4) we have found no evidence of a correlation between plasma beta (in the range from 0.23 to 1.09) and wave onset, amplitude, or ratio of compressional to radial components. These characteristics suggest that wave growth and energy dissipation, wave polarization, and pulsation frequency are all greatly dependent on the characteristics of the lowest energy plasmas present in this region and/or along the affected flux tubes, although the presence of more energetic plasma populations may well be a necessary precondition. In agreement with earlier studies, we have found that these pulsations occur during quiet times, when the IMF is radial or northward, usually several days after significant storm or substorm activity. Very low levels of the AE index correlate well with the onset of wave activity in most cases.

The localized and possibly nonpropagating nature of the observed waves suggests that they are caused by a local instability or source of free energy, perhaps triggered by the rapid magnetospheric reconfiguration accompanying outward motion of the convection/corotation boundary. Our observations have many features in common with the conditions required for the onset of bounce resonances and ballooning modes, and specifically the recently proposed drift Alfvén ballooning mode instability. The good correlation of wave onset with drops in the AE index to very low levels suggests that plasmaspheric refilling plays a key role in wave onset. We have noted, however, that further refinement of the available models is needed to account for the sharp spatial boundaries of these events in both L shell and local time; the dayside, longitudinally extended location of the events; and the apparently rapid growth of wave activity despite low beta values. Further multisatellite observations, including accurate determination of densities of both cold and hot plasma populations, will also be needed to confirm the association of these wave regions with outer plasmaspheric boundaries and bounce resonant energetic ions.

ACKNOWLEDGEMENTS

We thank the AMPTE project office and science team for the successful operation of the AMPTE satellite mission. We also thank K. Takahashi for providing the GOES 5 and 6 magnetic field data, G. Gloeckler for providing the AMPTE CCE CHEM proton data used to calculate beta, H. Luehr and W. Baumjohann for providing AMPTE IRM magnetic field and particle data, R. Treumann and R. Anderson for providing AMPTE IRM plasma wave data, and F. J. Rich for providing values of the DMSP auroral boundary index. Discussions with L. Chen, C. Z. Cheng, R. H. Comfort, C. T. Russell, G. Haerendel, and D. J. Southwood are also gratefully acknowledged. Both referees provided helpful suggestions which improved the quality of the presentation. This research was

supported by NASA under Grant NAGW-1567 to Augsburg College and under Task I of contract N00039-87-C-5301 to The Johns Hopkins University Applied Physics Laboratory and by subcontract to Augsburg College; efforts at UCLA were supported by NASA grant NAG5-863; and work at Lockheed was supported by NASA under contracts NAS5-30565 and NAS5-31213.

REFERENCES

- Anderson, B. J., M. J. Engebretson, S. P. Rounds, L. J. Zanetti, and T. A. Potemra, A statistical study of Pc 3-5 pulsations observed by the AMPTE/CCE magnetic fields experiment, 1, Occurrence distributions, J. Geophys. Res., 95, 10495, 1990.
- Anderson, B. J., T. A. Potemra, L. J. Zanetti, and M. J. Engebretson, Statistical correlations between Pc 3-5 pulsations and solar wind/IMF parameters and geomagnetic indices, Physics of Space Plasmas (1990), SPI Conference Proceedings and Reprint Series, Vol. 10, T. Chang, G. B. Crew, and J. R. Jasperse, eds., Scientific Publishers Inc., Cambridge, MA, 419, 1991.
- Arthur, C. W., and R. L. McPherron, The statistical character of Pc 4 magnetic pulsations at synchronous orbit, J. Geophys. Res., 86, 1325, 1981.
- Barfield, J. N., and R. L. McPherron, Statistical characteristics of storm-associated Pc 5 micropulsations observed at the synchronous equatorial orbit, J. Geophys. Res., 77, 4720, 1972.
- Barfield, J. N., and R. L. McPherron, Stormtime Pc 5 magnetic pulsations observed at synchronous orbit and their correlation with the partial ring current, J. Geophys. Res., 83, 739, 1978.
- Chappell, C. R., K. K. Harris, and G. W. Sharp, The dayside of the plasmasphere, J. Geophys. Res., 31, 7632, 1971.
- Chen, L., and A. Hasegawa, On magnetospheric hydromagnetic waves excited by energetic ring-current particles, J. Geophys. Res., 93, 8763, 1988.
- Chen, L., and A. Hasegawa, Kinetic theory of geomagnetic pulsations, 1,

Internal excitations by energetic particles, *J. Geophys. Res.*, 96, 1503, 1991.

Chen, L., Theory of ultra-low-frequency magnetic pulsations in the earth's magnetosphere, Technical report PPPL-2742, Princeton Plasma Physics Laboratory, Princeton, NJ, March, 1991.

Cheng, C. Z., K. Takahashi, and A. T. Y. Lui, Correlation between ULF wave events and instability conditions obtained from AMPTE CCE particle data, *EOS Trans. AGU*, 72, 255, 1991.

Cummings, W. D., R. J. O'Sullivan, and P. J. Coleman, Jr., Standing Alfvén Waves in the Magnetosphere, *J. Geophys. Res.*, 74, 778, 1969.

Engebretson, M. J., L. J. Zanetti, T. A. Potemra, W. Baumjohann, H. Luehr, and M. H. Acuna, Simultaneous observation of Pc 3-4 pulsations in the solar wind and in the earth's magnetosphere, *J. Geophys. Res.*, 92, 10053, 1987.

Engebretson, M. J., L. J. Zanetti, T. A. Potemra, D. M. Klumpp, R. J. Strangeway, and M. H. Acuna, Observations of intense ULF pulsation activity near the geomagnetic equator during quiet times, *J. Geophys. Res.*, 93, 12795, 1988.

Engebretson, M. J., N. Lin, W. Baumjohann, H. Luehr, B. J. Anderson, L. J. Zanetti, T. A. Potemra, R. L. McPherron, and M. G. Kivelson, A comparison of ULF fluctuations in the solar wind, magnetosheath, and dayside magnetosphere, 1, Magnetosheath morphology, *J. Geophys. Res.*, 96, 3441, 1991.

Gloeckler, G., F. M. Ipavich, W. Studemann, B. Wilken, D. C. Hamilton, G.

- Kremser, D. Hovestadt, F. Gliem, R. A. Lundgren, W. Rieck, E. O. Tums, J. C. Cain, L. S. MaSung, W. Weiss, and P. Winterhof, The Charge-Energy-Mass Spectrometer for 0.3-300 keV/e ions on the AMPTE CCE, IEEE Trans. Geosci. Remote Sens., GE-23, 234, 1985.
- Grubb, R. N., The SMS/GOES space environment monitor subsystem, NOAA Tech. Memo. SEL-42, Space Environment Laboratory, Boulder, CO, 80303, 1975.
- Gussenhoven, M. S., D. A. Hardy, and W. J. Burke, DMSP/F2 electron observations of equatorward auroral boundaries and their relationship to magnetospheric electric fields, J. Geophys. Res., 86, 768, 1981.
- Horwitz, J. L., S. Menteer, J. Turnley, J. L. Burch, J. D. Winningham, C. R. Chappell, J. D. Craven, L. A. Frank, and D. W. Slater, Plasma boundaries in the inner magnetosphere, J. Geophys. Res., 91, 8861, 1986.
- Horwitz, J. L., R. H. Comfort, and C. R. Chappell, A statistical characterization of plasmasphere density structure and boundary locations, J. Geophys. Res., 95, 7937, 1990.
- Horwitz, J. L., and N. Singh, Refilling of the earth's plasmasphere, EOS Trans. AGU, 72, 399, 1991.
- Hughes, W. J., R. L. McPherron, and J. N. Barfield, Geomagnetic pulsations observed simultaneously on three geostationary satellites, J. Geophys. Res., 83, 1109, 1978.
- Kokubun, S., Statistical characteristics of Pc 5 waves at geostationary orbit, J. Geomag. Geoelectr., 37, 759, 1985.
- Kokubun, S., K. N. Erickson, T. A. Fritz, and R. L. McPherron, Local time

asymmetry of Pc 4-5 pulsations and associated particle modulations at synchronous orbit, *J. Geophys. Res.*, 94, 6607, 1989.

Lakhina, G. S., M. Mond, and E. Hameiri, Ballooning mode instability at the plasmapause, *J. Geophys. Res.*, 95, 4007, 1990.

Lee, Y. C., and L. J. Cahill, Jr., Quiet time inflation of the inner magnetosphere in the afternoon and evening quadrants, *J. Geophys. Res.*, 80, 1003, 1975.

Lin, N., M. J. Engebretson, R. L. McPherron, M. G. Kivelson, W. Baumjohann, H. Luehr, T. A. Potemra, B. J. Anderson, and L. J. Zanetti, A comparison of ULF fluctuations in the solar wind, magnetosheath, and dayside magnetosphere, 2, Field and plasma conditions in the magnetosheath, *J. Geophys. Res.*, 96, 3455, 1991.

Madden, D., and M. S. Gussenhoven, Auroral Boundary Index from 1983 to 1990, GL-TR-90-0358, Environmental Research Papers No. 1075, Space Physics Division, Geophysics Laboratory, Hanscom AFB, MA, 1990.

McEntire, R. W., E. P. Keath, D. E. Fort, A. T. Y. Lui, and S. M. Krimigis, The medium-energy particle analyzer on the AMPTE CCE spacecraft, *IEEE Trans. Geosci. Remote Sens.*, GE-2a3, 246, 1985.

Miura, A., S. Ohtani, and T. Tamao, Ballooning instability and structure of diamagnetic hydromagnetic waves in a model magnetosphere, *J. Geophys. Res.*, 94, 15231, 1989.

Ohtani, S., A. Miura, and T. Tamao, Coupling between Alfvén and slow magnetosonic waves in an inhomogeneous finite-beta plasma, I, Coupled equations and physical mechanism, *Planet. Space Sci.*, 37, 567, 1989.

- Ohtani, S., A. Miura, and T. Tamao, Coupling between Alfvén and slow magnetosonic waves in an inhomogeneous finite-beta plasma, II, Eigenmode analysis of localized ballooning-interchange instability, *Planet. Space Sci.*, 37, 579, 1989.
- Olsen, R. C., Equatorially trapped plasma populations, *J. Geophys. Res.*, 86, 11235, 1981.
- Olsen, R. C., S. D. Shawhan, D. L. Gallagher, J. L. Green, C. R. Chappell, and R. R. Anderson, Plasma observations at the earth's magnetic equator, *J. Geophys. Res.*, 92, 2385, 1987.
- Orr, D., and J. A. D. Matthew, The variation of geomagnetic micropulsation periods with latitude and the plasmapause, *Planet. Space Sci.*, 19, 897, 1971.
- Pangia, M. J., C. S. Lin, and J. N. Barfield, A correlative study of Pc 5 magnetic pulsations with substorm onsets, *J. Geophys. Res.*, 95, 10699, 1990.
- Potemra, T. A., L. J. Zanetti, and M. H. Acuna, The AMPTE/CCE magnetic field experiment, *IEEE Trans. Geosci. Remote Sens.*, GE-23, 246, 1985.
- Rostoker, G., H.-L. Lam, and J. V. Olson, Pc 4 giant pulsations in the morning sector, *J. Geophys. Res.*, 84, 5153, 1979.
- Russell, C. T., and M. M. Hoppe, Upstream waves and particles, *Space Sci. Rev.*, 34, 155, 1983.
- Scarf, F. L., The AMPTE/CCE plasma wave investigation, *IEEE Trans. Geosci. Remote Sens.*, GE-23, 250, 1985.

- Shelley, E. G., A. Ghielmetti, E. Hertzberg, S. J. Battel, K. Altwegg-von Burg, and H. Balsiger, The AMPTE/CCE hot plasma composition experiment (HPCE), IEEE Trans. Geosci. Remote Sens., GE-23, 241, 1985.
- Singer, H. J., W. J. Hughes, and C. T. Russell, Standing hydromagnetic waves observed by ISEE 1 and 2: Radial extent and harmonic, J. Geophys. Res., 87, 3519, 1982.
- Singh, N., and K. S. Hwang, Perpendicular ion heating effects on the refilling of the outer plasmaphere, J. Geophys. Res., 92, 13513, 1987.
- Southwood, D. J., A general approach to low-frequency instability in the ring current plasma, J. Geophys. Res., 81, 3340, 1976.
- Southwood, D. J., and M. G. Kivelson, Charged particle behavior in low-frequency geomagnetic pulsations, 1, Transverse waves, J. Geophys. Res., 86, 5643, 1981.
- Takahashi, K., and R. L. McPherron, Standing hydromagnetic oscillations in the magnetosphere, Planet. Space Sci., 32, 1343, 1984.
- Takahashi, K., P. R. Higbie, and D. N. Baker, Energetic electron flux pulsations observed at geostationary orbit, Relation to magnetic pulsations, J. Geophys. Res., 90, 8308, 1985.
- Takahashi, K., R. W. McEntire, A. T. Y. Lui, and T. A. Potemra, Ion flux oscillations associated with a radially polarized transverse Pc 5 magnetic pulsation, J. Geophys. Res., 95, 3717, 1990.
- Tamao, T., Interaction of energetic particles with HM-waves in the magnetosphere, Planet. Space Sci., 32, 1371, 1984.

- Taylor, J. P. H., and A. D. M. Walker, Accurate approximate formulas for toroidal standing hydromagnetic oscillations in a dipolar geomagnetic field, Planet. Space Sci., 32, 1119, 1984.
- Vinas, A. F., and T. R. Madden, Shear flow-ballooning instability as a possible mechanism for hydromagnetic fluctuations, J. Geophys. Res., 91, 1519, 1986.

FIGURE CAPTIONS

Figure 1: Magnetic field components from AMPTE CCE from 1700 to 1900 UT September 2, 1984 (day 84246). From top to bottom the field components shown are radial (BR); azimuthal, or magnetically eastward (BE); and parallel to the earth's dipole axis, or magnetically northward (BN).

Figure 2: AE and A_0 (defined as $(AU + AL)/2$) Geomagnetic indices for September 2, 1984 (day 84246). The times of wave observations by GOES 5, GOES 6, and AMPTE CCE are also indicated.

Figure 3: Magnetic local time — L value plot of the AMPTE CCE, GOES 5, and GOES 6 satellite orbits from 1600 UT to 2200 UT September 2, 1984 (day 246). Regions of observed radially polarized oscillations are highlighted.

Figure 4: Radial components of the magnetic fields observed by GOES 5, GOES 6, and AMPTE CCE from 1700 to 1900 UT September 2, 1984 (day 84246). A sliding average has again been subtracted from the data before plotting.

Figure 5: Magnetic local time — L value plot of the AMPTE CCE, GOES 5, and GOES 6 satellite orbits from 1800 UT September 4, 1984 (day 84248) to 0400 UT September 5, 1984 (day 84249). Regions of observed oscillations are highlighted.

Figure 6: AE and A_0 geomagnetic indices for September 4–5, 1984 (days 84248–9), as in Figure 2.

Figure 7: Magnetic field waveform plot of the radial component of the AMPTE

CCE, GOES 5, and GOES 6 satellites covering approximately the same spatial (local time) region, but at successively later times September 4–5, 1984 (days 84248–84249). The GOES 5 plot is from 2000 to 2200 UT September 4; the GOES 6 plot is from 2130 to 2330 UT September 4, and the AMPTE CCE plot is from 0100 to 0300 September 5.

Figure 8: Magnetic local time — L value plot of the AMPTE CCE, GOES 5, and GOES 6 satellite orbits from 1400 UT September 6, 1984 (day 84250) to 0200 UT September 7, 1984 (day 84251). Regions of observed oscillation are highlighted.

Figure 9: Stacked dynamic power spectra from GOES 5, GOES 6, and AMPTE CCE. Each panel shows color-coded wave power of differenced radial component data vs. frequency and UT from 1400 September 6, 1984, to 0200 UT September 7, 1984.

Figure 10: AE and A_0 geomagnetic indices for September 6–7, 1984 (days 84250–1), as in Figure 2.

Figure 11: Radial components of the magnetic fields observed by GOES 5, GOES 6, and AMPTE CCE from 1500 to 2000 UT September 6, 1984 (day 84250).

Figure 12: Magnetic local time — L value plot of the GOES 5 and GOES 6 satellite orbits from 2000 to 2400 UT September 26, 1984 (day 84270) and of the AMPTE CCE satellite orbit from 2000 UT to 0800 UT the following day. Regions of observed oscillations are highlighted.

Figure 13: AE and A_0 geomagnetic indices for September 26–28, 1984 (days 84270–2), as in Figure 2.

Figure 14: Magnetic local time — L value plot of the AMPTE CCE, GOES 5, and GOES 6 satellite orbits from 1400 to 2400 UT September 27, 1984

(day 84271). Regions of observed oscillation are highlighted.

Figure 15: Magnetic local time — L value plot of portions of the AMPTE CCE, GOES 5, and GOES 6 satellite orbits during September 28, 1984 (day 84272). Times and regions of observed oscillation are highlighted.

Figure 16: Wave amplitudes at 30 and 178 kHz for three plasmopause crossings. The base 10 logarithm of the wave amplitude ($V/m/Hz^5$) is shown as a function of Universal Time for three plasmopause crossings where density structures may be present. The vertical arrows mark the times of the 10 and 400 cm^{-3} density levels as given in Table 1, assuming the signatures correspond to Upper Hybrid Resonance (UHR) waves. The passes on days 251 and 270 clearly show additional UHR waves at 30 kHz outside of the region indicated as the 10 cm^{-3} density level.

Figure 17: Schematic diagram of conditions before and after the onset of dayside radially polarized Pc 4 pulsations. A satellite is shown near synchronous orbit and the geomagnetic equator. A sharp drop in the AE index causes an expansion of the corotation/convection boundary outward beyond the satellite, and initiates plasmaspheric refilling which destabilizes the marginally stable ring current.

Table 1: Plasma density estimates inferred from AMPTE OCE Plasma Wave Data

DATE, UT, leg	P-P R _E range	Amp (nT)	Br/Bn	Plasma Beta	Location of 400 cm ⁻³	Location of 10 cm ⁻³
84248 1800 UT outbound	6.0-6.8	2-3 1-2 1-3	CCE: >=2 G5: 1 G6: 3	.29- .41	1610 UT L = 3.9 LMT = 10.1	No signal
84249 0200 UT inbound	6.4-7.3	3-6 4-8 4-8	CCE: >=3 G5: 3 G6: 3	.72- 1.09	0445 UT L = 2.8 LMT = 18.3	No clear signal. Main density gradient observed after 0315 UT (L = 5.5, LMT = 16.1)
84250 1600 UT outbound	5.2-6.8	2 2-7 1-6	CCE: >=3 G5: >3 to 2 G6: >3 to 1	.25- .31	1350 UT L = 3.4 LMT = 9.3	no signal
84251 0100 UT inbound	6.9-7.7	2	CCE: >5	.51- .60	0345 UT L = 2.7 LMT = 18.5	0200-0230 UT and ~0100 UT L = 5.0-5.7 L = 6.9 LMT = 16.4-15.9 LMT = 15.3
84270 2200 UT outbound	6.6-8.2	2 1-7 1-6	CCE: >5 G5: 2 G6: 2 to 1	.62- .75	1900 UT L = 2.8 LMT = 8.1	1950-2015 UT and 2030-2200 UT L = 4.4-5.1 L = 5.4-7.1 LMT = 9.7-10.2 LMT = 10.4-11.3
84271 0600 UT inbound	6.1-8.0	4-10	CCE: >5 to 2	.23- .39	0850 UT L = 3.4 LMT = 17.0	?? 0620 UT Very weak signal L = 7.2 LMT = 14.4
84271 2200 UT inbound	6.7-7.8	3-7 2-6 2-6	CCE: >5 to 3 G5: 3 to 2 G6: 3 to 2	.41- .81	2450 UT L = 2.5 LMT = 17.9	2215-2300 UT L = 5.7-6.7 LMT = 14.9-14.5
84272 1400 UT inbound	4.6-5.0, 5.8-6.4, 7.4-7.5	2-4 3-6	CCE: >5 G5: >5 to 3	.43- .68	1600 UT L = 3.6 LMT = 16.5	1415-1440 UT Complex Structure L = 5.8-6.3 LMT = 14.9-14.6
84272 1900 outbound	5.3-5.8	1 2-5 2-8	CCE: >3 to 2 G5: >3 to 1 G6: >3 to 1	.33- .43	1805 UT L = 3.0 LMT = 8.3	1900-1945 UT L = 4.8-5.9 LMT = 9.8-10.5

Table 2: Periods and inferred equatorial plasma densities for the pulsation events studied. Where necessary, AMPTE CCE entries are labeled as outbound (ob) or inbound (inb).

EVENT	SATELLITE	L SHELL	PERIOD (s)	DENSITY (cm ⁻³)
1	GOES 5	6.9	60-65	3.7 - 4.4
	GOES 6	6.8	57	3.8
	AMPTE CCE	6.2	55	7.5
		6.6	62	5.7
2	GOES 5	6.9	167-200	29.0 - 41.6
	GOES 6	6.8	167-200	32.7 - 46.9
	AMPTE CCE	6.8	50-67	2.9 - 5.3
3	GOES 5	6.9	52-86	2.8 - 7.7
	GOES 6	6.8	60-75	4.2 - 6.6
	AMPTE CCE	5.2	35	12.8
		(ob, inb) 6.8	67	5.3
4	GOES 5	6.9	100-125	10.4 - 16.3
	GOES 6	6.8	60-66	4.2 - 5.1
	AMPTE CCE (ob)	7.0	60	3.3
		(inb) 8.0	85-90	2.3 - 2.5
		6.1	85-90	20.5 - 23.0
5	GOES 5	6.9	55	3.1
	GOES 6	6.8	55	3.5
	AMPTE CCE	7.0	59	3.2
6	GOES 5	6.9	55-83	3.1 - 7.2
	GOES 6	6.8	53-125	3.3 - 18.3
	AMPTE CCE (inb)	7.4	55	1.8
		6.2	50	6.2
		4.8	33	22.0
		(ob) 5.6	30	5.1

AMPTE CCE MAGNETOMETER 84246

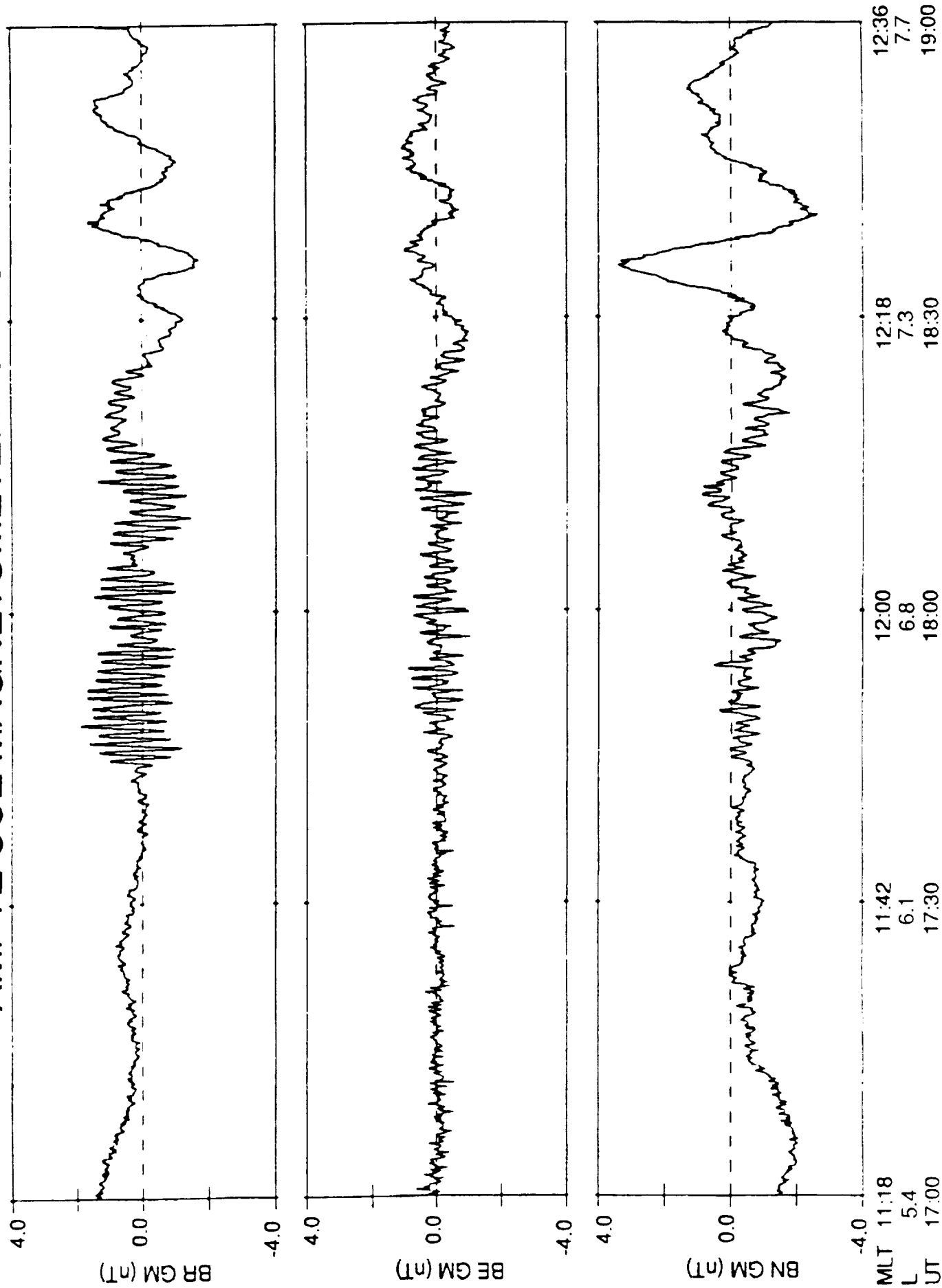


Figure 1

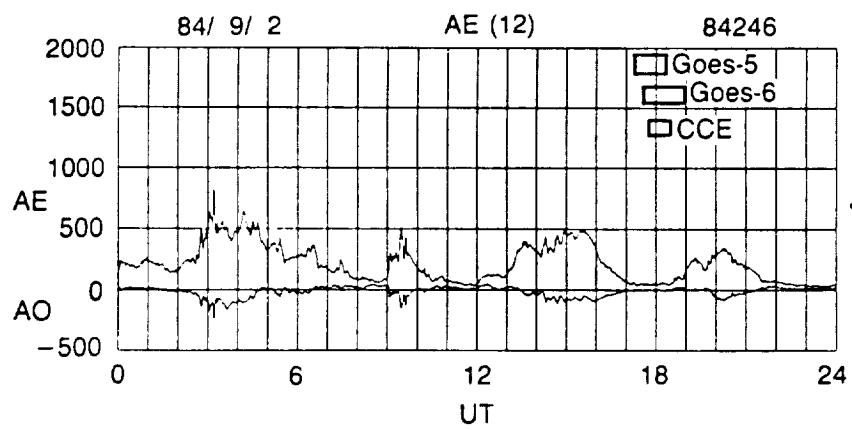


Figure 2

AMPTE CCE-GOES 5,6 ORBITS 12

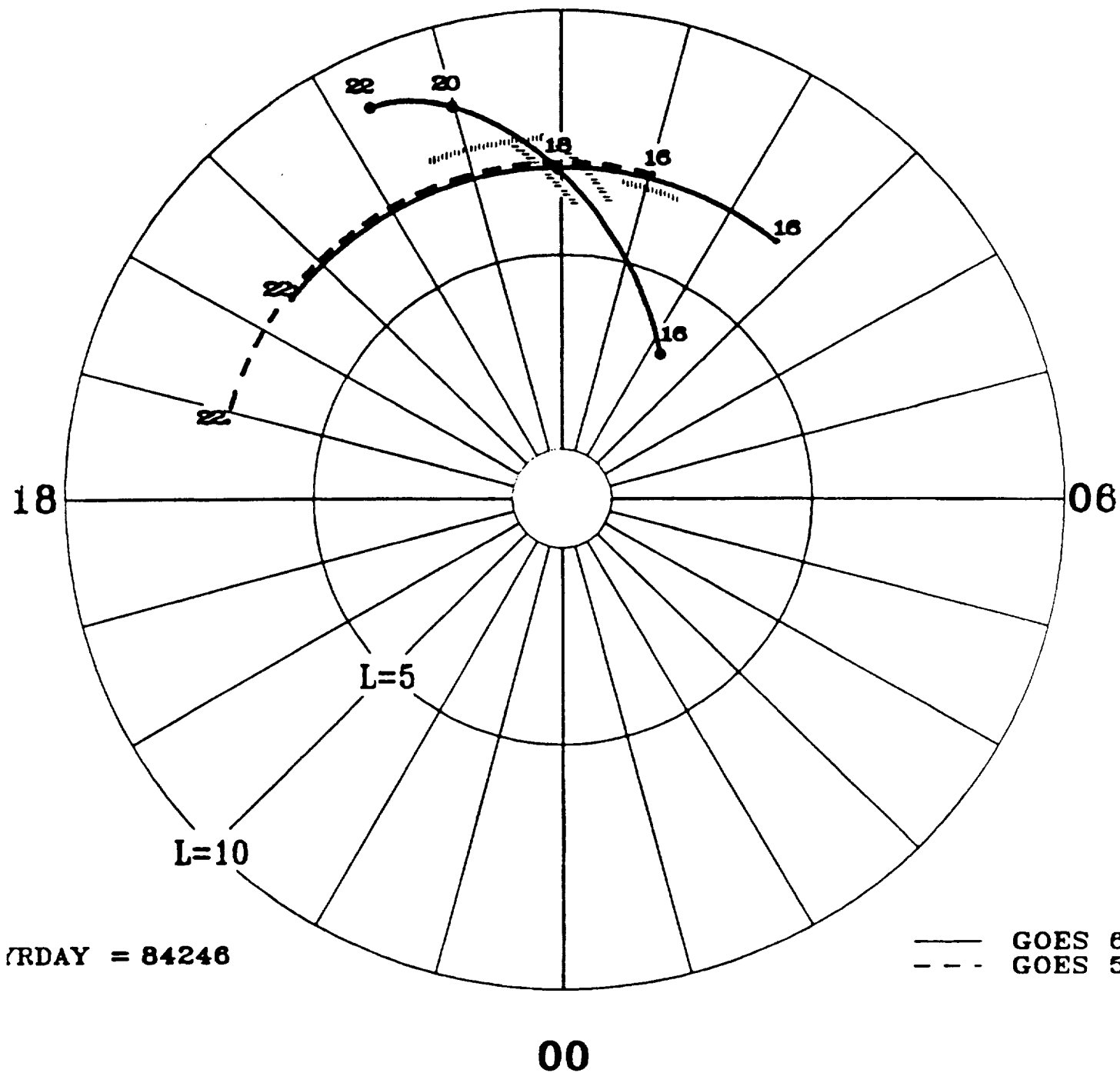


Figure 3

SEPTEMBER 2, 1984 84246

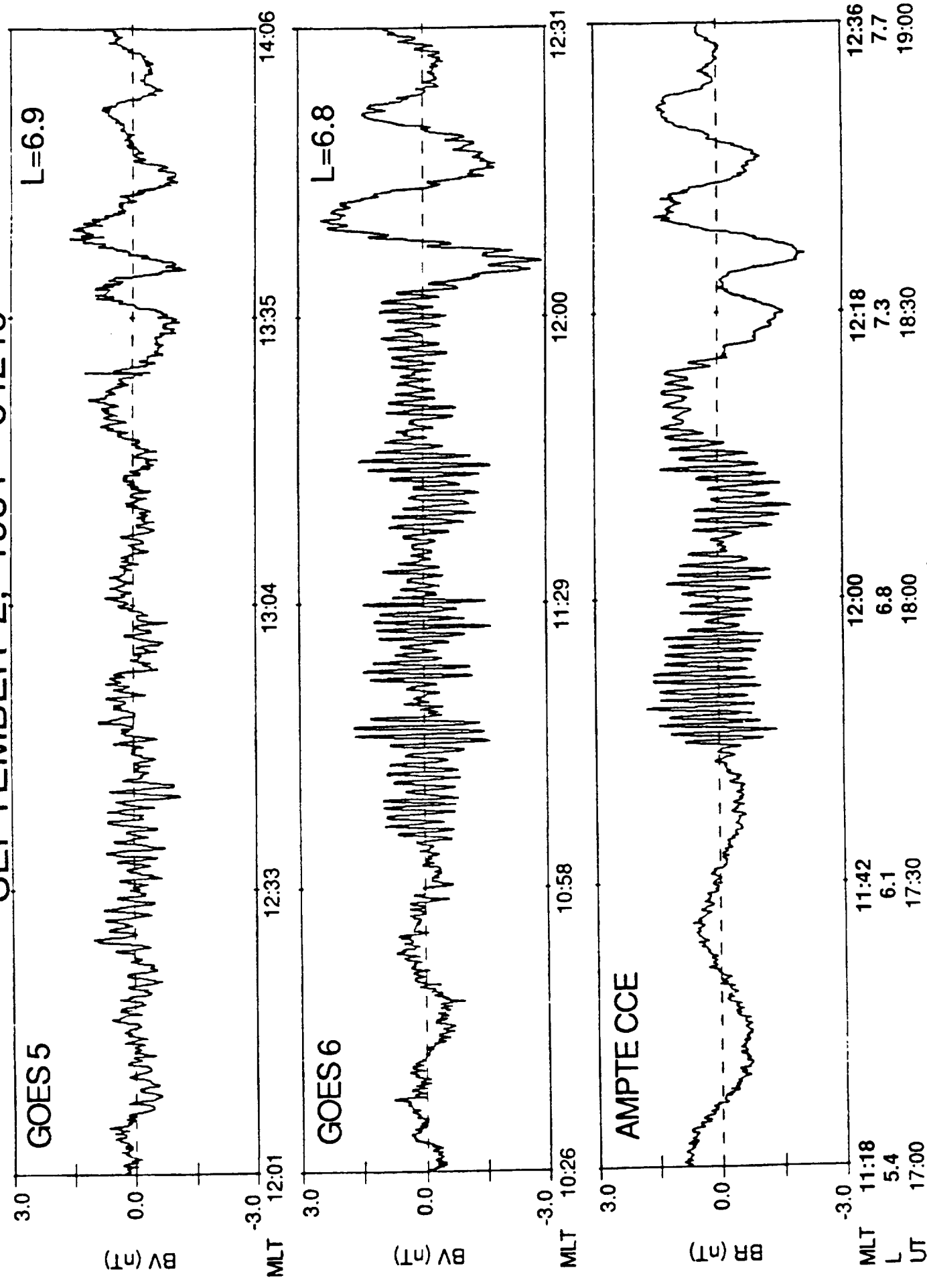


Figure 4

AMPTE CCE-GOES 5,6 ORBITS 12

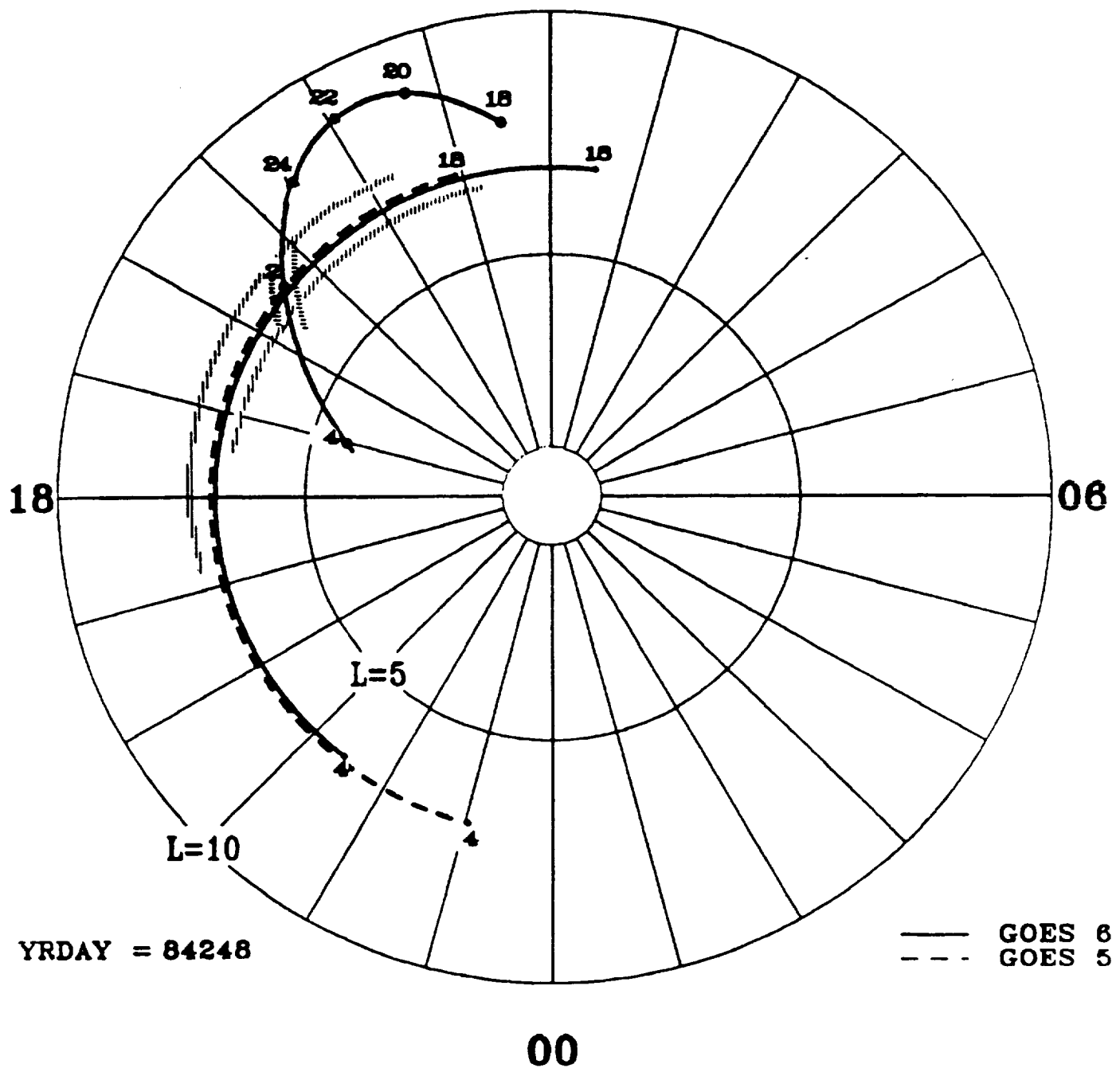


Figure 5

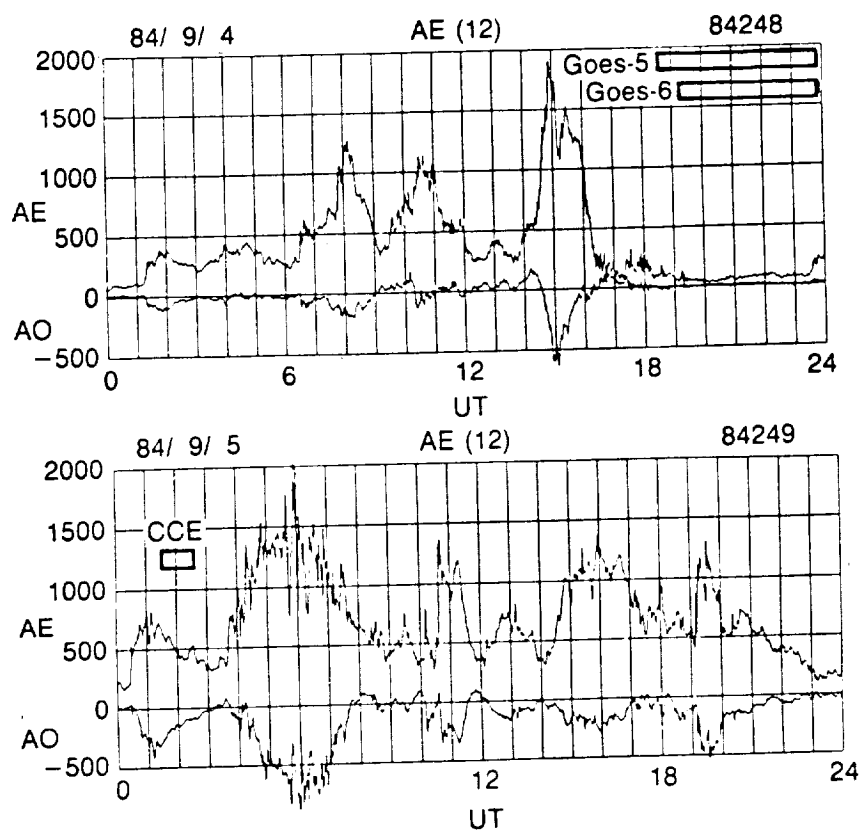


Figure 6

SEPTEMBER 4, 1984 84248

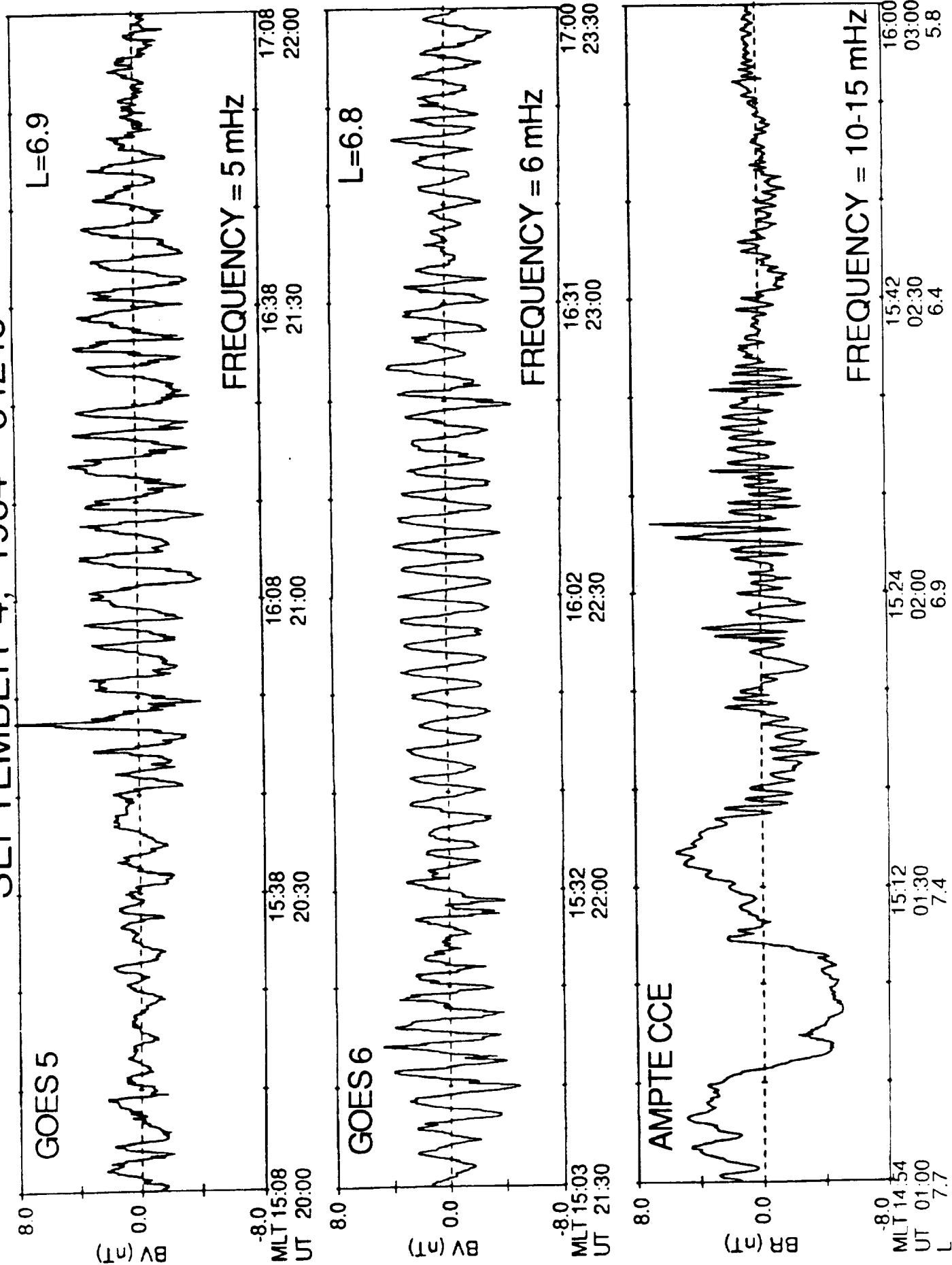


Figure 7

AMPTE CCE-GOES 5,6 ORBITS 12

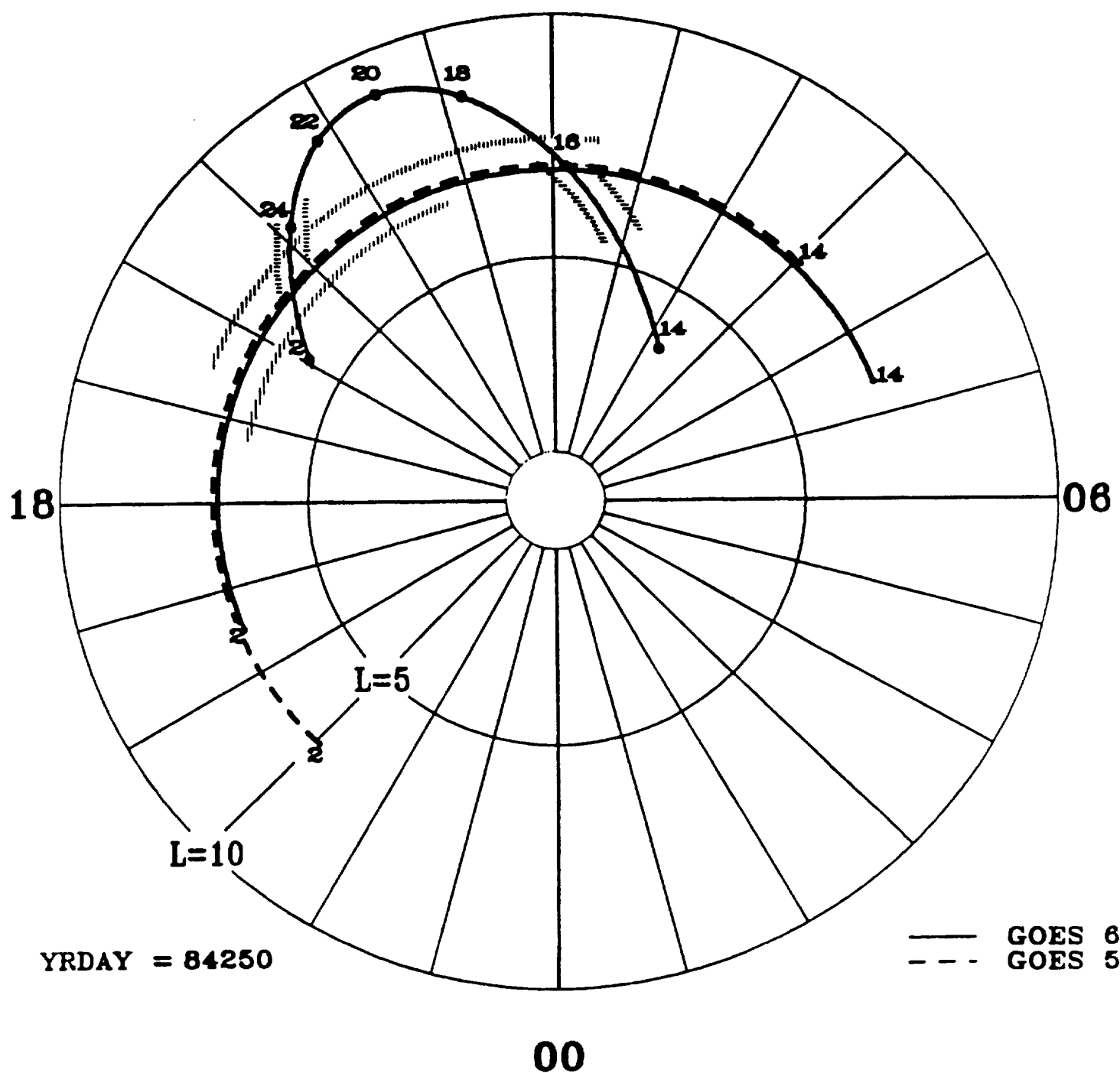


Figure 8

84250 September 6, 1984

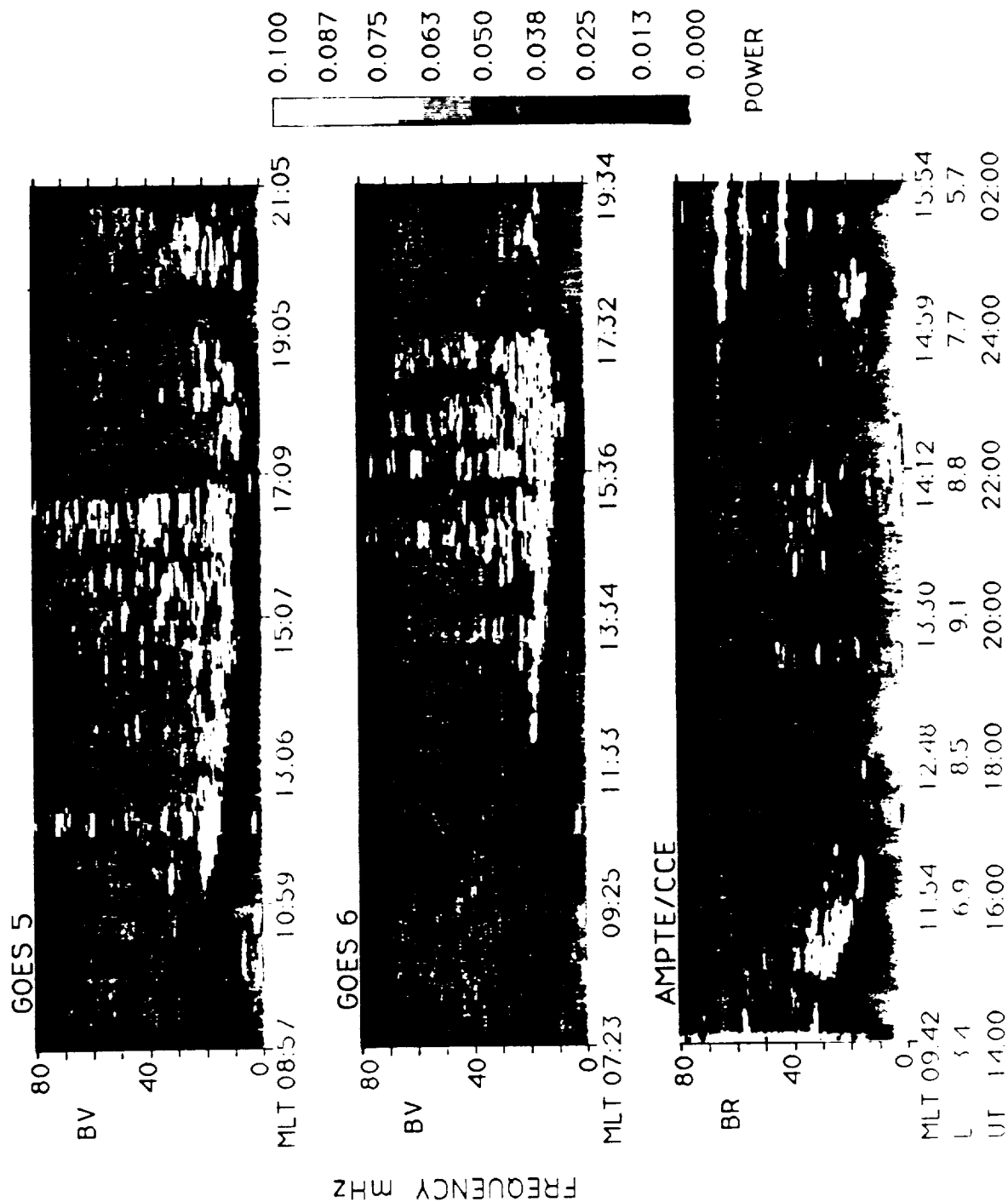


Figure 9

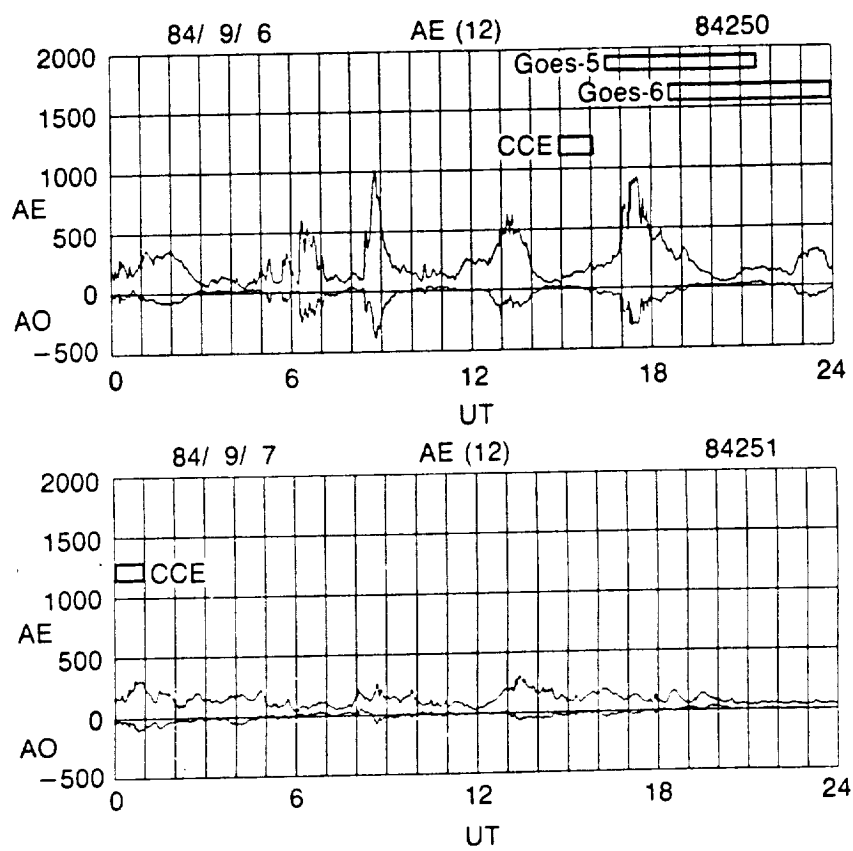


Figure 10

SEPTEMBER 6, 1984 84250

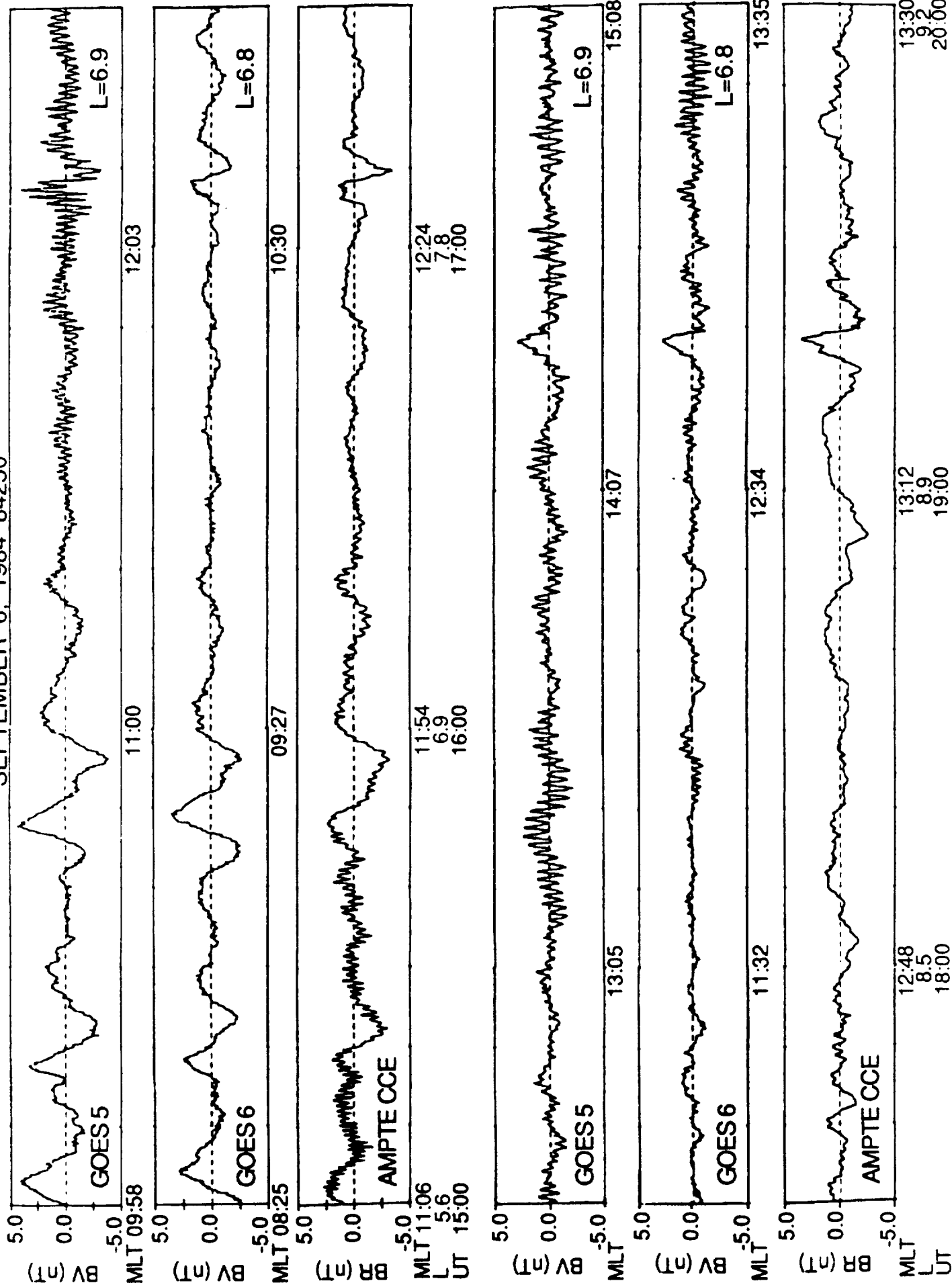


Figure 11

AMPTE CCE-GOES 5,6 ORBITS 12

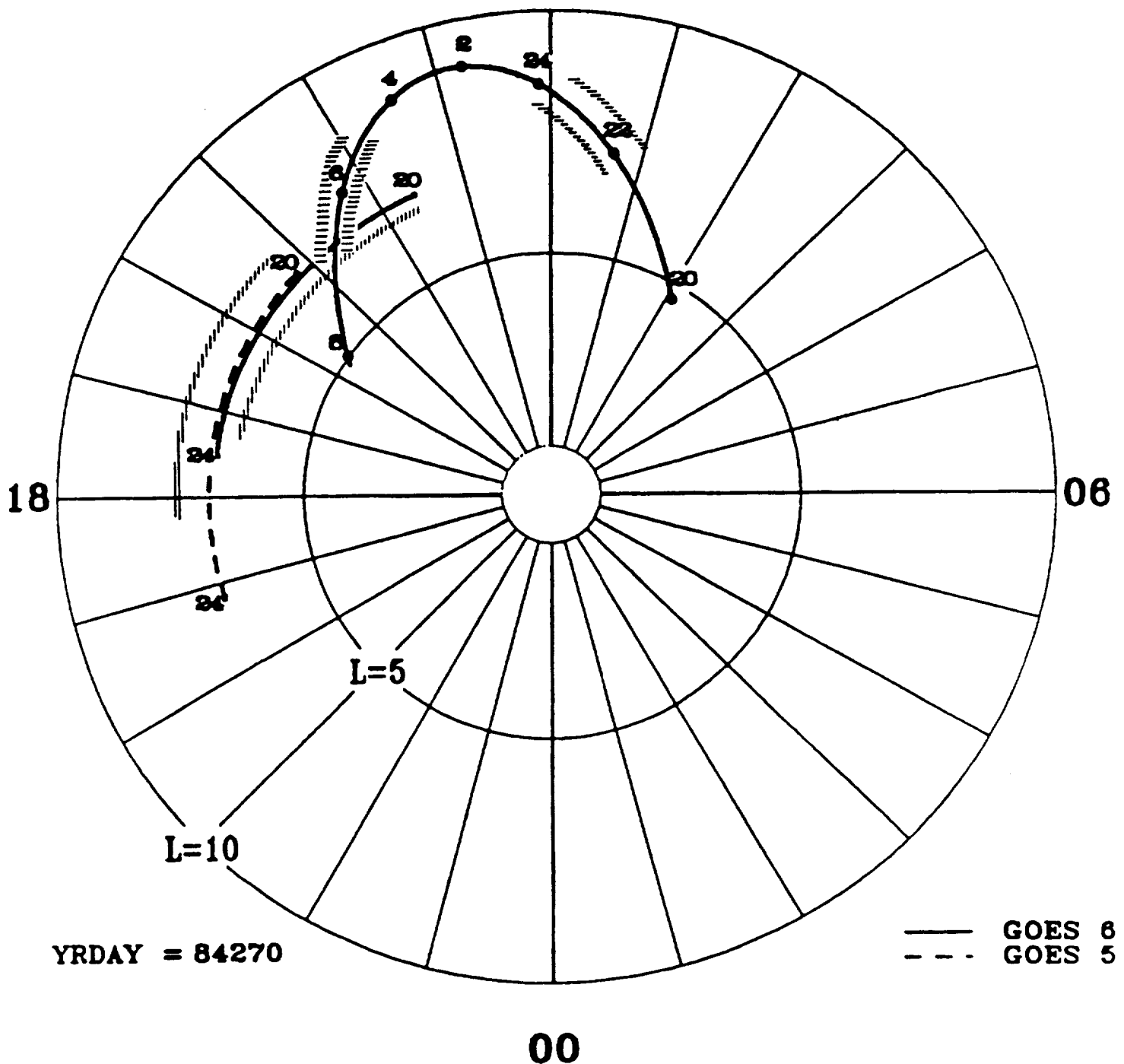


Figure 12

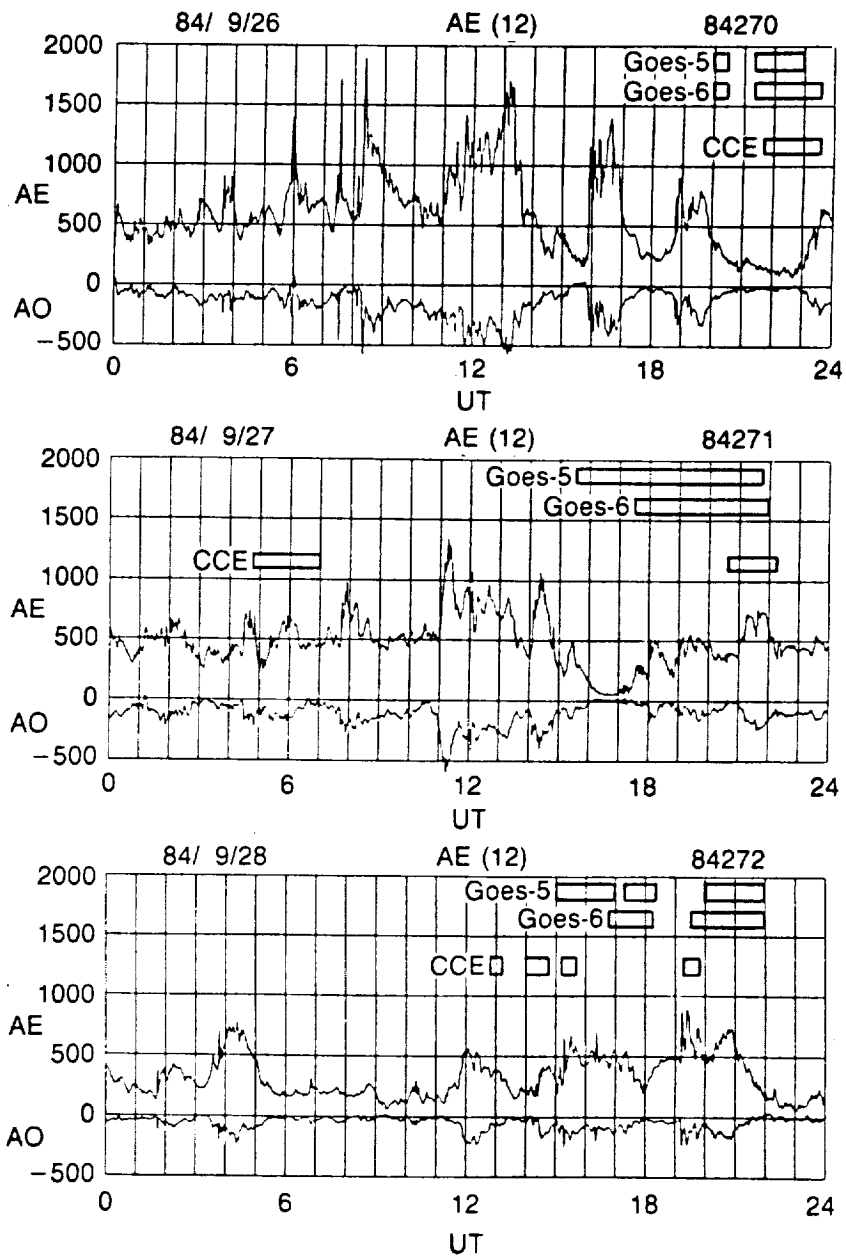


Figure 13

Figure 13

AMPTE CCE-GOES 5,6 ORBITS 12

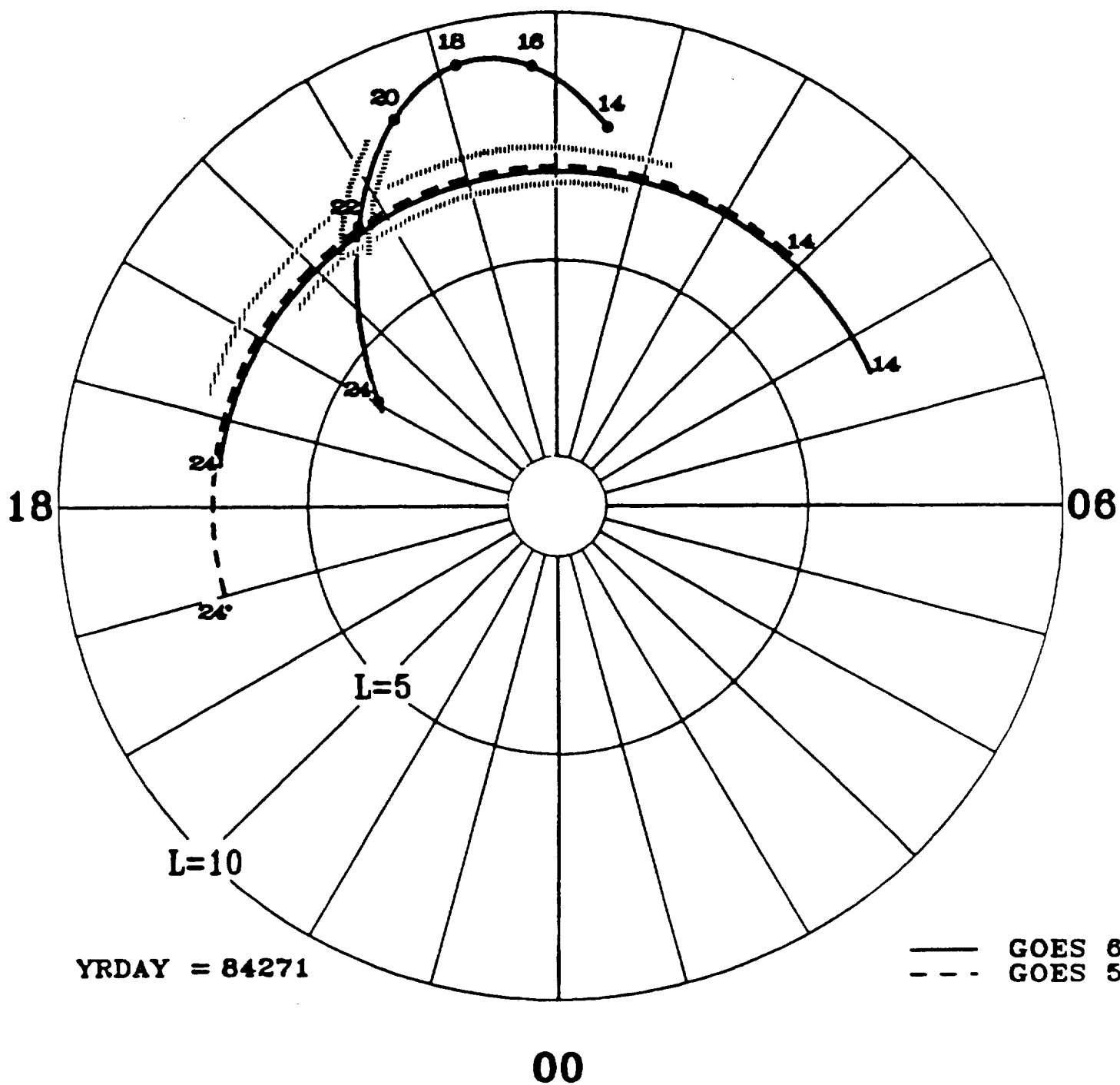


Figure 14

AMPTE CCE-GOES 5,6 ORBITS 12

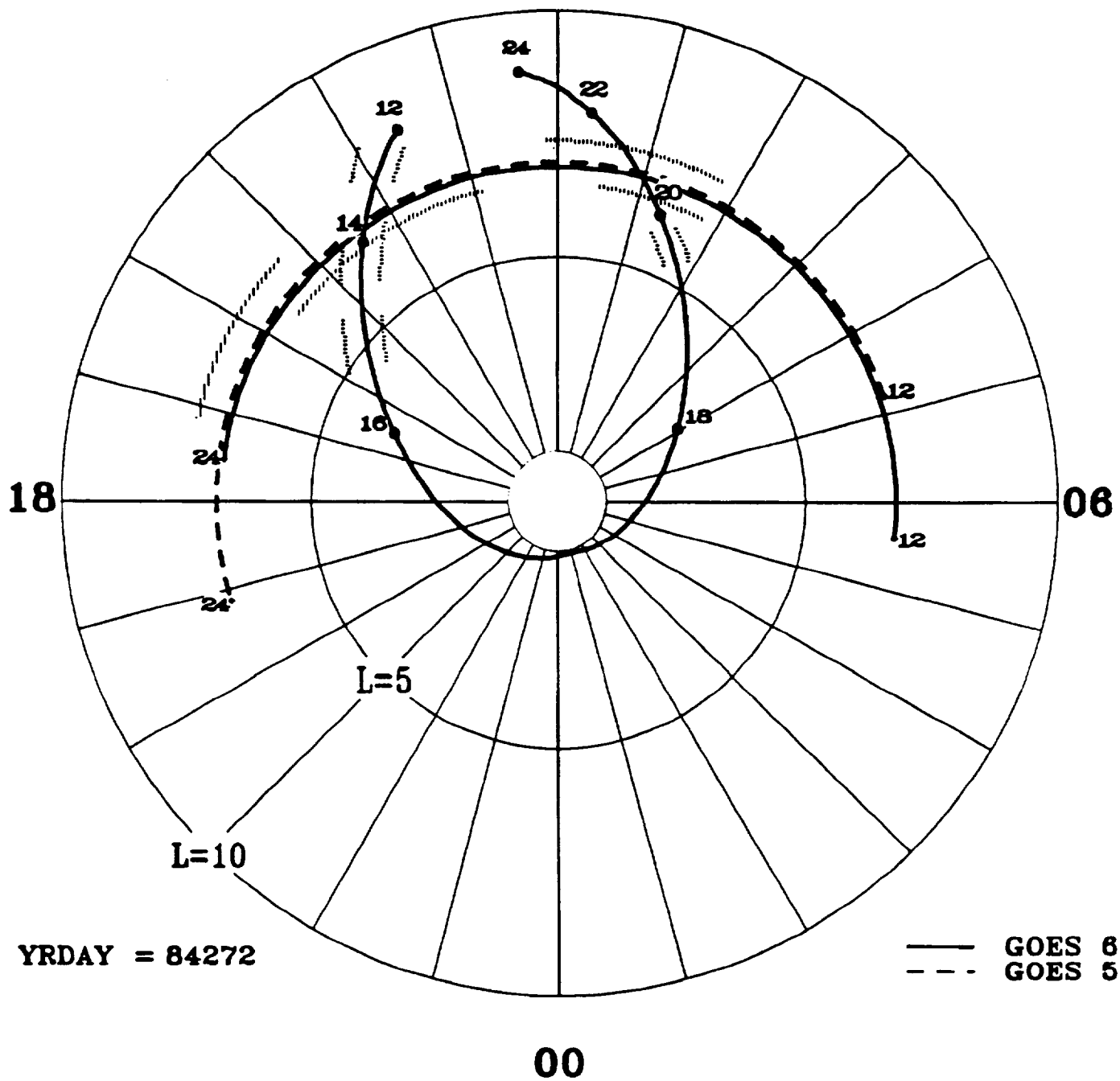


Figure 15

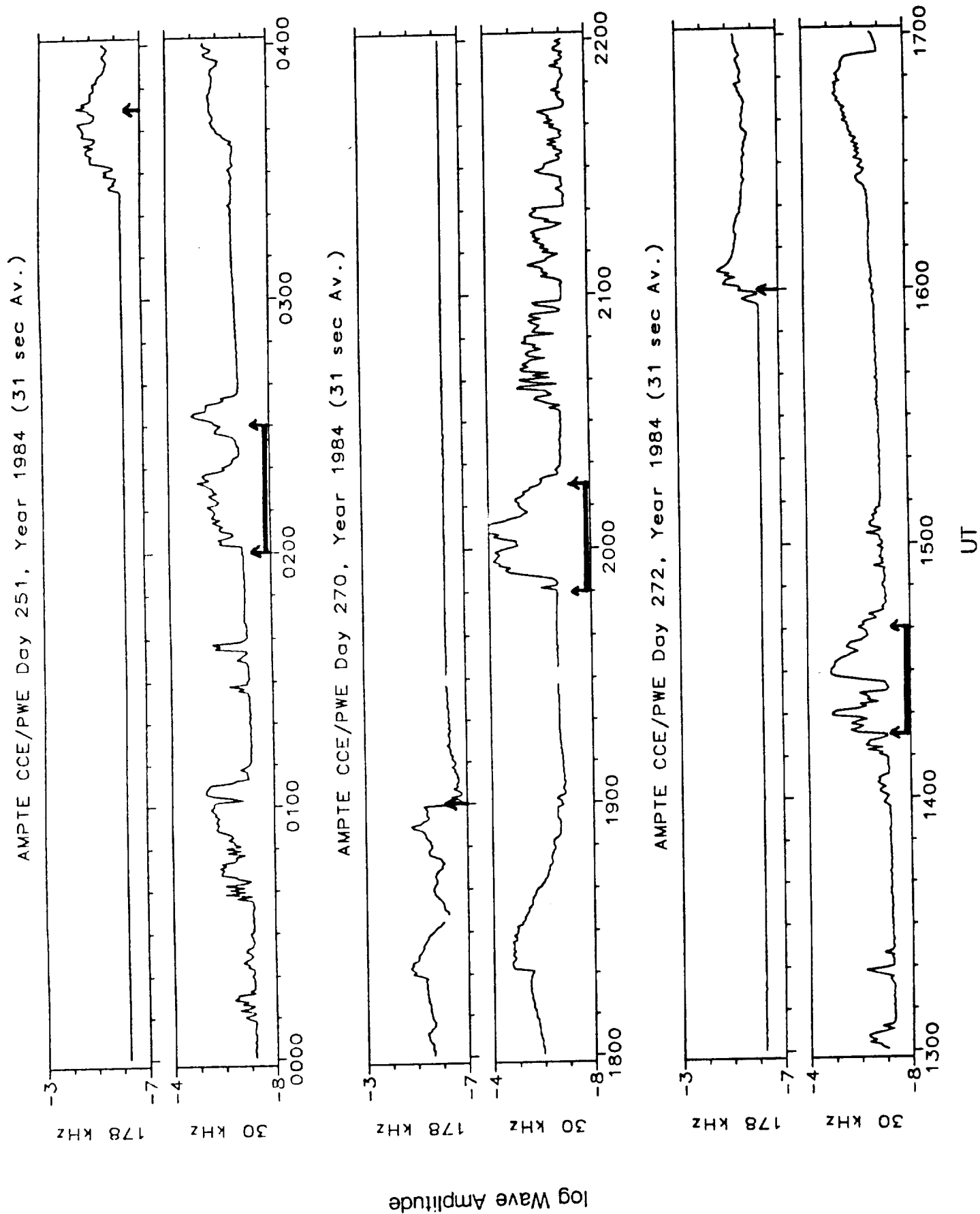
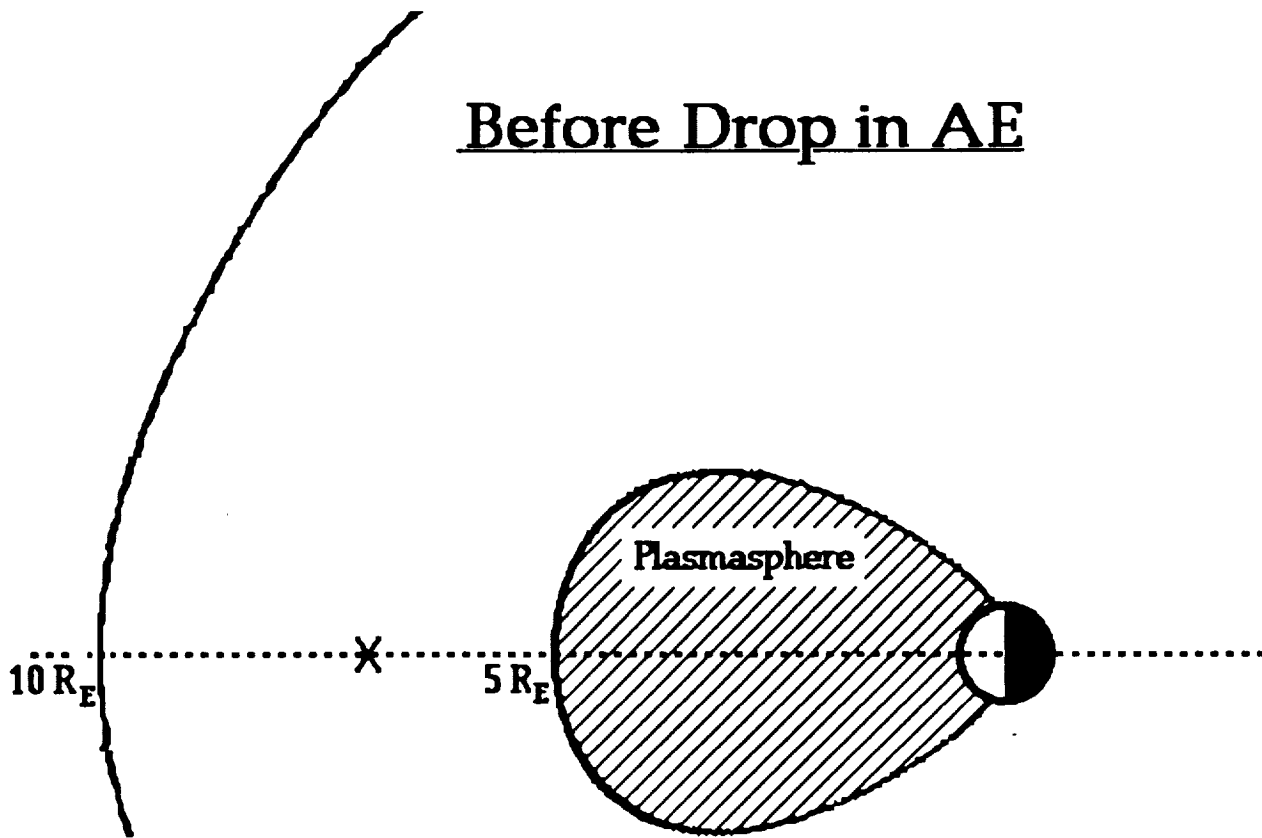


Figure 16

Before Drop in AE



After Drop in AE

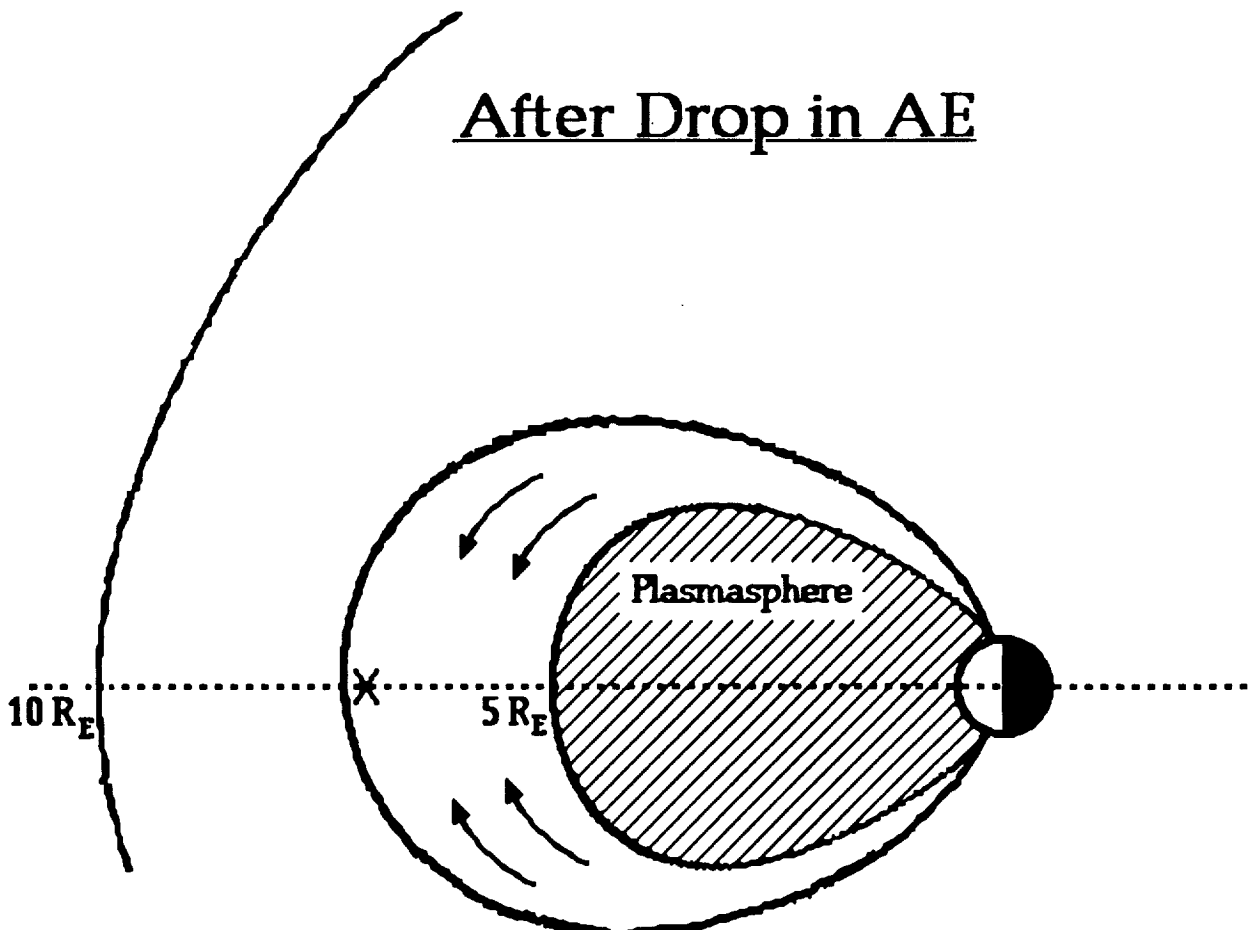


Figure 17

INSTRUCTIONS FOR COMPLETING THE NASA SCIENTIFIC AND TECHNICAL DOCUMENT AVAILABILITY AUTHORIZATION (DAA) FORM

The DAA Form, or its equivalent, is used to prescribe the availability and distribution of all NASA-generated and NASA-funded documents containing scientific and technical information. Either a suitable description (title, abstract, etc.) of the document or a completed copy must accompany this form. This form requires an appropriate Program Office review and approval, and in some cases, an International Affairs Division review and approval. The Center Representative for Document Availability Authorization should forward the completed DAA to the NASA Scientific and Technical Information Facility on completion. Specific guidelines for each Section follow:

- I. **Document/Project Identification:** Provide the information requested. If the document is classified, indicate security classification of the title and abstract. (Classified information must not be entered on this Form). Include RTOP numbers under the Contract number entry. Provide information on presentations or externally published documents as applicable. Documents intended for domestic presentation or publication must be approved in accordance with NASA STI Handbook (NHB 2200.2) while documents intended for presentation must also be screened. Documents that are to be printed as NASA series reports must be coordinated with the appropriate NASA installation or NASA Headquarters, Scientific and Technical Information Branch in accordance with NHB 2200.2. Note that information on the Report Documentation Page (if attached) is not to be entered here except for title, document date, and contract number.

- II. **Availability Category:** Check the appropriate category or categories.

Security Classification. Enter the applicable security classification for the document. Documents, if classified, will be available to all appropriately cleared personnel having a "need to know".

Export Controlled Document. If the document meets the provision of NHB 2200.2 Paragraph 5(g), the appropriate restriction must be checked, either International Traffic in Arms Regulations (ITAR) or Export Administration Regulations (EAR). This form must then be routed to the International Affairs Division for completion of Section VII. This category cannot be used with NASA Restricted Distribution documents.

NASA Restricted Distribution Document. If the document meets the provisions of NHB 2200.2, Paragraph 5(b), then the appropriate restriction must be checked, either "For Early Domestic Dissemination" (FEDD), or "Limited Distribution." If other special conditions apply to document availability, check the "Special Conditions" box and use Section III to determine the basis for such determination and the special handling required. This category cannot be used with Export Controlled Documents.

Document Disclosing an Invention. This box must be checked when documents contain information which discloses an invention. When this box is checked, an additional appropriate availability category must be checked. Authorization for use of this category must be provided by Installation Patent Counsel in Section IX.

Publicly Available Document. Check this box if the document is to be made available to the general public without restrictions. If this box is checked please indicate whether the document is copyrighted or not according to paragraph 203.2a in NHB 2200.2.

- III. **Special Conditions:** These boxes are checked only when the box designated "Special Conditions" in Section II has been checked. Both (a) and (b) are to be completed.

This subsection (a) describes the information content:

Foreign government information. Information provided by foreign governments under special agreements or the results of jointly sponsored research and development with agreed to limitations.

Commercial product test or evaluation results. Information resulting from the testing and/or evaluation of commercial products or processes that may unduly affect them if published.

Preliminary information. Preliminary or incomplete results, studies or recommendations for which wider distribution would be premature.

Special contract provisions. Information developed under NASA contracts that contain provisions providing limited rights to the data generated.

Other. Information that should be restricted for other reasons. The specific reason must be entered after "Other".

This subsection (b) on limitations refers to the user groups authorized to obtain the document. The special limitations apply both to the initial distribution of the documents and the handling of requests for the documents. The limitations will appear on and apply to reproduced copies of the document. Documents limited to NASA personnel should not be made available to on-site contractors. If approval of the issuing office is checked, the NASA Scientific and Technical Information Facility will provide only bibliographic processing and no initial distribution; the Facility will refer all document requests to the issuing office.

- IV. **Blanket Release:** This optional Section is to be completed whenever subsequent documents produced under the contract, grant or project are to be given the same distribution and/or availability as described in Section II. More than one contract number or RTOP Number can be entered. This Section may also be used to rescind or modify an earlier Blanket Release. All blanket releases must be approved by the Program Office (or its designee) and the International Affairs Division (if applicable), and concurred in by the Office of Management.

- V. **Project Officer/Technical Monitor:** The Project Officer or Technical Monitor should sign and date the form. The office code and typed name should be entered. The date signed should reflect the submission date to the program office whose approval will be entered in Section VI.

- VI. **Program Office Review:** This Section is to be completed by the duly authorized official representing the Program Office. Any delegation from NASA Headquarters to Field Installations in accordance with NHB 2200.2 should be entered here.

- VII. **International Affairs Division Review:** This Section is to be completed by the authorized representative of the International Affairs Division for all documents intended to be Export Controlled, for foreign publications or presentations, and for open domestic conference presentations.

- VIII. **Expiration of Review Time:** NHB 2200.2 provides twenty days for Program Office and International Affairs Division review. If no review has been received within twenty days, the Technical Monitor or Project Officer may release the document as marked in Section II. This release cannot be used for Export Controlled Documents, Conference presentations, or foreign publications.

- IX. **Document Disclosing an Invention:** In part a of this Section, the Installation Patent Counsel or the Intellectual Property Counsel may release a document in a time frame other than six months by entering the date and signing the alternate release. The NASA Scientific and Technical Information Facility will process and distribute these documents after six months in accordance with Sections II and III unless otherwise notified.

- X. **Disposition:** This form, when completed, is to be sent to the NASA Scientific and Technical Information Facility, P.O. Box 8757, B.W.I. Airport, Maryland 21240. When available, a printed or reproducible copy of the document should be sent with the form; otherwise, an abstract or Report Documentation Page should be sent. Forms that contain availability categories that have been disapproved by the Program Office or the International Affairs Division may be returned to the initiating NASA Technical Monitor or Project Office for resubmission.

NASA SCIENTIFIC AND TECHNICAL DOCUMENT AVAILABILITY AUTHORIZATION (DAA)

To be initiated by the responsible NASA Project Officer, Technical Monitor, or other appropriate NASA official for all presentations, reports, papers, and proceedings that contain scientific and technical information. Explanations are on the back of this form and are presented in greater detail in NHB 2200.2, "NASA Scientific and Technical Information Handbook."

- ☐ Original
☐ Modified

(Facility Use Only)

Control No.

Date

189278

I. DOCUMENT/PROJECT IDENTIFICATION (Information contained on report documentation page should not be repeated except title, date and contract number)

Title: ORIGINS OF UNUSUAL LOSS IN THE EARTH'S MAGNETOSPHERE - RURAL REPORTAuthor(s): S.A. Fuselier, M.G. Shelley and D.M. Stump

Originating NASA Organization: _____

Performing Organization (if different): Lockheed Palo Alto Research Laboratories, Palo Alto, CA 94304

Contract/Grant/Interagency/Project Number(s): _____

Document Number(s): NAS 5-51212

Document Date: _____

(For presentations or externally published documents, enter appropriate information on the intended publication such as name, place, and date of conference, periodical or journal title, or book title and publisher: CR - 189278)

These documents must be routed to NASA Headquarters, International Affairs Division for approval. (See Section VII)

II. AVAILABILITY CATEGORY

Check the appropriate category(ies):

Security Classification: ☐ Secret ☐ Secret RD ☐ Confidential ☐ Confidential RD ☒ Unclassified

Export Controlled Document - Documents marked in this block must be routed to NASA Headquarters International Affairs Division for approval.

☐ ITAR ☐ EAR

NASA Restricted Distribution Document

☐ FEDD ☐ Limited Distribution ☐ Special Conditions-See Section III

Document disclosing an invention

☐ Documents marked in this block must be withheld from release until six months have elapsed after submission of this form, unless a different release date is established by the appropriate counsel. (See Section IX).

Publicly Available Document

☒ Publicly available documents must be unclassified and may not be export-controlled or restricted distribution documents.

☐ Copyrighted ☐ Not copyrighted

P.138

III. SPECIAL CONDITIONS

Check one or more of the applicable boxes in each of (a) and (b) as the basis for special restricted distribution if the "Special Conditions" box under NASA Restricted Distribution Document in Section II is checked. Guidelines are provided on reverse side of form.

a. This document contains:

☐ Foreign government information ☐ Commercial product test or evaluation results ☐ Preliminary information ☐ Information subject to special contract provision
☐ Other - Specify _____

b. Check one of the following limitations as appropriate:

☐ U.S. Government agencies and U.S. Government agency contractors only ☐ NASA contractors and U.S. Government agencies only ☐ U.S. Government agencies only
☐ NASA personnel and NASA contractors only ☐ NASA personnel only ☐ Available only with approval of issuing office: _____

IV. BLANKET RELEASE (OPTIONAL)

All documents issued under the following contract/grant/project number _____ may be processed as checked in Sections II and III.

The blanket release authorization granted _____ is:

Date

☐ Rescinded - Future documents must have individual availability authorizations.

☐ Modified - Limitations for all documents processed in the STI system under the blanket release should be changed to conform to blocks as checked in Section II.

V. PROJECT OFFICER/TECHNICAL MONITOR

John D. Bullock
Typed Name of Project Officer/Technical Monitor

6002
Office Code

John D. Bullock
Signature

6/17/92
Date

VI. PROGRAM OFFICE REVIEW

☒ Approved☐ Not Approved

Stephen S. Holt
Typed Name of Program Office Representative

600
Program Office and Code

W. J. D. Bullock
Signature

6/30/92
Date

VII. INTERNATIONAL AFFAIRS DIVISION REVIEW

☐ Open, domestic conference presentation approved.☐ Export controlled limitation is not applicable.☐ Foreign publication/presentation approved.☐ The following Export controlled limitation (ITAR/EAR) is assigned to this document: _____☐ Export controlled limitation is approved.

International Affairs Div. Representative _____

Title _____

Date _____

VIII. EXPIRATION OF REVIEW TIME

The document is being released in accordance with the availability category and limitation checked in Section II since no objection was received from the Program Office within 20 days of submission, as specified by NHB 2200.2, and approval by the International Affairs Division is not required.

Name & Title _____

Office Code _____

Date _____

Note: This release procedure cannot be used with documents designated as Export Controlled Documents, conference presentations or foreign publications.

IX. DOCUMENTS DISCLOSING AN INVENTION

a. This document may be released on _____ Date _____ Installation Patent or Intellectual Property Counsel _____ Date _____

b. The document was processed on _____ Date _____ in accordance with Sections II and III as applicable. NASA STI Facility _____ Date _____

X. DISPOSITION

Completed forms should be forwarded to the NASA Scientific and Technical Information Facility, P.O. Box 8757, B.W.I. Airport, Maryland 21240, with either (check box):

☐ Printed or reproducible copy of document enclosed

☐ Abstract or Report Documentation Page enclosed. The issuing or sponsoring NASA installation should provide a copy of the document, when complete, to the NASA Scientific and Technical Information Facility at the above listed address.